POLITECNICO DI MILANO

School of Design
Master of Science in Design & Engineering

Analysis and development of additive manufactured novel Bio-inspired Lattice Structures

Supervisor: **Prof. Mario Guagliano**
Co-supervisors: **Dr. Sara Bagherifard; Dr. Federica Buccino**

Candidate: **Lucrezia Greco** - 941997

Academic year 2020/2021

I

Sommario

La natura, fonte di ispirazione pressoché inesauribile per scienziati e ingegneri alla ricerca di sistemi nuovi e ottimizzati, è alla base di questo lavoro di ricerca che mira alla progettazione di strutture bio-ispirate resistenti a compressione.

Le tecniche di *additive manufacturing* hanno aperto un mondo di possibilità nella produzione di strutture lattice, in un'ampia gamma di materiali e con un'elevata libertà geometrica, consentendo applicazioni di assorbimento di energia in vari settori industriali (*automotive*, protezione del corpo, campo biomedicale...).

Pertanto, la libertà di forma resa possibile dal processo produttivo, unita all'approccio biomimetico, ha dato la possibilità di definire strutture lattice innovative.

Gli obiettivi del progetto erano due: definire le caratteristiche morfologiche di alcune strutture presenti in natura resistenti a diversi tipi di carichi; generare nuove strutture bio-ispirate (BLS) pensate per applicazioni di assorbimento di energia.

L'ispirazione è partita dal bambù. Il suo diaframma, che permette alla pianta di resistere ai carichi di compressione e di flessione, ha consentito lo sviluppo di due *unit cells* quasi identiche tra loro: la seconda ha un profilo leggermente più sottile. Per ognuna delle *unit cells* è stata realizzata una struttura lattice periodica; in cui successivamente sono state introdotte alcune variazioni dimensionali (l'altezza delle *unit* è stata raddoppiata, dimezzata, o è stata variata la dimensione dei raggi di raccordo) al fine di analizzare il ruolo dei singoli aspetti geometrici sulle prestazioni meccaniche delle strutture lattice progettate.

Il lavoro è stato svolto in collaborazione con il Dipartimento di Ingegneria Meccanica e Industriale di NTNU che ha messo a disposizione tecnologie di stampa 3D per la produzione delle strutture fabbricate con la tecnologia FDM in PLA e successivamente sottoposte a prove di compressione quasi statiche. Dettagliate analisi FEM sono state condotte per analizzare ulteriormente le prestazioni e il comportamento a

compressione delle strutture; i risultati dei test sperimentali sono stati confrontati con la fase elastica ottenuta dalle analisi FEM.

Le strutture lattice basate sulla *unit cell* originale sono risultate migliori in termini di assorbimento di energia rispetto alle strutture dal profilo leggermente più sottile. In generale, i risultati migliori sono stati conseguiti con la struttura con *unit cell* con altezza dimezzata e con la struttura composta dalla *unit* originale con dimensione aumentata dei raggi di raccordo.

Un ipotetico campo di applicazione per questa struttura potrebbe essere quello biomedicale, approfondendone l'utilizzo per lo sviluppo di piedi protesici.

Abstract

Additive manufacturing technologies have opened a world of possibilities in the production of structures, such as lattices, in a wide range of materials with high geometrical freedom.

Lattice structures have been widely used in lightweight energy absorption applications, applied in a range of industrial sectors (automotive, body protection, biomedical fields...).

Scientists and engineers are seeking novel and optimized systems for which nature can be a source of innovation: the purpose of this project lies in designing bioinspired structures, capable of providing resistance to compression. The freedom of shape made possible by the manufacturing process, blended with the biomimetic approach, gave the possibility to define innovative lattices.

The objectives of the project were two: to define morphological features that characterise some structures found in nature, which make them resistant to different types of loads, and to generate novel bio-inspired structures (BLSs) thought for energy absorption applications.

In this context, bamboo was a source of inspiration: its diaphragm allows the plant to resist compression and bending loads. Two unit cells were developed: almost identical to each other, but the second with a slightly more slender profile.

For each of the unit cells, a periodic lattice structure was made; then, some dimensional variations were introduced to the original lattices (the height of the unit cells was doubled, halved, or the fillets dimension was varied) in order to analyse the role of individual geometrical aspects on the mechanical performance of the designed lattices.

The project was based on the collaboration with the Department of Mechanical and Industrial Engineering of NTNU. They offered the manufacturing and experimental instruments to deepen the topic of the project, contributing to 3D printing of the novel structures. The lattices were manufactured with FDM technology made of PLA and subsequently, quasi-static compressive tests were carried out. Detailed numerical finite elements (FE) simulations were

developed to further analyse the performance and deformation behaviour of the structures; the results of these experiments were compared with the elastic stage obtained with FE.

Lattice structures based on original unit cell were found to have better performance in terms of energy absorption compared to the structures based on the unit cell with a more slender profile. In general, the best results were shown by the lattice with halved height of unit cell and by the structure composed of the original unit cell with increased dimension of fillets.
A potential application for this structure could be in the biomedical field, with the possibility of introducing this lattice for the development of prosthetic feet.

Contents

List of figures

List of tables

1

1 Introduction

Scientists and engineers are seeking for novel and optimized systems or materials, for which nature can be a source of innovation. Organisms have evolved for millions of years to adapt to aggressive environments and the inspiration from plants and animals during the last decades has resulted in the development of very innovative systems or structures.

Different engineering fields are demanding solutions for energy absorption applications. From bigger scale (e.g., automotive) to the smaller one (personal protection, biomedical field), recent research works have been focused on the possibility to develop new structures thought for energy absorption applications.
One of the requirements for this typology of application is the lightweight: lattices are porous structures, and they could achieve a wide range of different desired physical properties.

Generally, lattice structures are strut-based, but because of additive manufacturing, novel unit cells could be designed in order to explore new possibility for energy-absorption applications. Consequently, the freedom of shape made possible by the manufacturing process, blended with the biomimetic approach, gave the possibility to define innovative lattices.

The project was based on the collaboration with the Department of Mechanical and Industrial Engineering of Norwegian University of Science and Technology (NTNU): they offered the manufacturing of the designed structures.
The objectives of the project were:
- to define morphological features that are inspired from design elements found in nature, which make them resistant to different types of loads
- to generate and analyse novel bio-inspired structures thought for energy absorption applications.

The starting point for the design of structures was the analysis and selection of morphological characteristics inspired from

nature, in order to mix these features. The research was not focused only on a typology of load, but it was considered the possibility to explore compression, torsion and bending.

Research → Evaluation → Design → Simulations

A review of varied bio-inspired structures, that are distinguished one from another for their typology of structures, materials, manufacturing processes, resistance to different typology of loads was carried out.

Therefore, the definition of the most interesting morphological characteristics was made and then some structures have been thought, modelled, designed and manufactured according to these features: a focus on resistance to compression was made.

Then, two unit cells were defined and eight bio-inspired lattice structures were modelled, 3D printed with FDM technology and numerical and experimental quasi-static compressive tests were carried out.

Results were analysed and the most prominent configuration and the outcomes have been highlighted.

In conclusion, future insights related to further development of the considered structures and possible applications are reported.

2
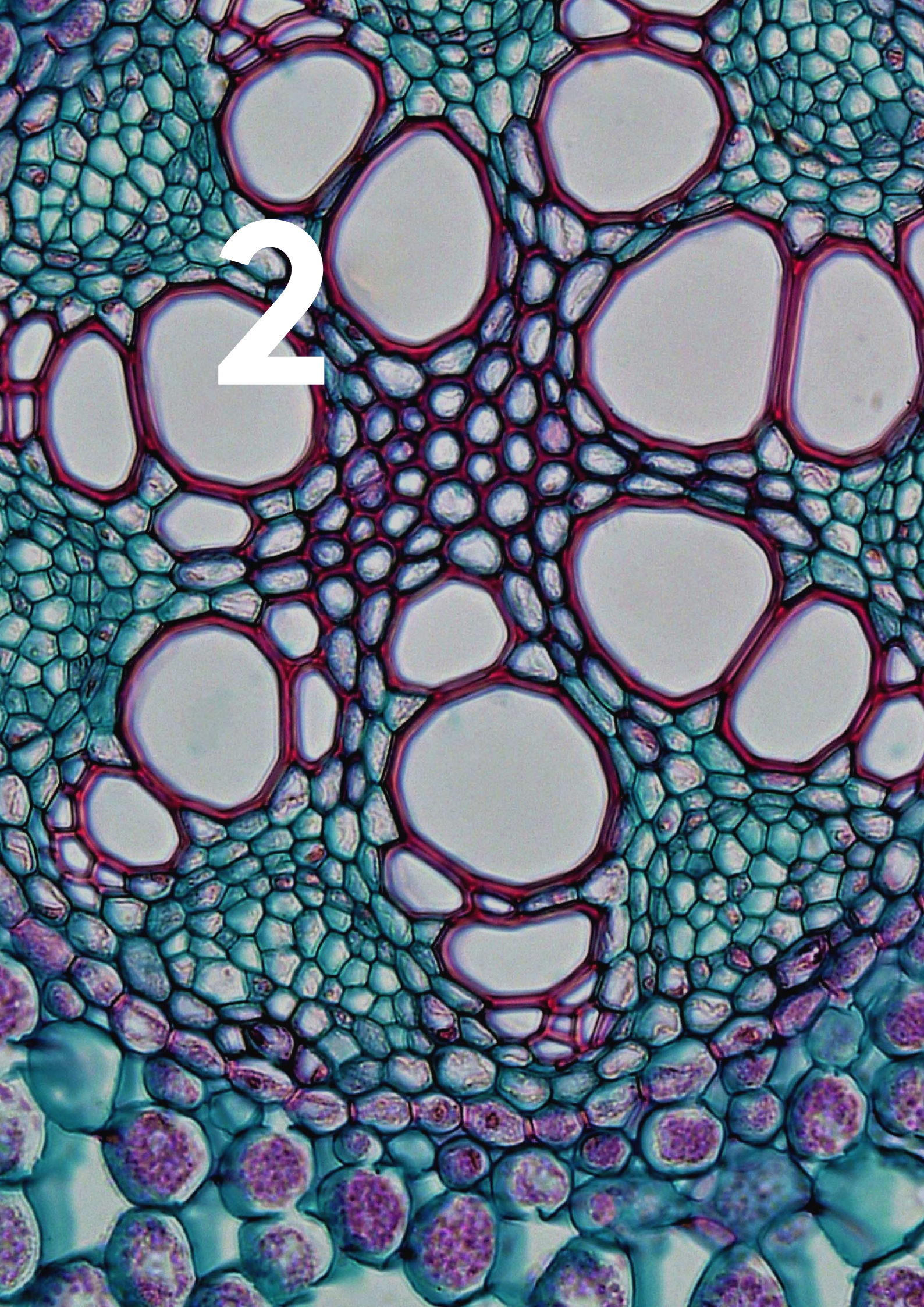
2 State of the art

Demand is increasing for lightweight structures with high energy absorption capacity in an array of engineering fields such as aerospace, transportation and civil engineering. In this chapter, common impact and energy absorbing systems or products that are part of everyday life are considered as case studies, in order to show the importance of energy absorption. A focus was made on the structures inspired by nature: very innovative systems have been developed during the last decades by taking nature as an inspiration.

Therefore, a short review of different typologies of structures with their materials and processes are analysed, in order to understand the main characteristics that an energy absorber should possess.

2.1 Energy absorbing structures

The research and development of energy-absorbing structure and materials, which dissipate kinetic energy during impact or intense dynamic loading, has received attention since 1970s: one of the major applications of energy-absorbing structures is the automotive, where crashworthy protection has become a challenging issue. In this case the "crashworthiness" refers to the vehicle response quality when it is involved in an impact: a high level of crashworthiness corresponds to low damage of the vehicle and the occupants after the event. This is the reason why the vehicles body structures are designed to resist different scenarios: the frame is optimized in case of frontal or rear impacts, doors and other components are reinforced; cushions are added on the internal part of the structure to avoid passenger's head impact in case of rapid deceleration. Also, seats, steering wheel system and other structural components have a certain absorption-capacity, in order to increase the total energy absorption of vehicles during collision. [1]

To reduce the damage caused by vehicles' collisions, various types of hardware have been also designed and installed along highways; the most common guardrail system consists of a

galvanized steel W-beam supported on steel or wood posts, that are buried in a foundation. When a vehicle impacts with the guardrail, the W-beam and the posts are deformed to dissipate most of the kinetic energy carried by the vehicle. Another type of protection consists of concrete parapets and wire rope safety: this system allows to redirect the vehicle to its original travelling direction and to convert part of its kinetic energy to potential energy. [1]

Another common application for energy absorbing structures is related to rockfall: when buildings, dams or roads are constructed in mountain or hill areas, an important safety concern is how to protect these structures from rockfall that has the potential to destroy or damage structures along its path or create an obstacle to public transportation networks. Depending on the geological conditions, some sites may require permanent protective barriers made of concrete or rock, while others may only need a protective net, which is relatively light and moveable from one site to another after being used during the construction period. In general, an ideal rockfall protective net should absorb the kinetic energy from a rockfall and plastically deform safely, no matter where the collision takes place on the net; it should be easy to install and maintain and the impact to posts should not result in a collapse of the structure. [1]

Personal safety is not an issue only during vehicles' collisions: various protective devices like bicycle helmets, hard hats and bullet-proof jackets are required to possess high energy absorption capacity. In constructions sites, workers may be hit by falling objects like tools, resulting in head and neck injuries. Therefore, the hard hat is widely used: its plastic hard shell can sustain and reduce the peak load of a falling object and it can partially dissipate energy; a similar application is considered for bicycles helmets to protect wearer's head if an accidental bike fall happens. A simulation and test of this situations is represented in **Figure 3**.
In games and sports such as football, boxing, skating and so on, crashworthiness and energy absorption capacity also have great safety values. Consequently, science and technology

need to find energy-absorbing solutions that could be applied not only on structures and vehicles but also thought for human body. [1]

Figure 3 Bicycle helmet crash test [87]

Protection is an important factor also to preserve goods while they are distributed, stored and transported: in general, the damage is due to dropping or impacts of other objects on them. Packaging has a fundamental role: product and package have become so interdependent that it cannot be considered the one without the other. In the past, cellulose wadding was widely used for shipment of liquid goods with the help of corrugated paperboard to block and cushioning the objects; these materials have later been replaced by polymers. As an example, during transportation, the packaging of fragile and valuable objects (such as electronic products and ceramic goods) is aimed at protecting the objects from a potential drop on a hard surface, in which a large impact force is created by the object's own weight.

Low density plastic foams (both rigid and flexible) are widely used for this purpose because of their excellent energy-absorption capacity as well as their light weight. In those situations, impact resistance and energy absorption become the main design criteria over static or low frequency dynamic loading.

Figure 4 *Polyurethane packing foam [88]*

Most of the foams (**Figure 4**) used for packaging are closed-cell ones, because the trapped gas within the cells provides pneumatic cushioning. Open-cell foams do not have this energy absorption mechanism, although there may be pneumatic losses as the air passes through restricted holes in the cell faces.

Some packaging applications involve simple blocks of foam, which are fixed to cardboard by adhesives and then assembled into the packaging. In this case extruded foam slab stock is the lowest cost manufacturing route and many polymers can be used. In some cases, also bubble sheets made of PE or PET can be used to transport and protect a broad range of fragile goods. [1]

More in general the materials that are used for energy-absorbing applications are mainly the ductile ones: low carbon steel or aluminium alloys, whilst among the non-metallic materials fibre-reinforced plastics and polymer foams are preferred when the weight is critical. [1]

In conclusion, there are various reasons to explain why the attention of scientists and engineers is focused on how structures and materials can be best designed to absorb kinetic energy in a controllable and predictable manner. Understanding of energy absorption is important in calculating the damage to structures caused by accidental collision, assessing the residual strength of structures after initial damage and in designing packaging to protect its contents in the event of impact. [1]

2.2 Structures for energy absorption applications

Over the last decades, energy absorption is a highly requested feature in various engineering fields: therefore, many typologies of energy absorbers such as columns, sandwiches, plates, cellular structures have been designed and tested.

COLUMNS

In seek of more efficient use of materials to achieve lightweight structures and higher energy absorption performance, thin-walled columns have become object of study. Thin-walled columns can be composed by single or multi cell; in general, it is well known that a multi-cell column absorbs more energy than corresponding single cell tube subjected to axial compressive load [2]. Referring to multi-cell tubes, hierarchical structures with self-similar have been credited with excellent mechanical properties [3], and this is due to their geometric configurations.

HONEYCOMBS

In recent research, a hexagonal multi-cell tube with hierarchy was designed and its performance under axial loading was evaluated; the honeycomb structure was made in aluminium alloy AA6061O and it was manufactured by Electrical Discharge machining (EDM) wire cutting method. In **Figure 5** is possible to see different structural configuration analysed in the research.

However, except the superior properties, the cost was a critical factor: as a result of the increase of the structural hierarchy order, the sub-structure size become smaller, which brings barriers in structural preparation and feasibility in large-scale industrial applications. [3]
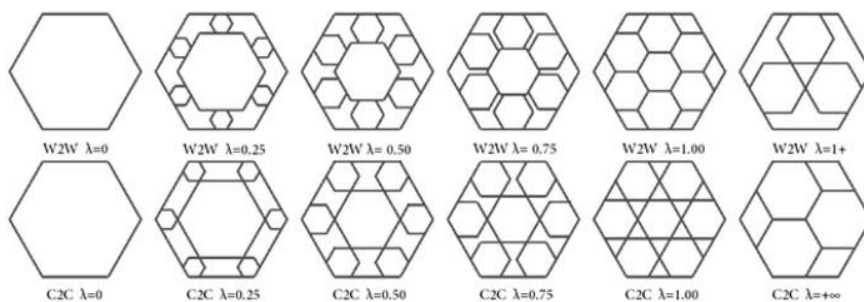
Figure 5 *Structural configurations [3]*

SANDWICHES

Tarlochan et al. show the potential of using tubular sandwich composite structures as energy absorber both for cladding structures and for crashworthiness application in vehicle design; the specimens were fabricated from glass fibre, polystyrene foam and epoxy resin.

The design of this composite sandwich addressed two main issues, the first one is the terrorist bombings: due to explosion and poor energy absorbing capabilities of civil structured, many buildings collapsed. A solution is the sacrificial cladding structure that is typically composed by two sub-structures [4]: the first and outermost one is a thin plate that distribute the blast pressure evenly across the second sub-structure (a core). Then the core absorbs the blast energy and reduces the effect of the blast force onto the building. In general, this protective structure should be an efficient energy absorber, light weight and easy to be installed.

Besides playing a role in cladding structures, energy absorbers are also fundamental in crashworthiness design. Crashworthiness is the capability of a material to absorb high energy in a progressive, controlled and irreversible manner during collisions. It ensures the vehicle to absorb crash energy with minimal attenuation of survivable space, determining the extent of occupant injuries. [5]

FOAMS

Energy absorption is required in many applications, but some of them also need the structures to be as lightweight as possible. One of the most interesting type of structure with this feature is the cellular structure: this typology is an attractive option because of its high specific strength and stiffness provided by the porous structure [6]. There are many different types of manufactured cellular structures, like metallic foams (an example in **Figure 6**): these are obtained by injecting gas or mixing a foaming agent into molten metal. The process is relatively inexpensive, but the main issue is the
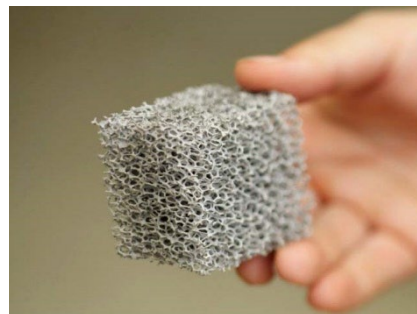
Figure 6 Metallic foam [89]

24

stochastic arrangement of open or closed cells rather than a prescribed cellular arrangement. This random structure results in an inconsistent mechanical response that is undesirable for these applications.

LATTICE STRUCTURES

Lattice structures are another type of cellular material that is differentiated from foams by the regular repeating structure of their unit cells. Gibson defines cellular materials as "an interconnected network of struts or plates" [7]. While Ashby refers to lattice structures as a form of cellular material that differ from large scale engineered structures (such as trusses or frames in terms of their scale), because of their millimetre or micrometre scale [8]. This means that while the unit cells of lattice structures can be analysed as space frames using classical mechanics, a lattice structure should be considered a material with its own mechanical properties, which allows direct comparison between the properties of a lattice structure and those of its parent material.

Lattice structures with simple geometry can be fabricated by a variety of traditional manufacturing process. However, since the proliferation of Additive Manufacturing (AM), much research attention has been paid to the AM fabrication of lattice structures [6]. An example of lattices obtained with AM technology is given in **Figure 7**.

Figure 7 Lattice structures obtained with AM technology [90]

As an example of how AM represents an opportunity to explore different possibilities for lattice structures design, the research

of Niknam and Akbarzadehab was considered. According to their research, a group of lattices were classified based on their topology and then it was proposed a strategy to enhance their energy absorption-to-weight ratio under compression: to vary the relative density across the lattice structures (**Figure 8**). The variation of the density over the structures was introduced thanks to the technology of stereolithography.

Six topologies were designed and the experimental compression tests were carried out. The results showed that the graded design with a rational variation of relative density enhanced the stiffness and energy absorption capability, when compared with the uniform design.

These results showed the possibility of designing single-phase lattice architectures that can combine lightweight and energy absorption properties by a rational variation of porosity within the cellular architecture, made possible with the use of AM technologies. [9]
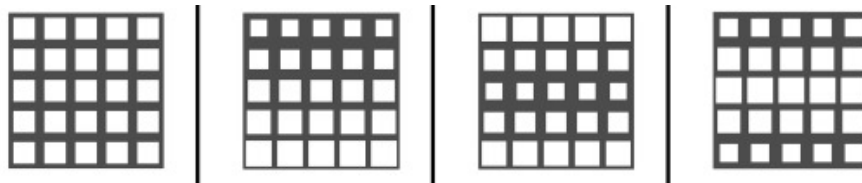
Figure 8 Gradient distribution [9]

The effect of the manufacturing process parameters on the mechanical properties of the 3D printed samples also needs to be analysed. Due to the advantages of simple equipment operation and low cost, fused deposition moulding (FDM) technology has become the most widely used 3D printing; but 3D printing PLA material has not been widely used as main load-bearing structures. The principal reason is that process parameters (printing temperature, speed and layer thickness) have a great impact on the mechanical properties of the samples during the forming process of 3D printing. Therefore, the research of Tang et al. focused on the impact of process parameters on the mechanical properties of tensile samples and lattice structures.

The prototypes, made for the tests, were prepared by FDM and then the compressive tests were carried out. Then, the

scanning electron microscope (SEM) was used to study the cross-section of the sample, and the mechanism of the influence of process parameters on the sample was analysed. According to the results, the tensile strength and elastic modulus increase with the increase of printing speed; while as the printing temperature increases, the yield strength, plastic platform stress and densification strain of lattice structure decrease. [10]

Particularly in the aerospace, a lightweight design of parts can reduce fuel consumption and increase the carrying capacity. For instance, Airbus has designed a new aircraft cabin area based on growth structures of organic cell and bone, leading to a weight decrease of the original structure by 45%. *Microlattice* (**Figure 9**), a light and strong structure produced from Boeing, enabled to balance on top of a dandelion. High specific strength of this structure offers great potentials for airplanes and vehicles. [11]
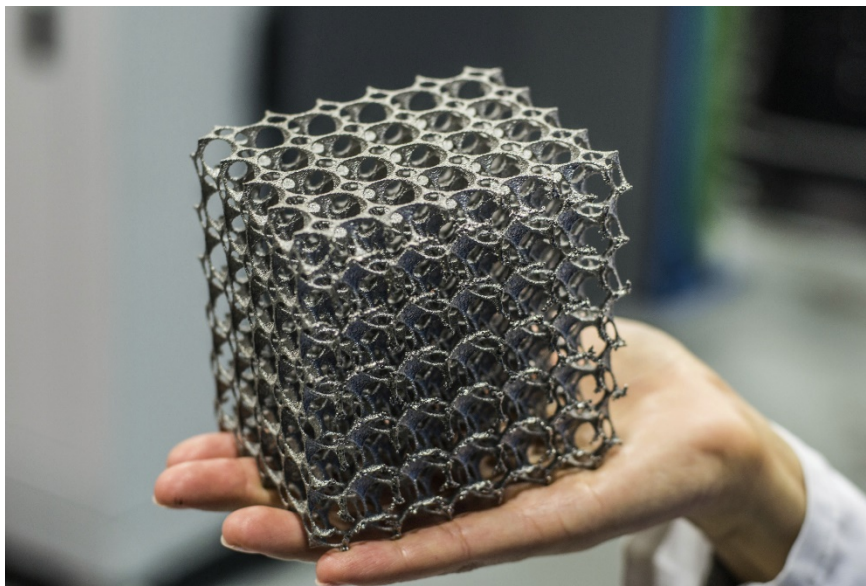
Figure 9 Microlattice by Boeing [91]

In conclusion, according to the different advantages and disadvantages, identified and listed in **Table 1**, different typologies of structures have been studied and implemented in various research. However, a lot of weak points are still present and need to be deepened; therefore, there is the need

to develop a structure based on different feature and characteristics. An innovative, yet interesting and "old and wise" source of inspiration could be nature: there are various example that could demonstrate how organisms have evolved in order to resist aggressive environments and then a novel structure could be developed starting from these inspirations.

There are different typologies of structures that could be considered for energy absorption application; however, compared to other types of cellular structures including foams and honeycombs, lattices are more flexible to achieve a wide range of different desired physical properties, such as high stiffness-weight ratio, low thermal expansion coefficient, negative Poisson ratio, and high heat dissipation rate through active cooling [12]. Another important aspect to consider is the development of AM technologies, that allow to easily vary the cellular architecture and prototype the structures.

Structure	Tested resistance to:	Numerical or experimental results	Advantages and disadvantages	Ref.
Columns (single-cell tube)	Axial compressive load	Numerical and experimental	+ Easy to manufacture - Mechanical properties are worse than multi-cell tubes	[2]
Honeycombs	Axial compressive load	Numerical and experimental	- Energy absorption performances are not enhanced by the hierarchy order increase; high manufacturing cost	[3]
Foams	(Generally used for energy absorption applications)	-	+ Lighweight - Stochastic arrangement lead to inconsistent mechanical response	[6]
Lattices	Axial compressive load	Numerical and experimental	+ Lighweight + Possibility to vary mechanical properties according to unit cells and density + Easy to manufacture (SLS)	[9]

Table 1 Recap of various typologies of structures

28

2.3 Nature as an inspiration

In the latest decades, there is an increasing interest in the research community in understanding how some structures present in nature have interesting qualities from a technical point of view: scientists and engineers are always seeking new inspirations and they are attracted by the unique qualities of the structure inspired by nature. Therefore, a review of interesting bio-inspired structures was made. The different typologies of structures and their material and processes were analysed.

2.3.1 Bio-inspired structures for energy absorption

In nature, plants and animals offer many excellent structures with low density, high strength and high energy absorption capacities that could inspire the design of novel structures with remarkable energy absorption.

For example, the pomelo fruit (Citrus maxima) has a spongy mesocarp layer that can dissipate energy of 80 J from free fall tests without leading to visible outer damage of the peel. Nut shells also exhibit excellent impact and puncture resistances. Lessons in high energy absorption can also be learned from animals: a beetle forewing can withstand a puncture force up to 23 N, which is much higher than the fighting force of the beetle. Thus, the beetle forewing plays a vital role in protecting the beetle's hindwing and thorax, a feature that can be applied to the design of protective structures. [13]

The biomimetic approach was first applied in an energy absorption application in 2000. In recent years, use of this approach is increasing for lightweight structures with high energy absorption capacity for different applications and it is a promising avenue for replacing conventional structures in future. Bio-inspired structures have been employed in a wide range of applications in the engineering and technical field, from the front structures of cars and trains, to design protective armours. Consequently, several energy absorbers with different structures such as columns, sandwich, plates and cellular structures have been proposed. [13]

Some crashworthiness criteria were used to evaluate the performance of bio-inspired structures; these criteria were defined based on the force-displacement curve of an energy absorber under crushing force; they are the IPCF, EA and SEA. Initial peak crushing force (IPCF) is the peak force at an early stage in the crushing process of a structure.

Energy absorption (EA) is mainly used to evaluate an energy absorber's ability to dissipate crushing energy through plastic deformation. It can be calculated as follows:

$$EA(D) = \int_0^{dmax} F(x)dx \qquad (1)$$

where F(x) is the crushing force as a function of displacement x during the crushing process, dmax is the effective deformation distance.

Specific energy absorption (SEA): the absorbed energy by a structure per unit mass given by:

$$SEA(D) = \frac{EA(d)}{m} \qquad (2)$$

The SEA is often used to compare the energy-absorbing ability of different materials and structures. [13]

2.3.1.1 Thin-wall structure

BAMBOO

The macrostructure of bamboo has inspired different types of tubes: the circular ones are the most common utilised in energy absorption since they are strong and stiff, inexpensive, easy to obtain with classical manufacturing process and very good energy absorber. Zorzetto and Ruffoni focused on the design of wall structures of the tubes, then proposed a novel wood-inspired helix-reinforced cylinder. The structure consisted of a main layer containing helicoidal fibres, bordered by inner and outer plies having thinner fibrils. The results of numerical and experimental tests demonstrated that failure resistance and energy absorption can be enhanced by

enclosing the main helicoidal layer with a minimum number of thin fibrils oriented perpendicular to the applied load. [13]

To improve the energy absorption capacity of circular tubes, multicell sections have been introduced to the circular ones. Some multi-cell tube' cross-sections were inspired by the bamboo vascular structures (**Figure 10**).

In their research, Zou et al. designed a multi-cell tube that consisted of four circular tubes connected through a series of bionic elements: numerical results indicated that this feature improved the SEA in both lateral and axial impact loading.

The effect of the bionic element shape on energy absorption capabilities was also studied in another research, in order to define the shape for the ribs that is more suitable for this type of application.

Although these structures showed positive numerical results, they have received limited attention, due to the difficulty of manufacturing the bionic element through traditional manufacturing processes. Even so, bamboo was considered to design a lot of different structure because of its particular macrostructure: the plant can resist not only compressive load, but also bending. This feature of bamboo will be detailed in chapter 3. [13]
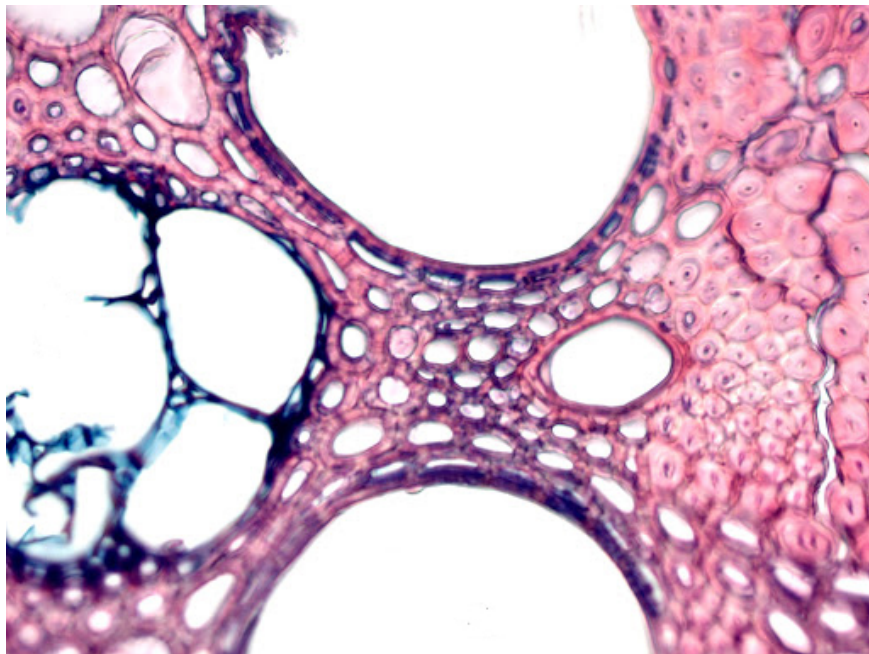
Figure 10 Bamboo vascular bundles [92]

HORSETAIL

Like bamboo, the horsetail plant contains hollow multi-cell structures (**Figure 11**); then a tube inspired by horsetail and filled with aluminium foam was tested. The results, that depended on the foam density and tube geometry, exhibited excellent performance under lateral loading, but the behaviour under axial loading was not fully understood. [13]
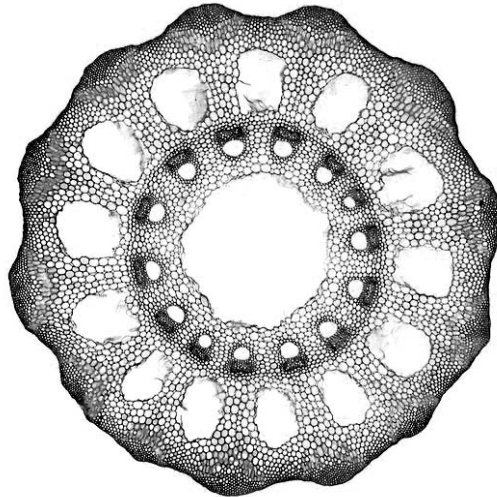
Figure 11 Horsetail plant cross section [93]

BEETLE FOREWING

Inspiration was also taken from animal world. Single-wall tubes were inspired by beetles' body: *Elytra* is the external protection of the insect (**Figure 12**); this structure is composed by circular tubes placed at the centre of hexagons that compose a honeycomb. Different structures were designed according to this feature, and the ability to resist impact was related to various geometrical parameters, such as column numbers, tube diameter, thickness and height of the columns. [13]

BONE AND TENDON

Two main structures were analysed: the first one was applied in the crash box of a vehicle, made of concave structure shell and an inner core (inspired by the cancellous bone structure of the human tibia) filled with negative Poisson's ratio material. The whole structure showed superior energy absorption capability than the original crash box.
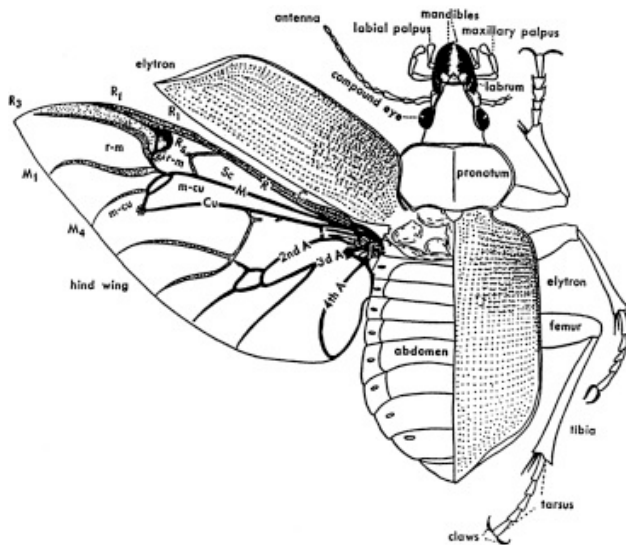
Figure 12 Anatomy of adult beetle [77]

In the second one, the tubes were constructed by packing smaller tubes into a tube of a higher hierarchical level: the energy absorption capability significantly improved for higher orders of hierarchy. This second structure was inspired by the architecture of tendon and muscles. [13]

Other examples include multi-corner, corrugated and tapered tubes. Multi-corner tube showed greater energy absorption capacity than traditional square columns under axial loading; this was also due to the feature of bulkheads (inspired by the structure of bamboo). [13]

The diatom, a *microalga* (**Figure 13**), inspired the design of a crash-pad as an energy absorber for vehicles in lateral collisions. The crash-pad, characterised by three undulations with different height, was produced from different materials: conventional talc reinforced polypropylene and a natural fibre reinforced plastic.
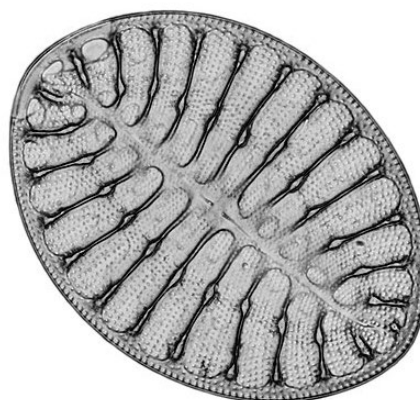
Figure 13 Corrugated structure of diatom [94]

Compression tests revealed that the bio-inspired crash pads performed equal than or even better to their technical counterpart.

Conical tubes with different cross-sectional shapes (circular, rectangular and square) have been investigated as energy absorbers. Li et al. designed three types of tubes based on the trabecular architecture of the beetle forewing: the structures consisted of a hexagonal tapered tube and an inner circular tapered tube. The plastic deformation under impact loading of the bio-inspired structure was compared to that of the double circular tube and double frusta tube, showing the most stable deformation among the three tube types. According to the positive results, this could be used as an ideal energy-absorbing bumper structure. In another research, horizontal grooves were added to the same tapered tubes, showing even a smoother deformation. [13]

In **Table 2** a recap of the given informations about thin-walled structures is represented.

2.3.1.2 Plates
BEETLE FOREWING
The trabecular microstructure of beetle forewing was mimicked to fabricate different type of tubes, but this architecture was also investigated in order to develop plates. Actually, the beetle forewing is a sandwich structure that has mechanical and thermal protection roles. It consists of two laminated plates; between the upper and lower plates it is placed a core made by a trabecular structure.
One of the structures proposed is a sandwich panel with the addition of circular tubes at the intersection of honeycomb walls: as a result, the structure showed an enhancement of energy absorption due to a shared mechanisms between the reinforced circular tube and the cell walls. In other research, it was also investigated the influence of radius and height of tubes and honeycomb on mechanical properties. [13]

34

WOODPECKER

Woodpecker was a source of inspiration for different structure. A sandwich beam mimicking its head structure (**Figure 14**) was developed to improve low-velocity impact behaviour; it was composed by carbon fibre laminated skins with rubber

Thin-walled structure inspired by:	Tested resistance to:	Numerical or experimental results	Observations
Bamboo: helix-reinforced cylinder	Axial compressive load	Numerical and experimental	Energy absorption can be enhanced by enclosing the main helicoidal layer with a minimum number of fibrils
Bamboo: multi-cell tube composed by four circular tubes connected through bionic elements	Axial and lateral impact load	Numerical	Bionic elements improve the SEA
Bamboo: multi corner tube with bulkheads	Axial compressive load	Numerical	Bulkheads improve the SEA
Horsetail: multi-cell tube and filled with aluminium foam	Axial and lateral load	Numerical	Excellent performance under lateral loading, but the behaviour under axial loading was not fully understood
Beetle forewing: hexagonal tube and an inner circular tube	Axial impact load	Numerical	The ability to resist impact was related to geometrical parameters (column numbers, heights, tube diameter and thickness)
Beetle forewing: hexagonal tapered tube and an inner circular tapered tube	Axial impact load	Numerical	According to the results, the structure could be applied as a energy-asborber bumper
Bone: concave structure shell and an inner core	Axial compressive load	Numerical	The structure showed superior energy absorption capability than the original crash box
Tendon: hierarchical tubes	Axial compressive load	Numerical	EA significantly improved for higher orders of hierarchy
Diatom: crash-pad with corrugation for vehicles	Lateral load	Numerical and experimental	Diatom crash pads performed equal than or even better to their technical counterpart

Table 2 *Recap thin-walled structures*

35

and aluminium honeycomb cores. The results showed superior energy absorption capacity compared to the conventional beams.
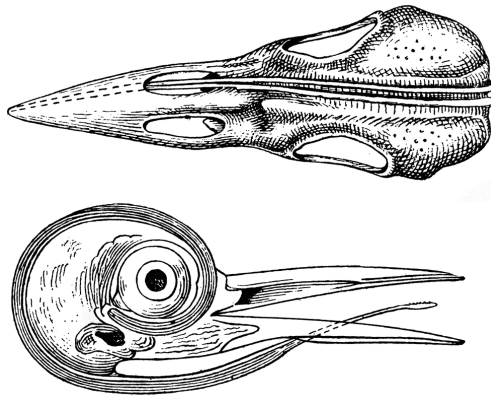
Figure 14 Anatomy of woodkpecker's head. Image via Yearbook of the United States Department of Agriculture (Washington: Government Printing Office, 1900) 293

Then, the microstructure of a woodpecker's beak was mimicked to propose a sandwich panel with corrugated core that exhibited superior energy absorption capability compared with a conventional honeycomb sandwich panel under dynamic crushing. [13]

CRUSTACEAN SPECIES

Bio-inspired composite plate with helicoidal structure was firstly proposed by Bouligand (**Figure 15**) and found in the cuticle of most crustacean species. The helicoidal structure enhances stiffness, strength and hardness: these types of laminates are significantly superior to standard lay-ups under quasi-static loading conditions. Therefore, a composite structure with helicoidal lay-up structures might improve damage tolerance and mitigate impact forces. [13]

Figure 15 Helicoidal or Bouligand structure [14]

NACRE AND CONCH SHELL

Other composite plates were inspired by the nacre and conch shells and even if they were made with ceramic materials, they showed non-brittle behaviour because of their structure. In **Figure 16** the graphical representation of conch shell structure.

For example, a Si3N4/BN ceramic composite laminate was fabricated using plastic forming methods: test results showed non-brittle behaviour and a fracture toughness 1.16 times greater than that of the monolithic plate.

Later, Flores-Johnson considered the effect of interlocking mechanisms between tablets. Numerical results showed that the nacre-like composite plate improved in blast resistance performance compared to conventional composite laminate with flat and continuous interface. This research also showed that the soft interlayer mortar has an important role in energy dissipation of the nacreous structure under dynamic loads. [13]
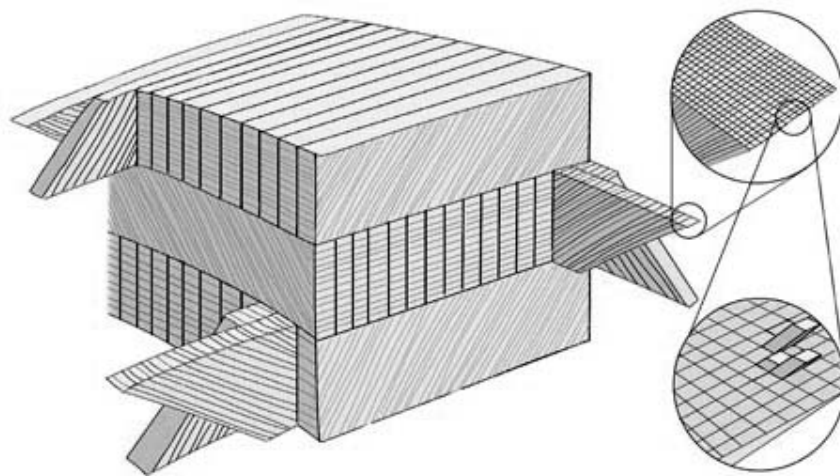
Figure 16 Conch shell layered structure. Image via Stephanie Freese/American Scientist

FISH SCALE

Fish possess flexible dermal armour for protection that could be source of inspiration for protective devices with high penetration resistance and energy absorption. In *Arapaima gigas* dermal armour (**Figure 17**), scales are made up of an external hard mineral layer on a multi-layered collagen

backing. Mimicking this structure, it was proposed a plate using a hard face and soft backing layers to create ceramic-composite panels for impact protection applications.

In modern teleost fishes, the overlapping of scales is fundamental for the protection of the fish. Using the overlapping strategy, a new composite architecture was proposed, and it was showed that flexibility was preserved but protection against penetration was ensured; moreover, the structure resulted more resistant than elastomers. [13]

Figure 17 *Arapaima Giga's scale [95]*

A similar structure was found on crocodiles: they have evolved flexible armoured skins in the form of osteoderms, which are hard plates of finite size embedded in softer tissues (**Figure 18**). The hard segments play the protection role while the relative motion of these segments provides the flexibility required for their locomotion. A bio-inspired segmented armour was fabricated using laser engraving and the results showed that glass segmentations reduce the size of the damaged area without reducing the protection in the centred impact. [13]

New topologically interlocked materials (TIMs) were developed in order to mimic the interlocking mechanisms from *Alligator gar* for impact applications. Research suggests that the TIMs were 10 times more impact resistant than their monolithic

form; it was also demonstrated that the structure significantly enhanced energy dissipation and toughness. [13]
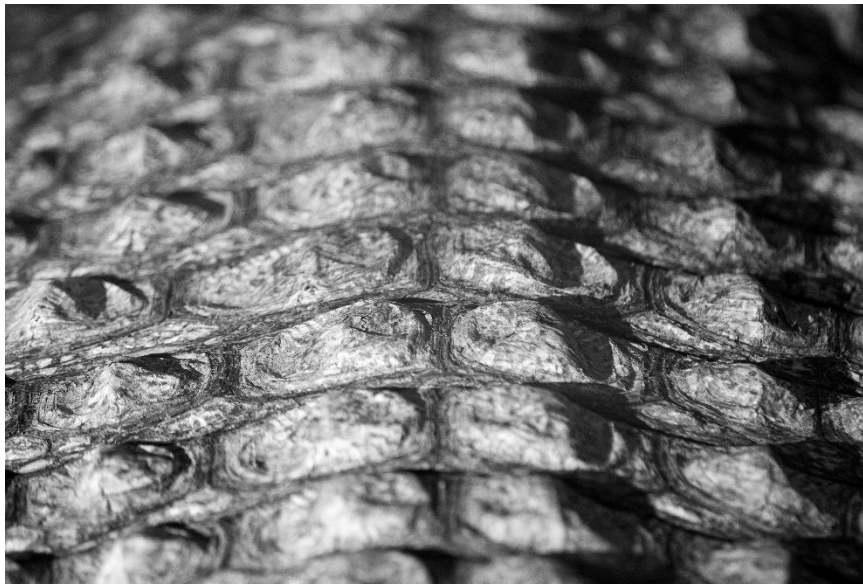
Figure 18 *Crocodile's osteoderm [96]*

In **Table 3** a recap of the given informations about plates structures is represented.

2.3.1.3. Cellular structures
HONEYCOMBS

The conventional honeycomb has been widely used in energy absorption applications, but a series of innovative geometries were considered to improve energy absorption capacity, such as triangular, square, hexagonal and kagome tessellations. All these geometries were inspired by the horseshoe mesostructure (**Figure 19**), and they all resulted to be better in energy absorption than the traditional honeycomb. [13]
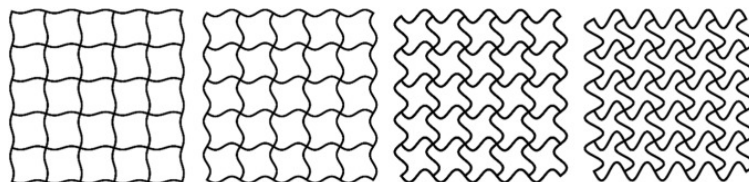
Figure 19 *Honeycombs with different wave amplitudes inspired by horseshoe [13]*

Plates inspired by:	Tested resistance to:	Numerical or experimental results	Observations
Beetle forewing: sandwich with circular tubes at the intersection of honeycomb walls	Axial compressive and impact load	Numerical	Tubes improve the EA
Woodpecker's head: sandwich beam	Axial impact load	Experimental and numerical	Improved the EA when compared to conventional beams
Woodpecker's beak: sandwich with corrugated core	Axial impact load	Numerical	Improved the EA when compared to conventional panels
Custaceans: bouligand structure	Axial impact load	Numerical	Helicoidal structure enhances stiffness, strength and hardness compared to standard lay-ups
Nacre: composite plate with tablets	Axial impact load	Numerical	This plate improved blast resistance compared to conventional composite laminate with continuous interface
Fish scale: composite panels with hard face and soft backing layers	Axial impact load	Numerical	Flexibility is preserved but protection against penetration is ensured too
Crocodiles: segmented armour	Axial impact load	Experimental and numerical	Segmentations reduce the size of the damaged area without reducing the protection
Aligator gar: interlocking elements (TIMs)	Axial compressive load	Experimental and numerical	TIMs were 10 times more impact resistant than their monolithic form; it was also demonstrated that the structure enhanced energy dissipation and toughness

Table 3 *Recap plates*

FOAMS

In their research, An and Fan investigated the behaviour of luffa-sponge-like hierarchical foam cylindrical structures and it was demonstrated that the SEA of the bio-inspired foam was greatly improved compared with that of pure aluminium foam cylinder due to the interaction between the CFRP tube and the aluminium foam. [13]

Another structure inspired by luffa was an aluminium foam for impact resistance application. Yin et al. proposed nickel-plated luffa sponges using electrochemical deposition method. They indicated that the energy absorption capacity of nickel-plated luffa sponges was far superior to that in other comparable materials, like CFRP honeycombs and stainless-steel lattices. [14]

Additionally, lotus was considered as an inspiration for bio-inspired foams: most of research about the lotus-like metal

foams are focused on the uniform density; it could be interesting to investigate how the gradient density of lotus foam may improve the energy absorption. [13]

LATTICE STRUCTURES

In their research, Han et al. mimicked the crystal structures of two natural solids: α-cristobalite (**Figure 20**) and LaNiO3/SrTiO3 in order to propose and study two novel auxetic materials with excellent mechanical properties. The materials were fabricated by forming helical wires into a wire-woven structure and then filling the tetrahedron or octahedron cells with another solid. It was demonstrated that the novel auxetic structures achieved superior energy absorption capability and ultrahigh strength and ductility, which are essential for heavy-duty applications.

An important aspect to lattices is the hierarchical architecture. In recent research of Wang et al. bio-inspired lattices were fabricated. The results showed an increase of energy absorption capability with the introduction of hierarchical order in lattices; furthermore, higher hierarchical of lattice indicated higher failure strain. [13]
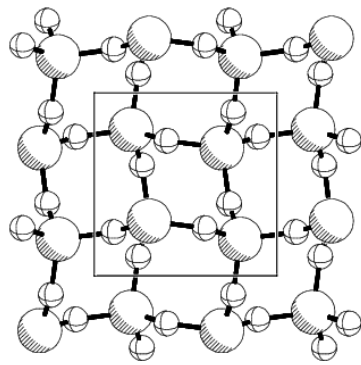
Figure 20 *Representation of α-cristobalite [84]*

In **Table 4** a recap of the given informations about plates structures is represented.

2.3.1.4 Other structures

The biomimetic approach was applied also on bigger scale for civil engineering, for applications that require high impact resistance and toughness. Nacre microstructure (**Figure 21**) was an inspiration for a structure made by ceramic composite, that showed significant improvement in impact resistance compared with the simple layered ceramic composite made by nonpartitioned tile layers. Tests were conducted on the

structure and the results showed better performance against high-velocity impact than that of monoblock cement-based materials.

Javan et al. proposed an alternative geometry for hard building blocks, introducing a topological interlocking mechanism for bricks mimicking nacre microstructure to improve the mechanical properties. The interlocking assembly plates with four curved side surfaces of the brick had significantly improved flexural performance compared with that of monolithic plates in terms of impact energy absorption capacity. [13]
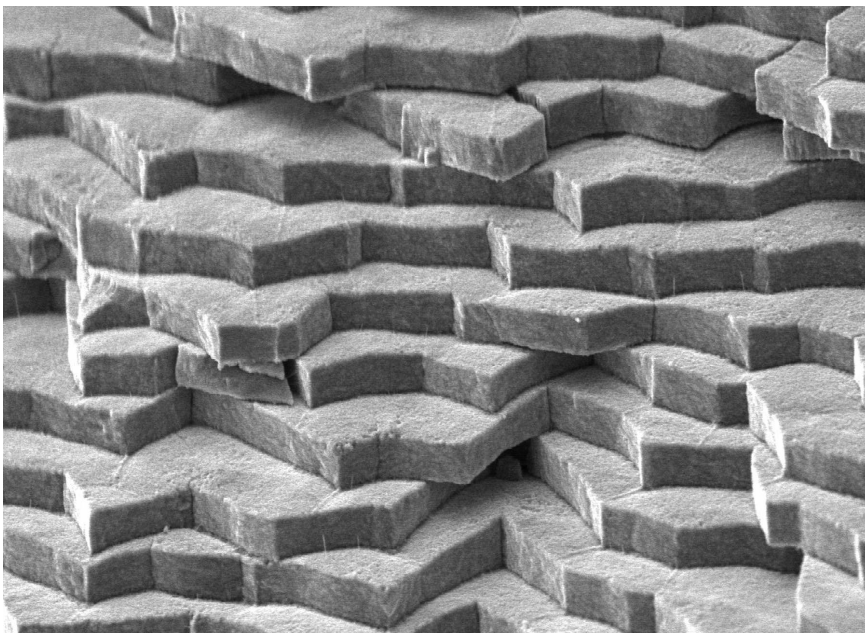
Figure 21 *Nacre structure view at the microscope [97]*

Besides the aforementioned categories of bio-inspired structures, other examples in nature were find and analysed.

The wing veins of dragonfly were mimicked to improve the impact resistance of E-glass/epoxy skins: the veins of dragonfly and other insects are specialised for mechanical loads like bending and torsion. The structure consists of E-glass/epoxy faces bonded to a polyurethane foam core and a cylindrical shell: using drop impact tests was demonstrated that the E-glass/epoxy skins with bio-inspired veins limited the damage propagation.

The seahorse tail is squared and composed of subdermal bony plates that are made of deformable materials and that can slide past one another and buckle if compressed (**Figure 22**). These plates overlap for controlled bending and twisting: with this unusual deformation mechanisms, seahorse tail plays a protective role against predators, that could inspire structures for defence applications.

Figure 22 A round-plated tail, typical of seahorses (right): the square segments create more contact points with the surface that it is gripping. Image via Michael Porter/Clemson University.

The chiral nature of DNA, composed by double-helix, inspired a structure that shows how the two intertwined helices are decisive to the compression-twisting coupling deformation mode. Experimental tests also showed the excellent recoverability and mitigation capability of the structure. [13]

The objective of the review of different bio-inspired structures was to identify some characteristics which allow for better mechanical properties, according to different type of loads. Therefore, some specific structures have been considered and analysed, with a focus on the possibility of mixing some of

these elements to create a novel unit cell for a uniform lattice structure.

Cellular structure inspired by:	Tested resistance to:	Numerical or experimental results	Observations
Honeycombs based on horseshoe mesostructure	Axial compressive load	Numerical	The horseshoe mesostructure increases plateau force and SEA compared with the traditional honeycomb
Foams based on luffa sponge	Axial compressive load	Experimental and numerical	SEA was improved compared with that of pure aluminium foam cylinder
Nickel-plated luffa sponges (electrochemical deposition method)	Axial compressive load	Experimental and numerical	The EA was far superior to that in other comparable materials (like CFRP honeycombs and stainless-steel lattices)
Lattices based on crystal structures	Axial impact load	Numerical	Improved the EA when compared to conventional panels

Table 4 Recap cellular structures

2.3.2 3D printed bio-inspired structures

Among all the typologies analysed, one of the most interesting structure for energy absorption application are the cellular structures, especially the lattices.

An example of lattice structures inspired by nature can be found in the research of Olsson and Naarttijärvi. The objective of this study was to investigate structures based on geometries found in nature and to optimize them to absorb as much energy as possible on impact meanwhile keeping the mass low. The manufacturing process considered for these lattices is 3D printing of Nylon, while the final application considered was the bicycle helmet, in order to create a lattice that could substitute the expanded polystyrene foams that are commonly used for this protective device.

Three main structural concepts were selected and evaluated: the first one is based on cellulose and the unit cell consists of two cubes stacked over each other with an offset. The offset is only in one direction to gain some strength and it is designed to transfer loads between the beams. The second structure is inspired by the trabeculae of human bone. A geometric figure that approximately resembles the stochastic pattern in trabeculae is a tetrahedron: then the unit cell consists of eight tetrahedrons and it is repeatable in all directions. The last inspiration for the lattice structure is the pyramid that like the tetrahedron it has some similarity to the stochastic pattern of the trabeculae (**Figure 23**).
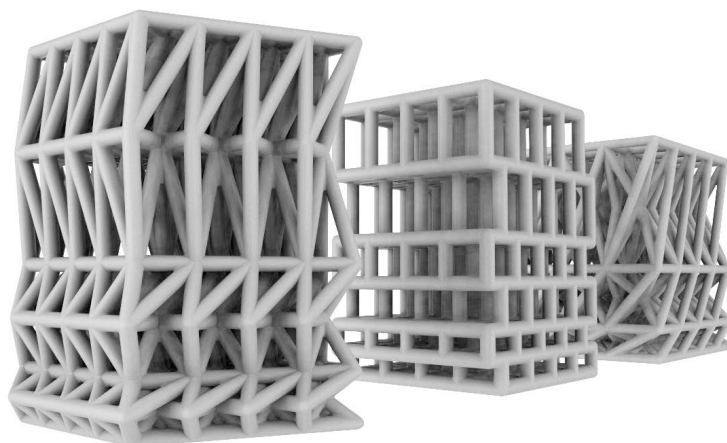
Figure 23 *The three bio-inspired lattice structures; the main inspirations were trabecular structure and cellulose [15]*

According to the results, the cellulose is the best structure among the three and it has both high energy absorption and SEA and it could be a good replacement for helmet foams. In fact, how the material in the helmet is structured is limited by available manufacturing techniques and materials. However, the manufacturing techniques are developing rapidly and with 3D printing it is now possible to manufacture complex geometries with very high precision. [15]

A novel lattice structure inspired from the front wing of beetles (adult *Allomyrina dichotoma*) was designed and fabricated by SLM technology of AlSi10Mg. The front wing has the dual function of protecting the body and promoting flight ability and its microstructure is composed by cylindrical tubes. Hence, the microstructure could be schematized as a circular column tube, and the shape of hyperboloid can be obtained (**Figure 24**). The novel structure was characterized by high degree of optimization, diverse design, lightweight and high strength. Therefore, bionic thin-walled structure based on the beetle's front wing microstructure was considered under impact load, showing excellent energy absorption; the effects of process parameters on densification level, microstructures, mechanical properties of SLM-processed lattice structures were also studied. [11]
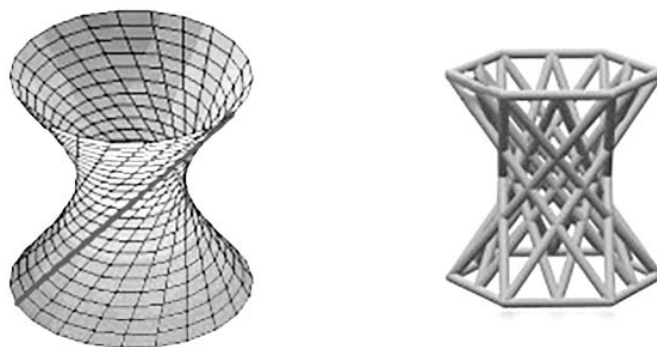
Figure 24 *Hyperboloid and unit cell structure inspired by front wing of beetles (adult Allomyrina dichotoma) [11]*

The biomimetic principle was also applied to design and 3D print four novel protective structures made in Nylon: the classic honeycomb structure, the concave honeycomb, the inclined column honeycomb, and the imitational peanut shell structure (**Figure 25**). The mechanical properties under the quasi-static compression have been analysed and the results between the different structures have been compared. Theoretical analysis has been conducted as well: the objective was to predict the quasi-static impact force and Poisson's ratio of the structures. To finalise the research, the 3D finite element models in the quasi-static compression have been established, and the mechanical properties of the models have been confirmed and verified by comparing the experimental, numerical simulation and theoretical results. The conducted analyses revealed the excellent properties of the structures and, as future developments, they could be considered to implement protective applications. [16]
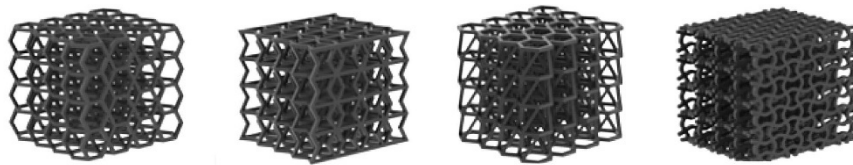
Figure 25 *The four bio-inspired honeycomb structures [16]*

All these lattices have in common complex geometrical shapes and then the manufacturing process: they were all realised through Additive Manufacturing (AM) technologies. AM allows to produce strong, lightweight structures with geometry that is unachievable by traditional manufacturing methods: it is extremely appealing thanks to several advantages such as time reduction in the design-to-manufacturing cycle, reduction of parts number or bolted connections/welding and capability to produce complex geometries in one part (**Figure 26**).
The design and manufacturing of cellular lattice structures is thought to provide high performance such as high strengths accompanied by a relatively low mass, good energy absorption characteristics and good thermal and acoustic insulation properties to aerospace, medical and engineering

products. Currently, there is great interest in manufacturing cellular lattice structures with tailored properties. Conventional manufacturing methods, (machining, laser cutting/engraving, precise casting process...) are commonly used to fabricate lattice structures with simple configurations. However, it is challenging for such methods to fabricate complex configurations: [6] additive manufacturing technologies have been developed to produce complex 3D components with bio-inspired efficient structures directly from a digital model by adding material layer by layer without the use of specialized tooling; advantages of this manufacturing process include greater geometric control, more efficient use of material, high customization and design flexibility. [17]

With AM "the design drives the shape" concept is valid, opposed to the strategy "the manufacturing drives the shape" which applies with traditional machined parts. Cellular complex structures may be included in AM components where lightweight, stiffness and high strength to mass ratios are needed. [18]

With additive manufacturing technologies, the research could be motivated to look at the structures and organisms in nature, shaped by the millions of years of evolution to inspire new ways to structure the materials to make them safer for energy absorption applications. [15]
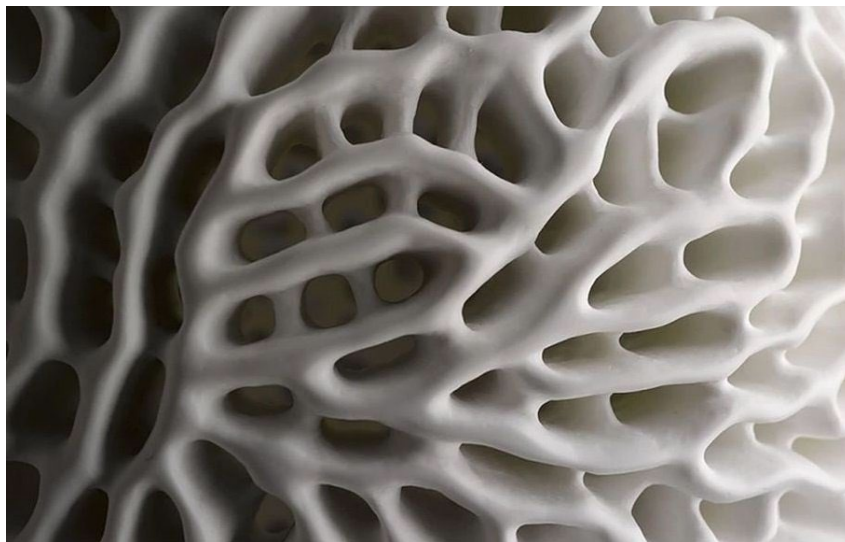
Figure 26 Complex design achieved with 3D printing [98]

2.4 Summary and setting the objectives

Different engineering fields are demanding solutions for energy absorption applications. From bigger scale (automotive, protection from accidents in different scenarios, from mountains to buildings in cities…) to the smaller one (personal protection, biomedical application), recent research works have been focused on the possibility to develop new structures that can resist different type of impact. [1]

The design of energy-absorbing structures could be inspired by nature. Organisms have evolved for millions of years to adapt to aggressive environments, which can provide good inspiration for novel structures. It is expected that the structures from organisms can develop the functional properties of the complex structures. [11]

One of the requirements for this application is the lightweight: cellular structures, like foams, honeycombs and lattices, are characterised by good mechanical properties and also, they are lightweight. Among cellular structure, lattices are more flexible to achieve a wide range of different desired physical properties. [12]

Generally, lattice structures are strut-based, but because of additive manufacturing, novel unit cells could be designed in order to explore new possibility for energy-absorption applications. [18]

Consequently, the freedom of shape made possible by the manufacturing process, blended with the biomimetic approach, gave the possibility to define novel lattices.

After the definition of the most interesting features, some structures have been thought, modelled and designed, but only two of them were developed in detail.

Therefore, two unit cells were defined and eight bio-inspired lattice structures (BLSs) for energy absorption applications were modelled, 3D printed and numerical and experimental tests were carried out. The objective was to identify the best configuration and more in general to analyse the behaviour of the structures in order to define the advantages and possible aspects to further improve.
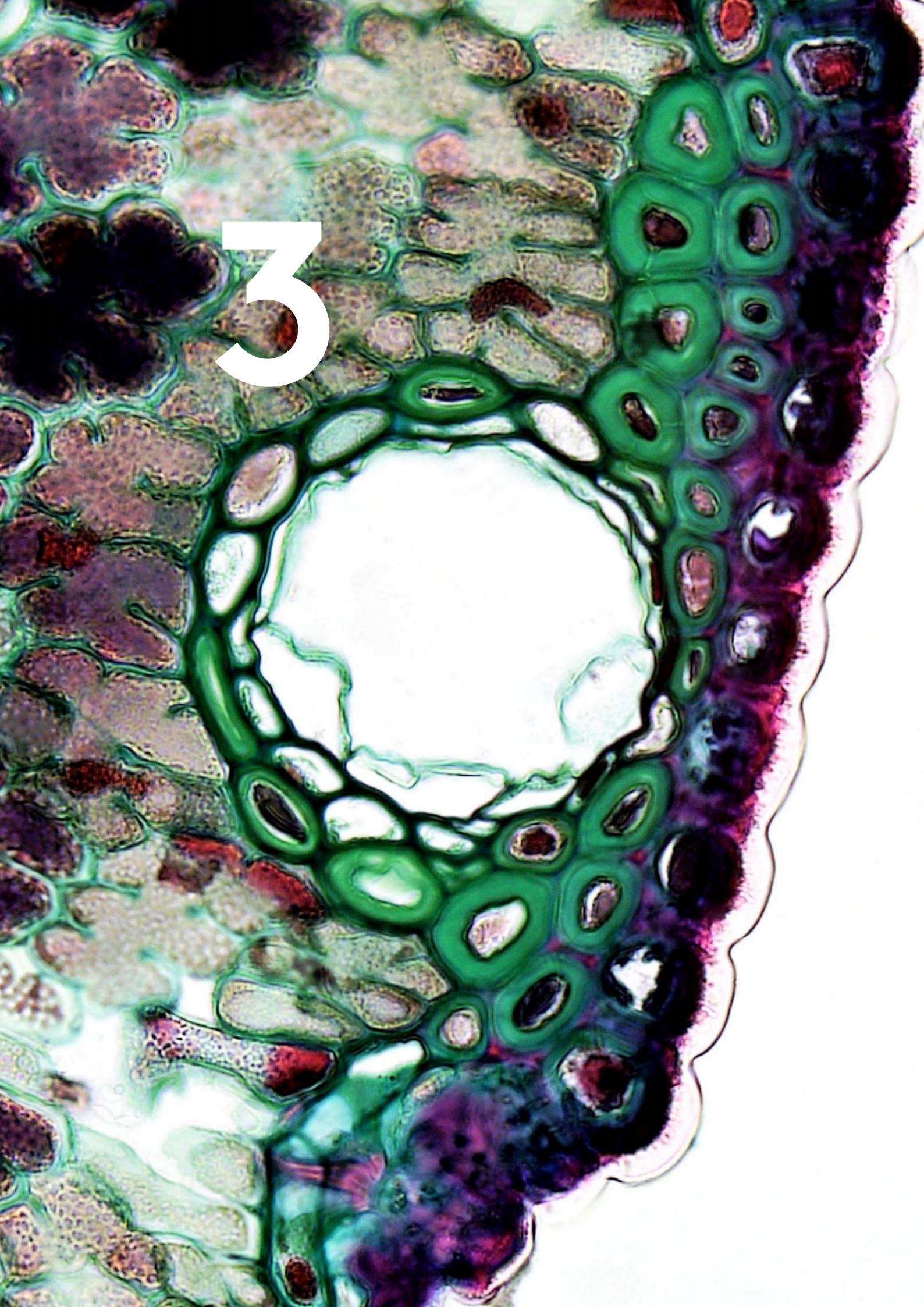
3 Design of the structures

Lattice structures are topologically ordered, three-dimensional open-celled structures composed of one or more repeating unit cells. These cells are defined by the dimensions and connectivity of their constituent strut elements, which are connected at specific nodes. These structures behave like homogenised meta-materials when considered at the overall structural level. [6]

3.1 Features

In order to design and develop a novel lattice structure, some common features identified among different biomimetic structures, thought for energy absorption applications, were chosen and mixed. Instead of creating a cell by connecting the classical struts, some interesting features or factors were identified and novel units were generated. All the considered elements were analysed according to their resistance to different types of loads (tension, compression, bending or torsion). Five main features were identified: nodes, tapered tubes, ribs, sinusoidal structure and structural hierarchy.

3.1.1 Nodes, bulkheads, or diaphragms

Bamboo is a giant woody grass composed of hollow culms, separated by solid diaphragms along its length [19]; the nodes are characterised by an internal diaphragm and an external ridge. (**Figure 28**) Therefore, its shape could be schematised as a tubular column with periodic nodes.

The diaphragm is a fundamental feature of the bamboo because it enhances both the bending and compressive strength: it raises the transverse tensile strength of bamboo and prevents the bamboo from expanding and splitting.

More in general, studies have confirmed that bamboo has some property of excellent tensile, compressive and bending strength. [20]

In fact, bamboo, such as many kinds of plants (reed, straw, cattail, horsetail grass) are of high slenderness ratio, but are able to effectively withstand the severe environmental loads

such as gravity, wind and snow pressure, attributable to the growth of sophisticated hollow tubular structures. Moreover, the hollow cylindrical shape of culm and relative uniformly distributed bamboo nodes give bamboo superior structural stability [21]. Also, due to its low density, bamboo has a higher stiffness-mass ratio than some metallic materials such as steel and aluminium. [20]

Zou et al. experimentally studied the mechanical parameters of bamboo under dynamic loading. Therefore, the parameters were extracted from the bamboo structure, and a novel bionic tube for energy absorption application was designed in order to understand the behaviour of the structure under axial and lateral loading.

Figure 28 Anathomy of a bamboo culm [79]

The results of dynamic tests showed that the energy absorption ability of bamboo was affected not only by vascular bundles and density of bamboo, but also from the nodes.

Generally, to resist deformation, single cell tubes are weaker in the lateral than axial direction; hence, it was designed a bionic node as a reinforcement rib for a thin-walled structure. The considered material for the thin-walled structure was Aluminium alloy 2A12.

The numerical results indicated that the bionic structure effectively improved the total energy absorbed and SEA; however, the bionic design also increased the initial peak load.

The topology of the bionic structure was too complex to manufacture, and the identified solution was the possibility to use 3D printing technology in future. [20]

Another structure with nodes or bulkhead was investigated; the cross section of the tube was defined as non-convex multi-corner. The energy absorption of the structure has been investigated numerically; a progressive deformation mode has been achieved and the structure showed a higher energy absorption than a similar column without the bulkheads. The nodes themselves absorb little energy, but their presence allow to change the deformation mode from an expansion-contraction mode to a progressive mode. [22]

3.1.2 Tapered tubes

According to various research, tapered tubes have been found preferable to straight tubes since they are capable of withstanding oblique impact loads as effectively as axial loads. Qi et al. investigated thin-walled square tubes with two types of geometries (straight and tapered) and two kinds of cross-sections (single-cell and multi-cell), in order to analyse the behaviour of these energy absorbing components under oblique impact loading with a plate velocity of 10 m/s. The numerical results showed that the SEA of multi-cell tubes was higher than that of the single-cell tubes for the complete range of load angle (0°–40°) under investigation. Also, a larger taper angle has to be preferred for both SEA maximization and PCF minimization. [23]

Another example is a novel lotus root filled tube that was thought for novel cars' crash-box. The lotus-inspired unit cell was a tapered tube with hexagonal cross section. Compared with the non-filled structure, the filled tube needed less mass and volume to absorb the same energy. The influence of geometric parameters on crashworthiness performance was also investigated: the results of performance study revealed that the novel filled structure has good energy absorption ability. [24]

By comparing the conical tubes could with straight tubes, the tapered ones could be considered more preferable in terms of energy absorption due to their relatively stable mean load–deflection response and resistance to oblique loading; in addition, conical tubes are less likely failed by global buckling. [25]

3.1.3 Ribs

Bitubal tubes with inner and outer rings connected by ribs exhibited superior energy absorption and load-bearing capacity. This is attributable to interactive effects between the tubes' walls and the ribs, which provide extra resistance to the crushing force: the increasing number of connections makes the structure more stable. [19]

Different types of ribs were analysed among the structures inspired by bamboo, horsetail and beetle forewing. The resistance of the considered structures depended on different features: the cross section (circular, quadrilateral, hexagonal or octagonal) [26], the arrangement in the space of the tubes (singular rings or honeycombs) and the shape (x, o, c) [19] and position of the ribs inside the tubes (on the corners, edges or both of them) [26] [27] [28].

In their research, Xiao et al. designed a horsetail-bionic thin-walled structures in order to investigates their crashworthiness under axial dynamic loading. Six configurations of the structure's cross section with different number of cells were evaluated using finite element simulations; the base material used for the structures was aluminium alloy AlMg0.5F22. The results of the analyses showed that the number of cells has significant effects on the crashworthiness of the structure. The best configuration was the one with 16 ribs; in general, it was demonstrated that all the configurations could be used as energy absorber in vehicle bodies and other engineering applications. [29]

Different thin-walled structures were designed and developed by Fu et al. inspired by bamboo. As already mentioned, bamboo is a giant woody grass composed of hollow culms, separated by solid diaphragms along its length. Inside the

cylindrical culm are longitudinal vascular bundles embedded a series of parenchyma cells. These parenchyma cells of the bamboo are made up by ribs of different shapes, which create critical effect on axial mechanical properties of culms.

Therefore, six cross-sectional configurations were considered for a comparative study: bitubal circular tubes without ribs; ribs with shape "I"; "V"; "X"; "double C"; "O". The ribs were assigned in different thicknesses to ensure the same tube mass. Aluminium alloy 6063T5 was used as the base material to achieve the lightweight of structures. The energy absorption capacity of the tubes with ribs was found to be higher than that of bare bitubal circular tube, which was attributable to the interactive effect between the ribs and tubal walls. The bionic tube with X-shaped rib exhibited the highest SEA value in comparison with other sectional configurations within the same tube mass. [19]

Not only the plants have been an inspiration for thin-walled structures with ribs: the beetle and its forewing were subject of research and study too. In nature, the beetle forewing can resist the impact load represented by droplets of rain or produced by the opponent. Therefore, the bionic thin-walled structure based on the microstructure of beetle forewing may be an excellent energy absorber when subjected to impact loading. Indeed, a group of bionic multi-cell tubes with quadrilateral, hexagonal and octagonal sections were proposed. The structures were constructed by filling the cylindrical tubes into different position of multi-cell tubes.

As results, the general increase of SEA of bionic structures can be attributed to the addition of cylindrical tubes, which required more energy for plastic deformation.

According to the configuration one, no noticeable improvements were showed because cylindrical tubes were simply filled into the gaps of the multi-cell tube, and global buckling occurred. These results demonstrate that the advantage of ribs is based on the interaction between the internal tube and the external one.

In case of the configuration three the cylindrical tubes are connected to three ribs, which results in excessive local stiffness.

Finally, octagonal cross-section was identified as the best cross-section configuration considering the SEA. [26]

3.1.4 Sinusoidal structure

This feature is mainly found in plates or panel. The woodpecker's beak inspired the generation of a hexagonal honeycomb with wave structure; the results of the dynamic compressive tests showed that the high stress is concentrated on the upper part of the core, meanwhile, the lower part experienced a small stress because of the stress wave propagation. [30]

A more complex structure was developed and it was based on peacock mantis shrimp's dactyl club, was composed by a double sinusoidal core placed between two plates to enhance the impact resistance. During the quasistatic crushing load test, the shape of the core makes it easier to induce a larger centralized plastic zone and generate the localization of deformation. Compared with the regular triangular and sinusoidal corrugated core sandwich panels, the novel panels significantly improved the crashworthiness and reduced the initial peak force. Besides, the specific energy absorption of the double-sine corrugated sandwich structure was proved to be strongly dependent on the wave number, wave amplitude and core layer thickness. [31]
Both of the tested sandwich panels were made in Aluminium alloys (AA6060 and 1060). [30] [31]

3.1.5 Structural hierarchy

Biological materials, featuring hierarchical microstructures, can exhibit excellent mechanical properties. Sea sponges, for example, are constituted by a hierarchical skeleton with more than six levels, spanning the length scale from nanometres to centimetres. Analogously, diatoms possess silicified cell walls with hierarchical structures from a wide range of scales and a diversity of species, which provides high structural flexibility and toughness. [32]
Therefore, the hierarchical order is a feature that could characterise the arrangement in the space of lattices; various
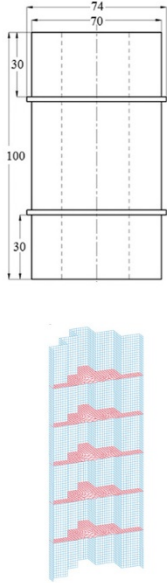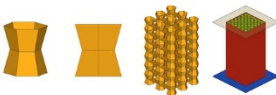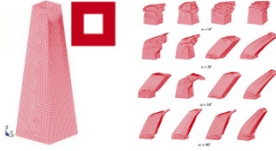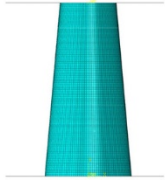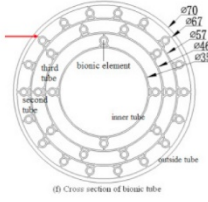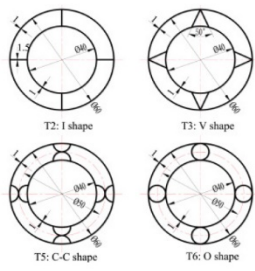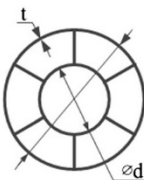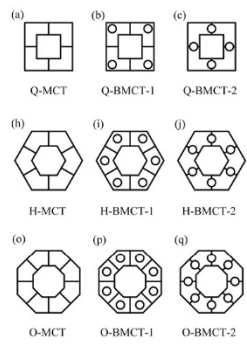
research and structures development have been focused of bamboo and tendons. [33] [34]
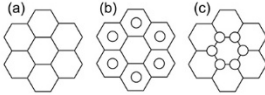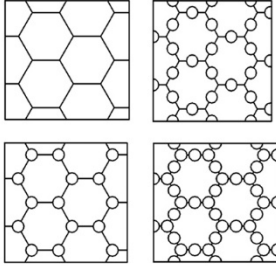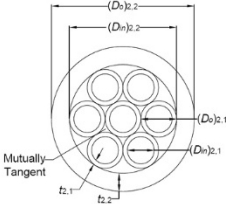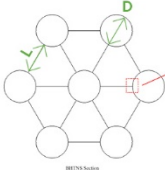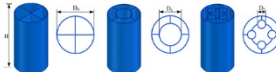
The advantage identified by testing a tendon-inspired structure is that the stress is distributed amongst different levels of hierarchy in higher-order tubular sections, whereas in the case of first-order tubular section, only one level of hierarchy is bearing the total stress. The results indicated that the energy absorption of the lattices increased with hierarchical order. [35]

This way to organize elements in space is also interesting because it could help to tailor mechanical properties of structures. In recent research of Wang et al. bio-inspired lattices were fabricated through selective laser melting techniques. Three types of macroscopic configurations were selected to build up the 2nd order hierarchical lattice materials: an octet-truss unit (fully rigid) an octahedron unit (periodically rigid) and a tetrakaidecahedron (non-rigid). The fully and periodically rigid lattice materials possessed stretch-dominated behaviours, while the former one was generally more efficient than the latter one in terms of stiffness and strength. In contrast, non-rigid materials were bending-dominated, which had much lower rigidity than the rigid ones. In general, the results showed an increase of energy absorption capability with the introduction of hierarchical order in lattices; furthermore, higher hierarchical of lattice indicated higher failure strain. [32]

Further research have been focused on pomelo peel and spider web [36] [37]. More detail could be found on **Table 5**.

Element/feature	Examples and functionalities	Material, process and characteristics of test	Ref.
Nodes/bulkhead/ diaphragms	Bamboo 1. compression and bending (impact loading) 2. compression · The structure of bamboo (made of walls and diaphragms) with vertical and horizontal correlation has good stability, especially as its **nodal diaphragm** raises the **transverse tensile strength** of bamboo and prevents the bamboo from **expanding and splitting**. · Effects: uniform progressive buckling between the diaphragms; superior energy absorption under axial compression. · The energy absorption of the column increases monotonically with the wall thickness. With the increasing thickness, the number of bulkheads to ensure the stable progressive deformation becomes smaller. · The bionic nature of the column prevents the column from undergoing the expansion-contraction deformation mode.	1. Aluminium alloy 2A12 Impact mass: 20 Kg, impact velocity 1): 0 m/s; impact velocity 2): 9.9 m/s 2. Aluminum alloy AA6060 T4 Constant velocity of the rigid plate: 10 m/s	[20] [22]
Tapered tubes 	3. Lotus root · compression (impact loading) Application: novel structure for cars' crash-box · Compared with the non-filled structure, the lotus filled tube needs less mass and volume to absorb the specified energy. 4. Tapered square tubes · compression and bending (oblique impact loading) · Tapered tubes have been found preferable to straight tubes since they are capable of withstanding **oblique impact loads as effectively as axial loads**, and appear to have fewer chances to fail via global bending. 5. Tapered tubes with various cross section · compression and bending (axial and oblique impact loading) · Conical tube is less likely failed by **global buckling** compared with straight tube.	Aluminium alloy AL5182 Impact mass of one filled tube: 200 Kg, impact velocity: 13.8 m/s Aluminum alloy AA6060 T4 Constant velocity of the rigid plate with various α angle: 10 m/s (typically encountered in passenger vehicle crash event) Aluminum alloy AA6061T4 Impact mass: 100 Kg, impact velocity of the rigid plate with various α angle: 10 mm/s	[24] [23] [25]

Element/feature	Examples and functionalities	Material, process and characteristics of test	Ref.
Ribs (f) Cross section of bionic tube	Bamboo 6. compression and bending (impact loading) The ratio of the number of vascular bundles in the three regions was 56:25:12. The bionic elements were distributed with 18, 9 and 4 elements in each layer from the outside to the inside of the tube.	Aluminium alloy 2A12 Impact mass: 20 Kg, impact velocity 1): 0 m/s; impact velocity 2): 9.9 m/s	[20]
Inner and outer rings with connecting ribs T2: I shape T3: V shape T5: C-C shape T6: O shape	7. compression · Bitubal tubes with ribs exhibited superior energy absorption and load-bearing capacity. This is attributable to **interactive effects** between the tubes walls and the ribs, which provide extra resistance to the crushing force. · Ribs with shapes "C" and "O" have a small ratio of diameter to thickness, leading to a global bending mode. · T1, T2, T3, T4: deformed in progressive concertina mode; T5: mixed mode; T6: diamond mode. · Deformation of T3 more stable than T2 (due to ribs shape). · Best result: T4; the **number of corners** of the T4 tube was **more** than that of the other profiles.	Aluminum alloy 6063T5 Constant velocity of the rigid plate: 10 m/s	[19]
	8. Horsetail · compression (impact loading) · Generally speaking, **the more cells of the HBTS**, the higher the SEA and MIF of structure: the tube with 16 cells was found to have the best overall crashworthiness.	Aluminum alloy AlMg0.5F22 Impact mass: 1000 Kg, impact velocity: 15 m/s	[29]
 Q-MCT Q-BMCT-1 Q-BMCT-2 H-MCT H-BMCT-1 H-BMCT-2 O-MCT O-BMCT-1 O-BMCT-2	9. Beetle forewing · compression (impact loading) · The increase in SEA of BMCT structures can be attributed to the **presence of cylindrical tubes**, which required more energy for plastic deformation. · Case 1: No noticeable improvements because cylindrical tubes are simply filled into the gaps of the multi-cell tube, and global buckling occurred · Case 3: the position of cylindrical tubes is too concentrated and they are connected to three ribs, which results in excessive local stiffness. · Octagonal cross-section is the best cross-section configuration considering the SEA; also the middle wall of the outer tube filled with the cylindrical tubes is the best position for achieving higher SEA and lower ULC.	Aluminum alloy AA6060 T4 Impact velocity: 10 m/s	[26]

Element/feature	Examples and functionalities	Material, process and characteristics of test	Ref.
Honeycombs with tubes 	10. compression (impact loading) · The energy absorption efficiencies of BHTS-2 (c) and BHTS-1 (b) are very closed, and obviously both higher than BHS (a) but comparing the SEA and the CFE, the BHTS-2 is the best structure. · The highest energy absorption efficiency was found when the filled column number is 6. · By changing thickness between 0.5 mm and 3.0 mm, the total absorbed energy and energy absorptive effectiveness gradually increase.	Aluminum alloy AA6063 T6 Impact mass: 500 Kg, impact velocity: 10 m/s	[28]
	11. compression (impact loading) · In BHTS-1, each hollow column is connected with two walls on both sides, while the hollow column is connected with three walls in BHTS-2. The increasing number of connections will make the structure more stable. · On average, the energy absorption characteristic of BHTS-3 is slightly better than that of other structures · The growth rate of the absorption energy and crushing force of BHTS is getting slower and slower with the increase of the column diameter.	Aluminum alloy AA6063 T6 Impact mass: 500 Kg, impact velocity: 10 m/s	[27]
Structural hierarchy 	12. Tendon · compression (impact loading) · The energy absorption capability of tubular sections is significantly improved with increasing order of hierarchy · The **stress is distributed** amongst different levels of hierarchy in higher-order tubular sections, whereas in the case of first-order tubular section, only one level of hierarchy is bearing the total stress.	Aluminium alloy 7075-T6 Impact mass: 200 Kg, impact velocity: 20 m/s	[35]
	13. Bamboo · compression (impact loading) · Failure mechanisms exhibited a progressive diamond mode	Aluminum alloy Al 6061-T5; Wire electrical discharge machining (WEDM) Impact mass: 261.1 Kg, impact velocity: 4.4 m/s	[33]
Structural hierarchy; in 2nd order, the internal ribs are replaced with sub-circle 	14. Beetle forewing · compression	Aluminum alloy 6061-O; Wire electrical discharge machining (WEDM) Constant velocity of the rigid plate: 5 mm/min	[34]
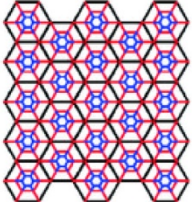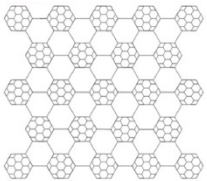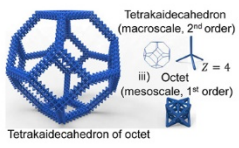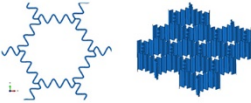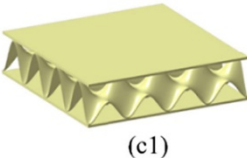
Element/feature	Examples and functionalities	Material, process and characteristics of test	Ref.
Hierarchical honeycomb	15. Spider web · compression (impact loading) · The global response tends to become stiffer because the buckled cell walls of the added hexagons and the original hexagons increasingly contact with each other and provide **additional support** to carry the compressive load, facilitating the energy absorption capacity.	Aluminum alloy 6060 T4; 3d printing Impact mass: 400 Kg, impact velocity: 15 m/s	[37]
	16. Pomelo peel · compression (flatwise/edgewise) · When compared to other typical engineering and natural materials as well as hierarchical structures, it is indicated that pomelo peel inspired honeycombs possess high energy absorption performance and high specific strength.	Aluminum alloy AA3003 H18 Constant velocity of the rigid plate: 15 m/s	[36]
Hierarchical lattice structures	17. compression · Introducing non-rigid lattice configuration in hierarchical lattice material is recommended to achieve **better toughness**, while rigid* lattice configurations for greater **stiffness or strength**.	Polyamide PA 2200 powder (Nylon 12); selective laser sintering method (SLS) Constant strain rate: 10^{-3}/s	[35]
Hexagonal honeycomb with wave structure	18. Woodpecker's beak · compression (flatwise/edgewise) · The high stress was concentrated on the upper part of the core. Meanwhile, the lower part of the experienced a small stress because of the s**tress wave propagation** from the top to the bottom.	Aluminium alloy AA6060 Constant velocity of the rigid plate: 10 m/s	[30]
Double sinusoidal core	19. Mantis shrimp · compression · The DSC sandwich structures can dissipate more energy and have a better energy absorption capacity. · The stress concentration occurred at the top and the bottom of the DSC sandwich panel. · The shape makes it easier to i**nduce a larger centralized plastic zone** and generate the localization of deformation.	Aluminium alloy 1060 Constant velocity of the rigid plate: 2 mm/min	[31]

Table 5 *Review of bio-inspired structure for features definition*

3.2 Unit cells and lattice structures (BLSs)

A unit cell is the base building component of non-stochastic cellular structures. By replicating a specific unit cell in the 3D space, a structure of desired dimensions is created. Due to late advances in additive manufacturing (AM) it has been possible to produce cellular structures with a high level of geometric freedom. Two unit cells were developed after the analysis of different elements; the second one consists in a slight variation of the first one.

3.2.1 Triangulation and closest packing

The first issue with the shape generation of the unit cell was the hypothetical structural arrangement in space of the elements. In fact, the classical lattice structures are composed of struts, which could be organised in space in several alternative ways. [6] With the purpose of generating a novel structure, a detachment from the classic concept of strut-based lattice structures was required, in order to design something completely new. As a result, starting from the organization in space of the cells was necessary not to neglect this fundamental aspect. Therefore, the geometrical rules that underlie the arrangement of elements in nature were observed.

Plato was apparently the first person to attempt a geometrical description of structures in nature. In his *Timaeus* (ca. 360 b.C.) he detailed the generation of regular solids from triangles: the tetrahedron; the octahedron and the icosahedron, in addition he also constructed the cube and the pentagonal dodecahedron, that are not based on the shape of triangle.

The Platonic solids (**Figure 29**) demonstrate how the triangle is the only polygon that is stable (rigid) by virtue of its geometry. This can be demonstrated by the construction of a
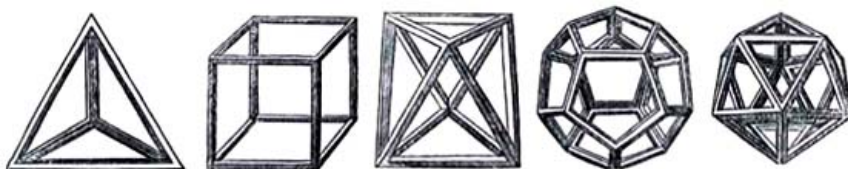
Figure 29 The five Platonic Solids drawn by Leonardo da Vinci [99]

triangular frame joined at its vertices with hingeable connectors; this frame remains rigid, in contrast to polygons of more than three sides, any of which will readily collapse when assembled with hinged joints. Therefore, of the Platonic polyhedra only the tetrahedra, octahedra, and icosahedra are stable by virtue of their geometry. This demonstration has far-reaching significance for the study of structure: triangulation imparts strength to structures even before the physics of materials is considered; it provides a head start to, and a guarantee of, structural rigidity. [38]

The shape of the triangle it is also related to the organisation of elements in space. The closest packing is a structural arrangement of inherent geometric stability that finds expression in the three-dimensional arrangement of polyhedral cells in biological systems as well as in the dense arrangement of spherical atoms in the structure of certain metals. The principle of closest packing is equivalent to that of triangulation, and it is known that triangulated frameworks exhibit inherent geometric stability. Such properties enable framework structures to be built without moment joints, insuring axially loaded members; and this results in high strength-per-weight minimum-energy structures. The principle of closest packing/triangulation is one of remarkable universality. It operates independently of scale or materials, with the same energetically conservative effect. Whether at the molecular level, the cellular level, or at the man-made structural level, its inherent stability always establishes a condition of

Figure 30 Bees' honeycomb [100]

minimum of potential energy. [38]

If a stacking of cylinders of equal diameter is considered, as they are stacked upon each other, their natural tendency is to arrange themselves in a triangular order. The end view of such an arrangement looks like the packing of equal circles. This is simply the arrangement which requires the least effort to maintain: it is a minimum-energy configuration or the minimum-resource state. If circles are tightly packed, as densely as possible, and their centres joined, triangles are formed; when the centres of packed hexagons are joined, an array of triangles also results.

Perhaps the most familiar example of closest packing in nature, and certainly the most sublime, is the honeycomb of the bee. This system, in plan one of regular hexagons, contains the greatest amount of honey with the least amount of beeswax and is the structure which requires the least energy for the bees to construct.

The repeated pattern of triangles is a pervasive geometrical arrangement in the physical world; it can range in scale from structures easily seen with the unaided eye, like the aforementioned bee's honeycomb, the association of cells in tissues or closest packed atoms in certain crystals.

The ubiquitousness of such energy-efficient solutions is important, because the development of a general morphological system rests on the possibility of discovering fundamental relationships among the broadest range of possible structures. [38]

In order to recreate the closest packing principle, the profile that was used for the generation of the original unit cell was
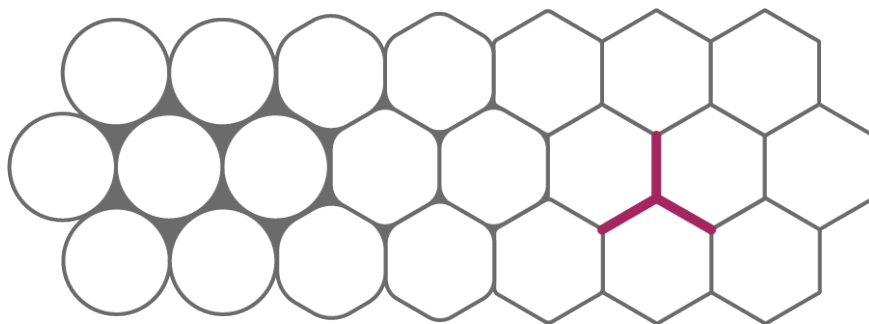
Figure 31 *Closest packing principle and profile generation*

taken from this arrangement in space (the purple profile in **Figure 31**).

3.2.2 Unit cell modelling

The shape generated for the unit cell was modelled with the software SolidWorks 2020, to immediately visualise and eventually change dimensional parameters.

The only dimensional constraint considered was the thickness of each element, which shouldn't have been less than 0.65 mm. The dimensional freedom was fundamental for the generation of a novel structure and certainly is related to additive manufacturing. This typology of process has paved the way to the rapid prototyping of structures whose fabrication would not be convenient via traditional, subtractive manufacturing techniques.

Fused deposition modelling, the most widespread AM technology, can be handled by low-cost 3D printers. This technique resorts to a spool of thermoplastic filament to be melted and extruded through a heated nozzle and, subsequently, deposited in two-dimensional layers that will form a 3D printed object. [6] In term of constraints, since the product body no longer emerges from a mould, design requirements such as draft angles, undercuts and tool access do not apply. Moreover, whilst some restrictions on the minimum size features that can be accurately printed do exist, most of these limitations revolve around how a print should optimally be orientated to reduce support dependency and the likelihood of print failure. This enables to create very complex geometries. Furthermore, cost and time requirements for complex part production are essentially the same as those for simple parts: form simplification stops being an economic requirement. [39]

3.2.3 Unit cell 1

The unit cell has been obtained in three main steps: the generation of the 2D profile on top and bottom view; the generation of the 3D shape with the command loft and finally the addition of

Figure 32 Profile of unit cell

65

circular fillets. The honeycomb, based on the repetition of geometrical shape of the hexagon, follows the principle of triangulation and closest packing; then the shape for the unit cell was extrapolated from this arrangement (**Figure 32**).
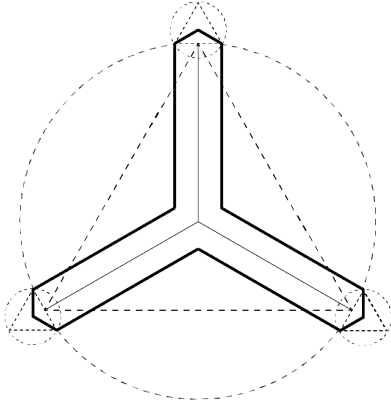
Figure 33 Geometrical construction of the profile based on equilateral triangle's medians

In order to reproduce the honeycomb when packing the unit cells, the geometrical construction of the profile was based on an equilateral triangle inscribed in a circle: the medians of the angles meet in the barycentre of the figure and these three segments are the starting point for the generation of the form (**Figure 33**).
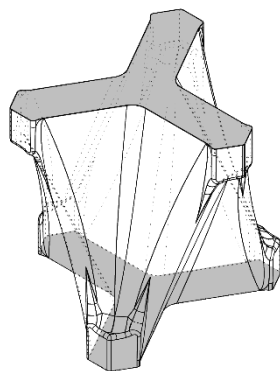
Figure 34 Unit cell 1 top and bottom profiles

For the generation of the cell two planes were created, one on the ground and the other at a distance of 6 mm, that is the height of the single unit (**Figure 34**). On the base the profile was designed and rotated of 60 degrees on the other plane: then, the 3D shape is obtained by using the command "loft", that allows to introduce one of the elements resistant to compression, the nodal diaphragm.

In fact, there is a gradual change of the horizontal cross section of the unit: the loft creates a feature through transitions between the profiles. By selecting two specific points, the transition creates a change in the section: if the cell is cut in half, it can be noticed the shape of a solid hexagram (the third section in **Figure 35**); this element constitutes a thickening of the original profile and represents the nodal diaphragm of the unit cell that, according to

research works, improves the compressive and bending strength of bamboo (**Figure 36**).

Figure 35 Unit cell 1 horizontal cross sections

In order to avoid critical contact point between the cells, an extrusion with constant section was added on the top and bottom profile, to allow for the generation of a honeycomb.

The fillets were added to avoid sharp corners that are not easily printable, and that could also constitute a possible issue for numerical analysis and experimental tests. More dimensional details are given in **Figure 41**.
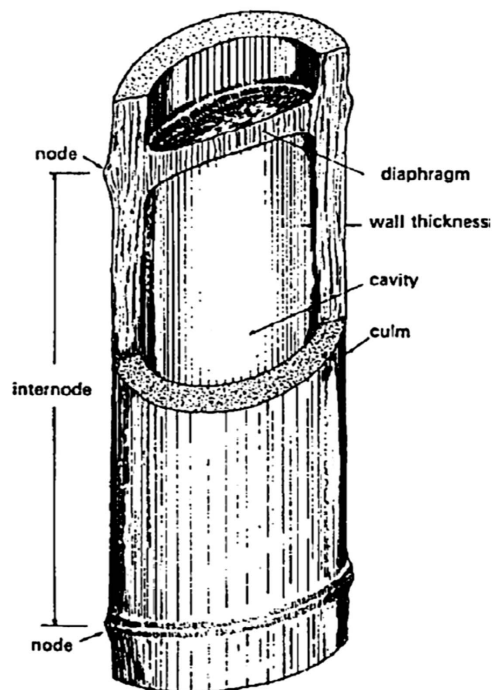
Figure 36 Bamboo culm section [86]

67

3.2.4 Unit cell 2

Figure 37 Burj Khalifa [101]

The second one is a variation of the first unit cell and its profile was also inspired by Burj Khalifa, the skyscraper in Dubai (**Figure 37**). The tower has triangular footprint and tapering form to reduce the effect of the wind and enhance the stability: owing to it super height (~ 830 m), wind is one of the biggest structural design challenges. A buttress core system was used as the major structural system: a strong central core is connected to three building wings. As each wing is buttressed by the other two, the stability of the structure is greatly enhanced (**Figure 38**).

The hexagon-shaped central core plays an essential role in torsional strength of the tower. The support wings give adequate stiffness towards horizontal actions (wind and earthquake): this system is effective for both lateral and gravity load resistance. [21]
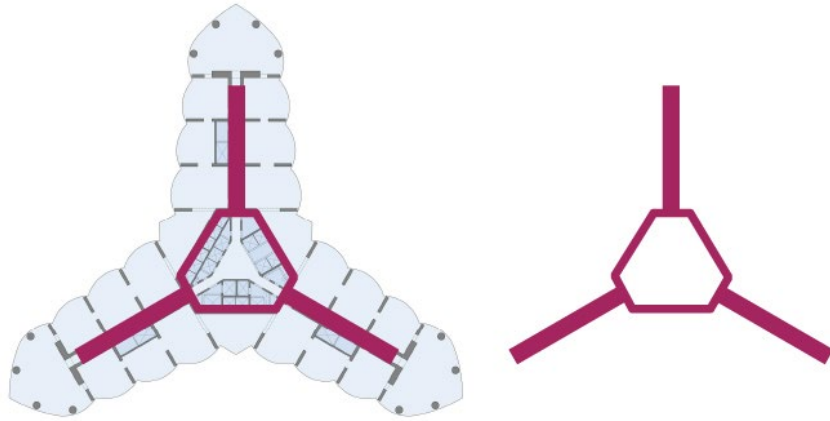
Figure 38 Burj Khalifa buttress core

This shape of the profile could be schematized as a core with three "wings".

As for unit cell 1, the geometry was generated with the "loft" command.

At first, the loft was applied to twist the structure as it is done with the DNA: Zheng et al. demonstrated that its two intertwined helices are decisive to the compression-twisting coupling deformation mode. [40]

But, as it could be observed in unit cell 1, the loft allows to introduce the nodal diaphragm into the unit.
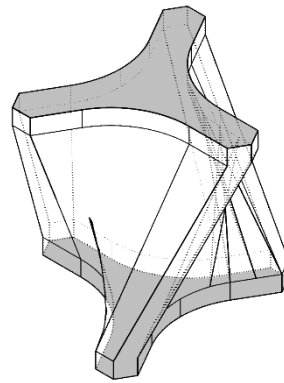
Figure 39 Unit cell 2 top and bottom profile

Also in this case, the height of the unit cell is 6 mm, and by observing the horizontal cross section of the cell (**Figure 40**), it is evident the presence of a solid shape that constitutes the nodal diaphragm inspired by the bamboo.
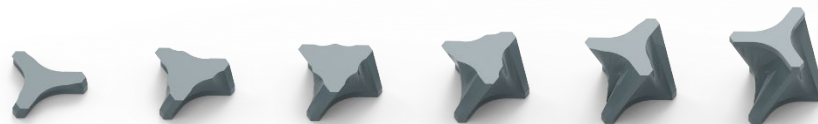
Figure 40 Unit cells 2 horizontal cross sections

Compared to the first unit cell, the unit cell has three wings too, but the bigger core should confer the ability to resist torsion. In **Figure 39** the unit cell 2 is shown.

Note that both of the unit cells' wings are characterised by pointed ends: this shape allows the units to enter in contact. The pointed ends too are geometrically obtained by considering an equilateral triangle and its medians (**Figure 33**).

The most important dimensions of the unit cells are detailed in **Figure 41**, while a recap of features and characteristic is shown in **Table 6**.
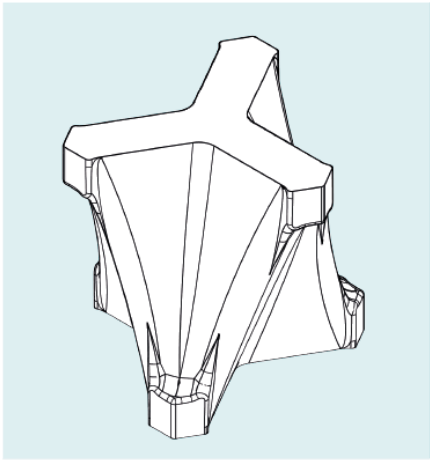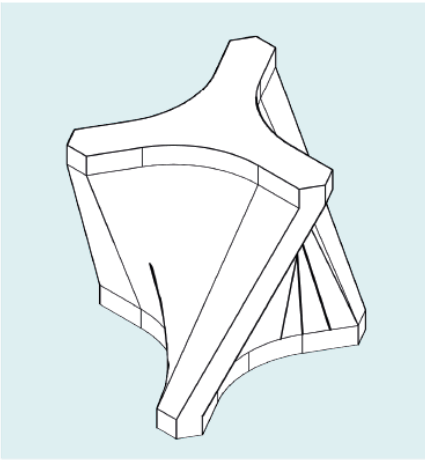
Unit cell 1		Unit cell 2	
Features or elements:	Nodes	Nodes; buttress core	
Inspirations:	Bamboo, honeycombs	Bamboo, Burj Khalifa	
Expected resistance to:	Compression, bending	Compression, bending, torsion	

Table 6 Comparison between unit cells

Unit cell 1

D= 6 mm

H= 6 mm

r_1= 0.5 mm

t_1= 1.2 mm

h_1= 1 mm

Unit cell 2

D= 6 mm

H= 6 mm

r_2= 2.55 mm

t_2= 1 mm

h_2= 0.5 mm
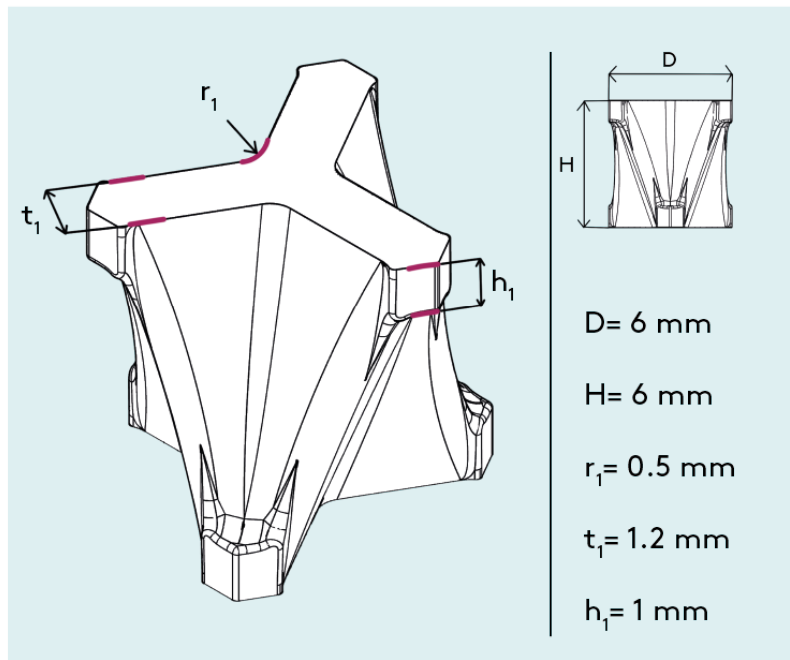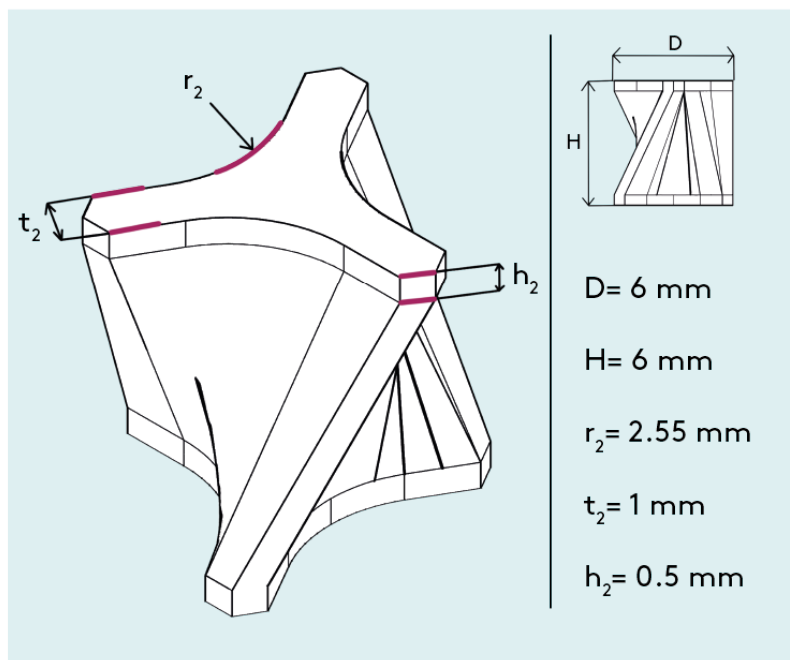
Figure 41 Unit cells dimensions

The final uniform lattice was obtained by assembling five unit cells in each direction to create a cube of side 30 mm; a homogeneous lattice structure consists of unit cells with exactly the same shape periodically distributed in the design space. Thus, this type of lattice structures can be considered as homogeneous materials on a macroscale during the design process. For homogeneous lattice structure, most of research is focusing on its unit cell. In order to achieve the fabricable unit cell, the manufacturing constraints such as the minimum member size can be considered in the optimization procedure of microcell structure. [12]

By modifying design parameters, such as the unit cell size and fillets, the mechanical performance, and so the functionality of the structure can be modified, and the strength-to-weight ratio characteristics could be optimized. [41] For each unit cell, three variations of the original version were considered.
The unit cells 1 and 2 were modified as follows: the height was halved, doubled and the value of fillets was changed (in the first case it was multiplied by 1.5, while in the second it was doubled).
For the first unit cell, the parallel faces of the cube are identical, in order to compare the results after the experimental tests. For the second unit cell, it is not possible to have identical parallel faces, then the model of the specimen was thought to obtain at least two out of three symmetrical pair of faces: the top and bottom view could not be symmetrical, unless the number of cells' row is an even number.

3.2.5 Porosity
Porosity has a great impact on mechanical performance of open-porous lattice structures [42]. In **Table 7** the porosity of each structure is presented.
Porosity is defined as the percentage of void volume in solid material. The structures were 30x30x30 mm with different value of porosity, P, that was calculated according to the following relation:

$$P(\%) = \frac{Vvoid}{Vtot}100 = \frac{Vsolid - Vtot}{Vtot}100 = \left(1 - \frac{Vsolid}{Vtot}\right)100$$

where V_{tot} is the volume of the box enclosing the unit cell, V_{void} is the void volume within the enclosing box and V_{solid} is the volume of the lattices, obtained from CAD models.

BLS 1	1.1.1	1.1.2	1.1.3	1.2.1
Porosity (%)	48	48	48	46

BLS 2	2.1.1	2.1.2	2.1.3	2.2.1
Porosity (%)	57	57	57	55

Table 7 *Porosity of BLSs*

The **Table 8** shows an overview of the BLSs' variations and some information about the structures are given. Note that 1.1.1 and 2.1.1 are the BLSs composed by the original unit cells.
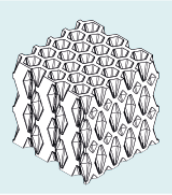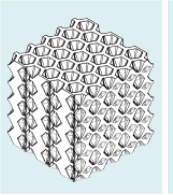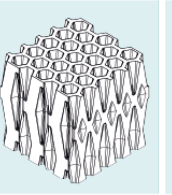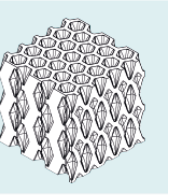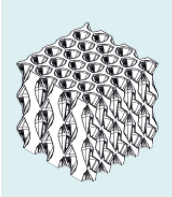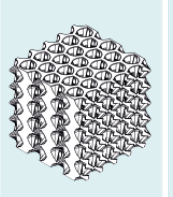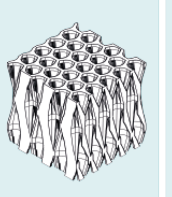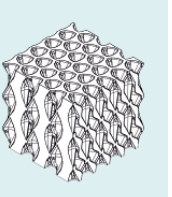
1	1.1.1	1.1.2	1.1.3	1.2.1
Unit cell's height	6 mm	3 mm	12 mm	6 mm
Fillet radius	0.5 mm	0.5 mm	0.5 mm	0.75 mm
Number of layers	5	10	2.5	5
Porosity	48%	48%	48%	46%

2	2.1.1	2.1.2	2.1.3	2.2.1
Unit cell's height	6 mm	3 mm	12 mm	6 mm
Fillet radius	2.5 mm	2.5 mm	2.5 mm	5 mm
Number of layers	5	10	2.5	5
Porosity	57%	57%	57%	55%
Analyses' focus	Possibility to investigate dimensional variations' effects on the compressive resistance of the lattice structures			To investigate the effects of radius fillets at connection points among cells

Table 8 BLSs variations and porosity

3.3 3D printed structures

In **Figure 42**, **Figure 43** and **Figure 44** it is possible to see all the 3D printed specimens of the lattice structures.

Figure 42 BLSs 1 and BLSs 2

Figure 43 3D printed bio-inspired lattice structures

The specimens were printed at the Department of Mechanical and Industrial Engineering of NTNU. The 3D printer used was the Original Prusa i3 MK3 [43], while the manufactory for PLA filament is 3D Net; the diameter of the black filament used was 1.75 mm. [44]

The tensile properties, later considered for the numerical analyses, have been determined from tensile tests carried out at NTNU: standard ASTM D638 Type II specimens made in PLA with 3 mm thickness were used for testing.
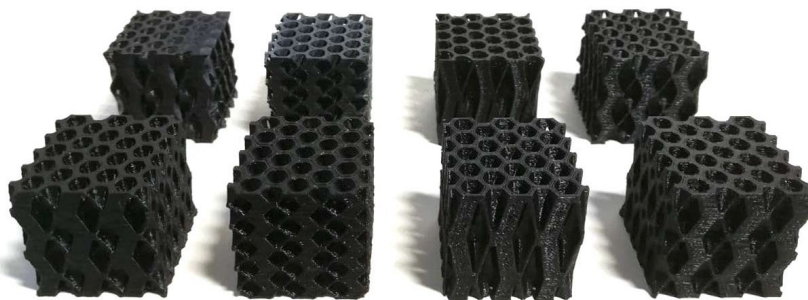
Figure 44 3D printed bio-inspired lattice structures

The machine used for testing was the MTS Criterion model C42 electromechanical load frame with maximum load limit of 5kN [45].
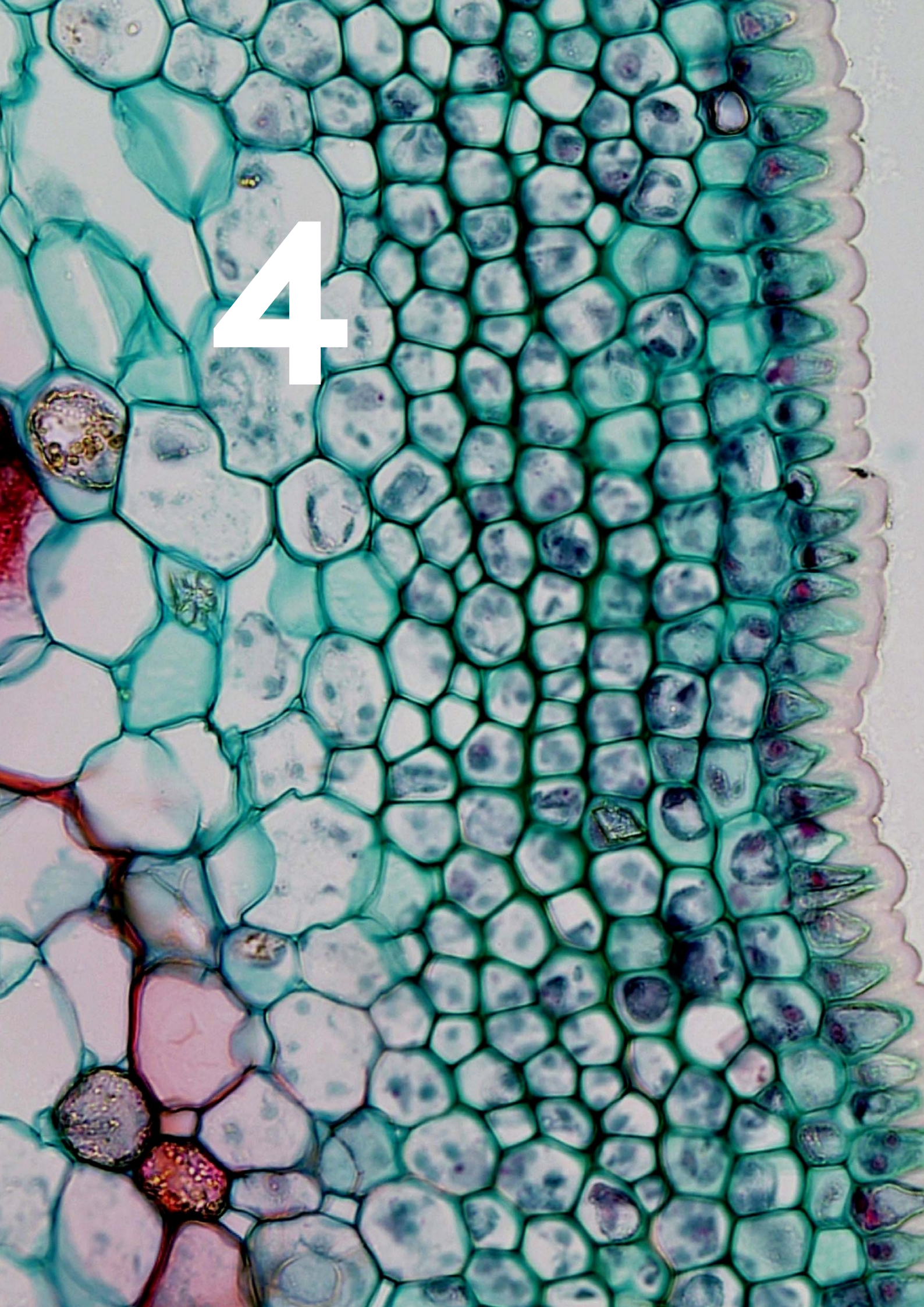
4 Materials and methods

Late advances in additive manufacturing have contributed to the possibility to produce lattice structures with almost complete geometric freedom, and so to the deepening of knowledge regarding these types of structures. However, there is still a lot to be understood: finite element analysis allows to investigate the mechanical behaviour at reduced costs and provides guidance for structural optimization. Hereafter the samples were tested under compressive test and then a finite size solid finite element model is developed to predict the mechanical properties of BLSs, then it is validated through comparison with experimental data.

4.1 Experimental tests

The experimental tests were carried out on all the typology of the lattice structures: overall, the 3D printed specimens were 49. For each BLS, at least three tests were carried out in order
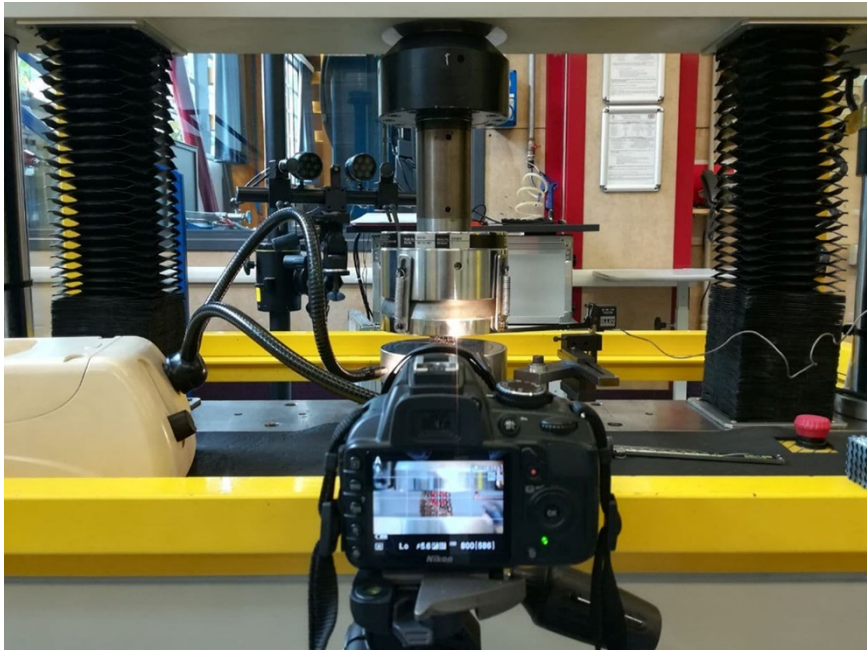
Figure 46 *Experimental test setting*

to understand if, for each experimental test, the behaviour of the structure was repeatable.

All the structures were tested at Material Testing laboratory at Department of Mechanical Engineering of Politecnico di Milano.

4.1.1 Characteristics of the tests

For the conducted tests carried out at Politecnico di Milano, the machine used was an electromechanical machine, the MTS Alliance RF150 System with maximum load limit of 150 kN **Figure 46**). [46]

The testing campaign was performed following the standards for compression ISO 604 [47]. The displacement rate was set as 2 mm/min and the structure was compressed of the 50%, with a displacement of 15 mm. An extensometer was used to measure the actual displacement on the samples during the test.

4.2 Numerical model

Finite element analysis allows to investigate the mechanical behaviour of lattice structures at reduced costs, validated through comparison with experimental tests made on the lattice structures. A finite size solid finite element model is developed to predict the mechanical properties and deformation mechanisms of BLSs.

The 3D finite element explicit model was developed by means of the commercial software package ABAQUS/explicit. A lattice structure based on the unit 2.1.3, having approximately 43% material volume fraction (or 57% porosity) was used for the model validation. Two analytical rigid shells were created to replicate the upper and lower compression plates of a testing machine. A reference point located at their centre was used to define the boundary conditions: all the degrees of freedom were blocked in the lower plate by using the command encastre, while the upper one was only allowed to have a displacement in the vertical direction to compress the structure by 7% of its initial height, in order to reach the Yield stress.

In order to define the boundary conditions directly on the reference point, the "rigid body" constraint was used: a rigid body is a collection of nodes, elements, and/or surfaces whose motion is governed by the motion of a single node. The relative positions of the nodes and elements that are part of the rigid body remain constant throughout a simulation. [48] The upper and lower plates were respectively connected to RP-2 and RP-1 by using this command. Then, RP-2 was used to extract the displacement and reaction force from the structure, which is converted into the corresponding stress-strain curve.

After different attempts (made with different typology and dimension of mesh, velocities and BLSs) it was decided to remove the rigid shells, since its use generated too many distorted elements that led to aborted analyses.
Therefore, it was created a coupling constraint between the RP-1 and RP-2 and the last and first level of voxels of the BLS, in order to apply the previously mentioned boundary conditions.

4.2.1 Material properties

To characterise the deformation behaviour of a material when a load is applied, the most conventional way is to conduct a tensile test on cylindrical or flat specimens made of the material. Most engineering materials show and elastic deformation stage when the applied tensile force is relatively small. The behaviour of the material in its linear elastic stage is characterised by two material constants: Young's Modulus E and Poisson's ratio υ. The first one represents the constant slope of the stress-strain curve in the elastic stage, while the second stands for the ratio of the negative strain in the transverse direction to the longitudinal tensile strain.
For metals and polymers, when the applied load reaches a certain value, the material will yield. This implies a deviation from the linear stress-strain path, and it marks the onset of non-recoverable plastic deformation. For most of the materials, the required stress increases, and the deformation continues: this phenomenon is called strain-hardening. The plastic deformation stage will end when the specimen is

eventually broken under tension: before fracture happens, the stress will reach a maximum, the ultimate stress (UTS); while when fracture occurs the corresponding fracture strain is ε_f. These two quantities represent respectively strength and ductility of the material in tension. [1]

To establish theoretical models in order to analyse the energy-absorption capacity of structures and materials, the materials' mechanical behaviour should be idealised, in order to express the stress-strain relationship by simple analytical functions. When the deformation (strain) is small, a linear elastic
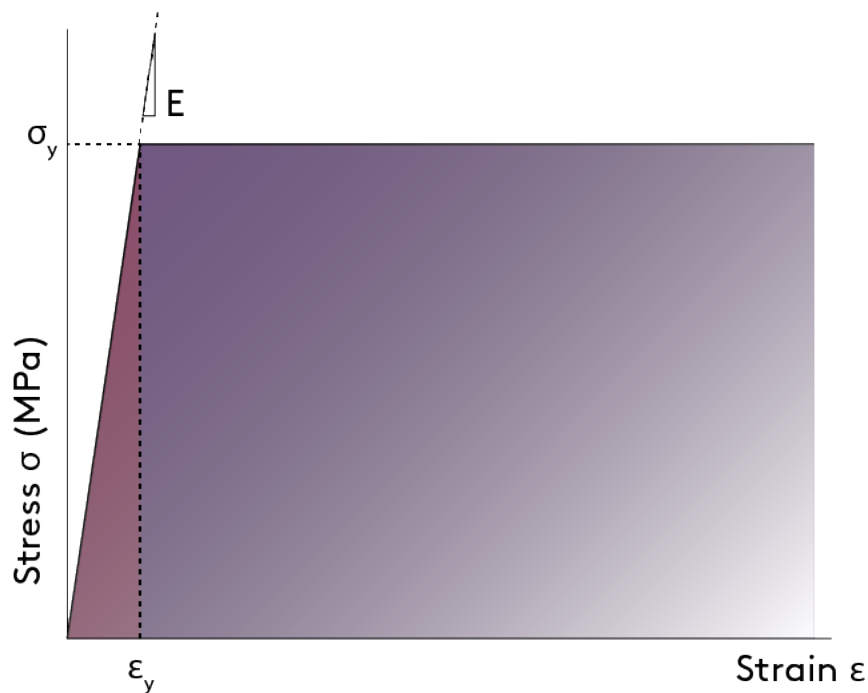
Figure 47 *Elastic-perfectly plastic stress strain curve*

material model can be adopted, while Young's modulus and Poisson's ratio are considered as two material parameters. After the yielding stage, if the strain-hardening is insignificant, then the elastic - perfectly plastic material model can be adopted: this means that the strain-hardening is negligible and so the material will continue to deform plastically from the initial yielding till fracture, whilst the stress remains σ_y [1]. The stress-strain curve of an elastic-perfectly plastic material is shown in **Figure 47**.

Initially, an elasto-plastic material model was assigned to the structure based on the information found on the Granta Edupack 2021 database, and a density of 1.3 g/cm^3 was assigned.

Then, after the tensile tests, the obtained values were considered for the analysis: the elastic modulus was set to 3120 MPa and Poisson ratio to 0.36.

The tensile properties, considered for the numerical analyses, have been determined from tensile tests carried out at NTNU: standard ASTM D638 Type II specimens made in PLA with 3 mm thickness were used for testing. The machine used for testing was the MTS Criterion model C42 electromechanical load frame with maximum load limit of 5 kN.

The tensile properties determined from the tensile tests are collected in **Table 9**.

In order to define the elastic-perfectly plastic material model, the Yield strength σ_y and the corresponding elongation EL were inserted in the section Plasticity in Abaqus: the focus of these analyses was the elastic stage and the characteristic values related to this aspect.

Property	Results
UTS (MPa)	56.83 ± 0.49
σy (MPa)	52.53 ± 0.65
%EL	2.62 ± 0.06
Poisson's ratio	0.36 ± 0.02
E (GPa)	3.12 ± 0.05

Table 9 PLA tensile properties

4.2.2 Contact interaction

There are two algorithms provided in Abaqus/explicit to model contact interactions: the contact pair algorithm and the general contact algorithm [48]. Among the two, the general contact algorithm was chosen because does not generate any limitations in domain decomposition for domain level parallelization, since parallel execution was implemented to

reduce computational time due to large number of increments, nodes, and elements.

Three sets of surfaces were involved in this interaction: the lower, the upper plate and a mesh surface consisting of all the element faces and edges of the lattice structure model.

The general contact pairs selected were three: the first one simulating the contact between lower plate and the lattice structure, another between the upper plate and again the lattice, and for the last one, it was imposed the contact between the lattice structure and itself. The contact properties were set with the penalty method taken as tangential behaviour with a coefficient of friction of 0.2.

4.2.3 Mesh

The models were meshed taking into consideration the geometry and the dimensions of the cells. At first, the software used was ABAQUS CAE. The command "mesh control" allows to choose the element shape and, considering the geometrical characteristics of the unit cell, the tetrahedral mesh typology was applied on the model with approximate global size of 0.5. The quality of the mesh was verified, and no errors were detected by the software. Different analyses were carried out with various mesh sizes; however, the computational time required was too high and the analyses were aborted by the software.

Then, instead of considering a whole lattice cube, whose dimensions are 30x30x30 mm, the analyses were carried out on a smaller cube (15x15x15 mm) and also on a single unit cell, in order to reduce the computational time: however, the results were not acceptable.

To solve this problem, the HyperMesh 2019 software was used to generate the mesh of the lattices. HyperMesh is a finite element pre-processor that prepares models, starting from imported CAD geometry to export an analysis run. The pre-processor provides several methods of generating a tetrahedral mesh, according to the features of the models.

The standard method creates tetras from an enclosed volume (bounded by a shell mesh, tria and/or quad elements). Two options are available to control the mesh:

- proximity, that creates smaller elements next to small features to make a smooth transition from small to large elements
- curvature, that will place more elements along curved surfaces based on user specified settings.

Both options were selected since the geometry of the unit cell is rich of details and fillets; but the computational time was too high.

Then, *shrink wrap* meshing was used to generate the mesh (**Figure 48**). This method creates a simplified mesh of a complex model: the model's size, mass, and general shape remains, but the surface features and details are simplified, which can result in faster analysis computation. However, the level of detail can be determined by modifying the mesh size to use and other parameters. [49] Since the STEP models have a very large size and they are rich of details too, this method was used to mesh the geometries and to find a compromise between the accuracy and computational cost.
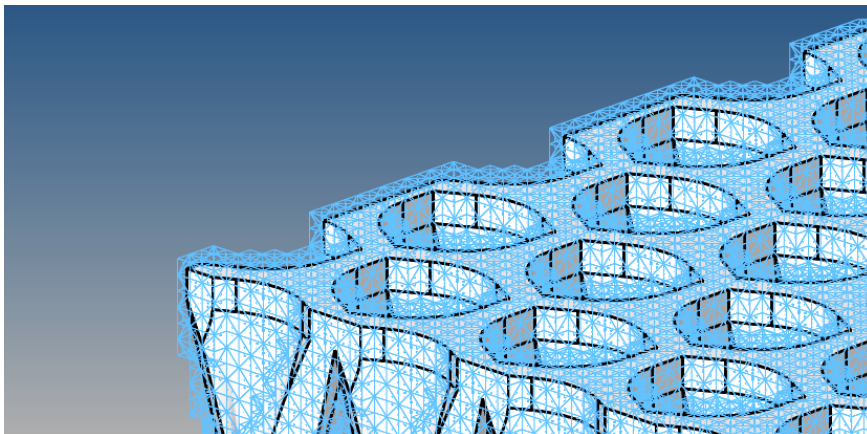
Figure 48 BLS 2.1.3 meshed with shrink wrap

Shrink wrap meshing method automatically select the element type of first order, then the element C3D4 was considered. As results of different analyses, it was evident that the typology of element was not ideal, according to the numerical data obtained by the test. In **Figure 49** it is possible to observe the different trend of various numerical tests, conducted with C3D4 element and different mesh size, compared to the results of the experimental test.
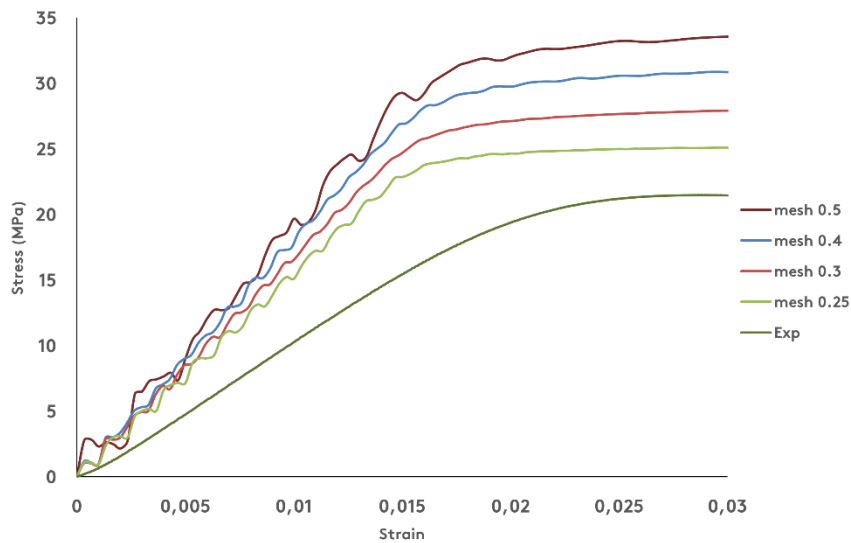
Figure 49 *BLS 2.1.3 with different mesh dimensions*

Hypermesh allows to change elements' order: therefore, the quadratic element C3D10M was considered. The modified version of C3D10 was used because of the Explicit model of the numerical tests.

Shrink wrap mesh allow to define the size of the element but also a fundamental quality parameter, the minimum tet collapse. The results with quadratic element and linear element (both with mesh size 0.4 and min tet collapse=1) showed very similar results (**Figure 50**). Then, the value of min tet collapse was reduced in order to improve the quality of the
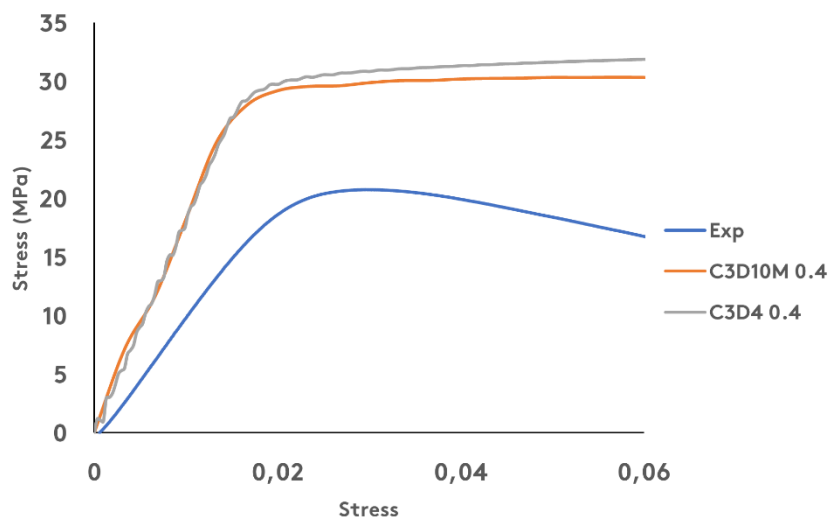
Figure 50 *Comparison of stress-strain curves among experimental test and numerical tests (with linear and quadratic elements)*

86

mesh. Note that the decrease of min tet collapse value led to an increasing of computational time.

4.2.4 Computational time reduction

One crucial factor in performing a finite element simulation is the computational time. In the case of ABAQUS/Explicit, it is directly dependent on both size and number of elements, as well as the time period simulated. The simulations are based on quasi-static compression of the lattices at a deformation rate of 2 mm/min. If the numerical analyses were to be carried out up to the 30% compression of the structures at the actual deformation rate, it would be necessary to set up a simulation time of 270 seconds; this run time is unfeasible since it would require extremely high computational times to be completed. Thus, a time reduction method had to be considered and there are two different possibilities: it could be applied time or mass scaling. The first one speed up the analysis as opposed to the event's natural time scale; this approach can be used only when rate-dependent material properties are not used since the increase in loading rate could trigger unwanted effects on the results: it could introduce undesirable kinetic effects, like increased inertia forces that may change the outcome of the simulation.

The second approach is mass scaling, that increases the stable time increment of the analysis by increasing the density of the material, this decreases the wave speed propagation through the elements and make the simulation run faster. Rate-dependent parameters are not influenced by this option; however, it is necessary not to apply excessive mass scaling because it could lead to inertial effects and then erroneous solutions. Hence, it was opted to apply time scaling to reduce computational time. To make sure the increase in loading rate did not affect the results, two aspects were considered:

- The kinetic energy was monitored to make sure it did not exceed 10% of the internal energy throughout most of the process.
- The compressive force-displacement had to be independent from the applied velocity. [48]

In **Figure 52** an example of energy-time graph is represented in order to monitor the internal energy and the kinetic energy during the numerical analysis.

Many attempts were made before using the shrink wrap meshing method; values of 0,1 m/s, 0,2 m/s, 0,4 m/s, 0,8 m/s, 1m/s, 2 m/s, 6 m/s were implemented while keeping the real density of the material. Since the model's mesh was not correct, the results were also influenced and the analyses aborted with error messages: "the ratio of deformation speed to wave speed exceeds 1.0000 in at least one element"; "the analysis may need a large number of increments (more than 20,000,000), and it may be affected by round-off errors".
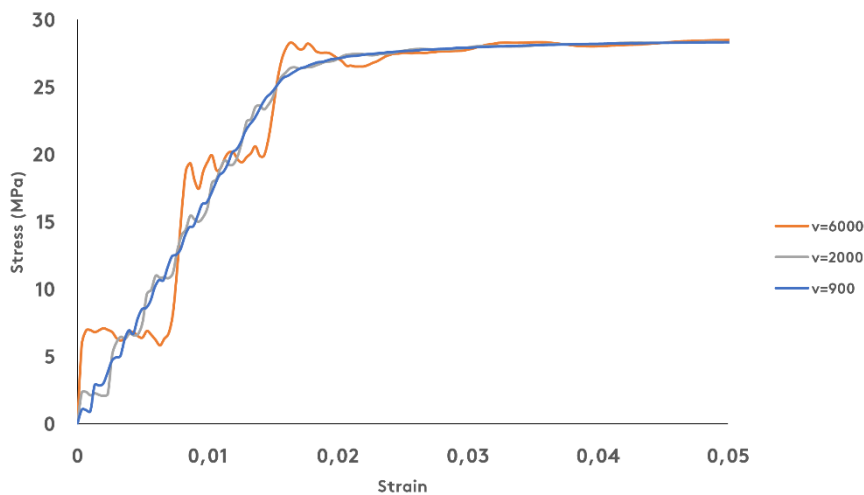
Figure 51 BLS 2.1.3, with mesh size 0.3 with different velocity

Once the model's mesh was corrected, analyses with values of 6 m/s, 2 m/s and 0,9 m/s were carried out in order to investigates if the resulted values of Young's Modulus were influenced by the velocity of the plate (**Figure 51**). It was evident that E is not related to this parameter, but in order to obtain the curve with a regular trend, a lower value of velocity was chosen for the analyses. Therefore, it was decided to consider a velocity of 2 m/s.
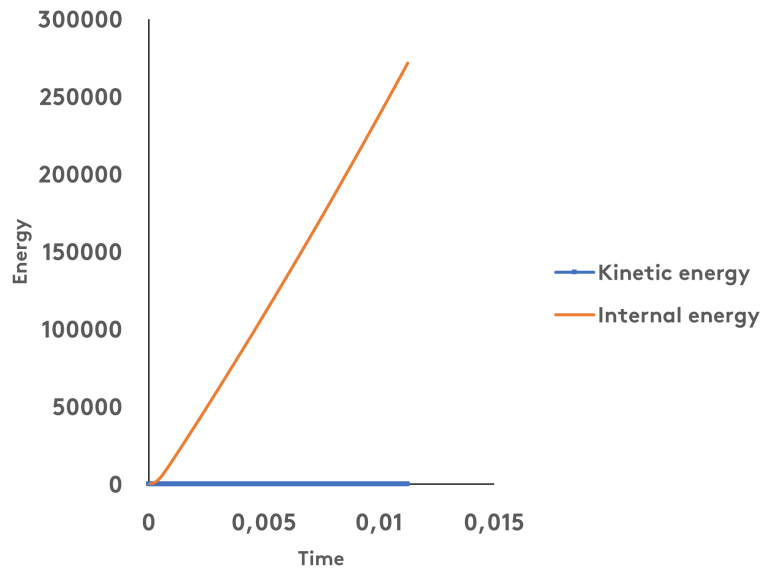
Figure 52 *Comparison between kinetic energy and internal energy*

4.3 Model validation

Mechanical properties

The elastic modulus was obtained as the slope of the straight line given by linear fitting of data points within the linear deformation region at the beginning of the compressive stress-strain curve. The yield stress was computed as the intersection between the compressive stress-strain curve and the 0.2 % offset line parallel to the elastic region.

Mesh convergence analysis

At first, the BLSs were meshed taking into consideration two important factors. Given the morphological properties of the unit cell, the element size could not be reduced too much because it would highly increase the total number of elements in the model, and consequently the computational time. Additionally, this would also increase the analysis time for BLSs with lower porosity. After the convergence analysis, the mesh size was set as 0.25, while the min tet collapse considered was 0.2, in order to find a compromise between computational costs and accuracy of results.

The constant velocity applied as boundary condition to the RP-2 was higher than the natural time period of the quasi-static
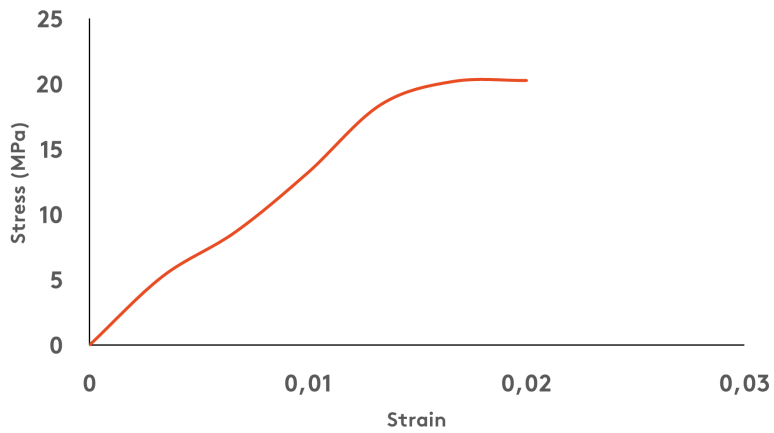
Figure 53 2.1.3 numerical results

process, which was 2 mm/min. Then, a value of 2 m/s was applied. In **Figure 53** and **Figure 56** the results of numerical analyses are represented, while in **Figure 54** a comparison of the stress-strain curve of numerical and experimental test is shown. In **Table 10** a recap of the mechanical properties is shown.

In **Figure 55** it is possible to observe where the structure is affected by higher level of stress: the contact points among the cells result to be the most critical point of the structure. This stress distribution is confirmed by the experimental test: the
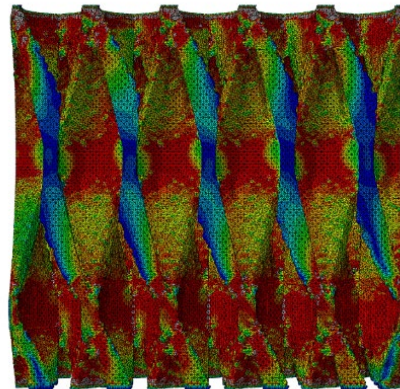
Figure 55 Stress distribution
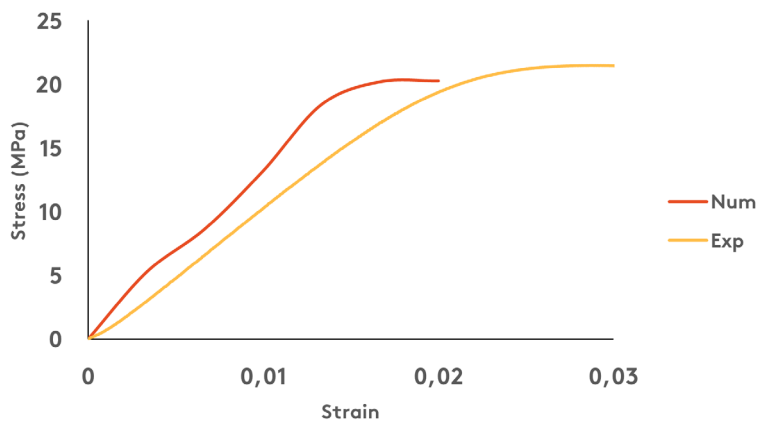
Figure 54 Comparison between numerical and experimental results of BLS 2.1.3

cracks in fact appear among the cells.

The numerical value of Young's modulus results to be 20% higher than the highest experimental results (1040 MPa). The discrepancy between these two values is acceptable and it is due to the anisotropy and the internal defects of the specimens (both related to the manufacturing process).
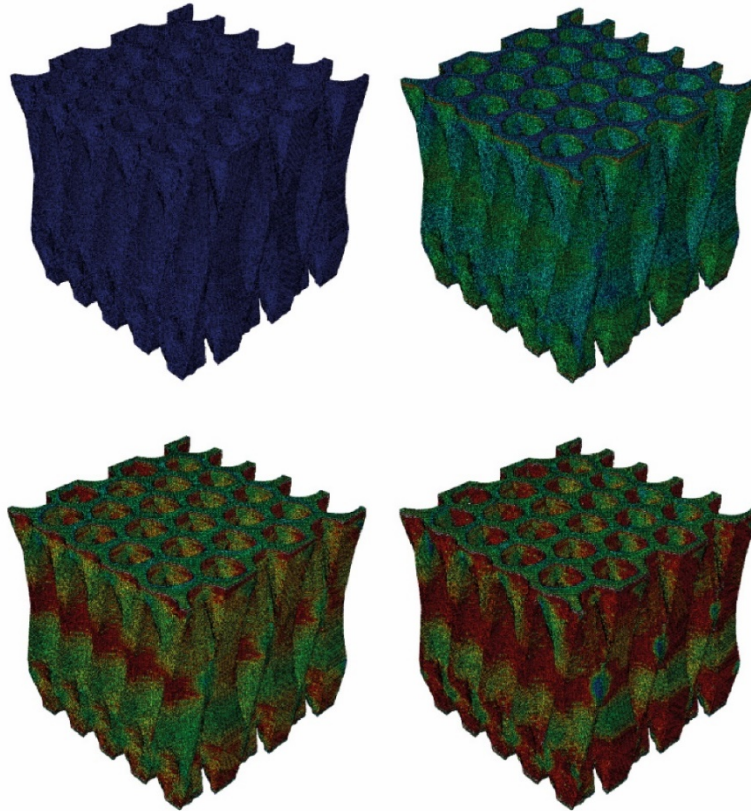
Figure 56 2.1.3 Von Mises at different strain (from strain 0 to strain 0.02)

2.1.3	NUM	EXP
Young's Modulus (MPa)	1240	989.3±51
σy (MPa)	21.5	19±1
εy	0.018	0.02±0

Table 10 Comparison of mechanical properties
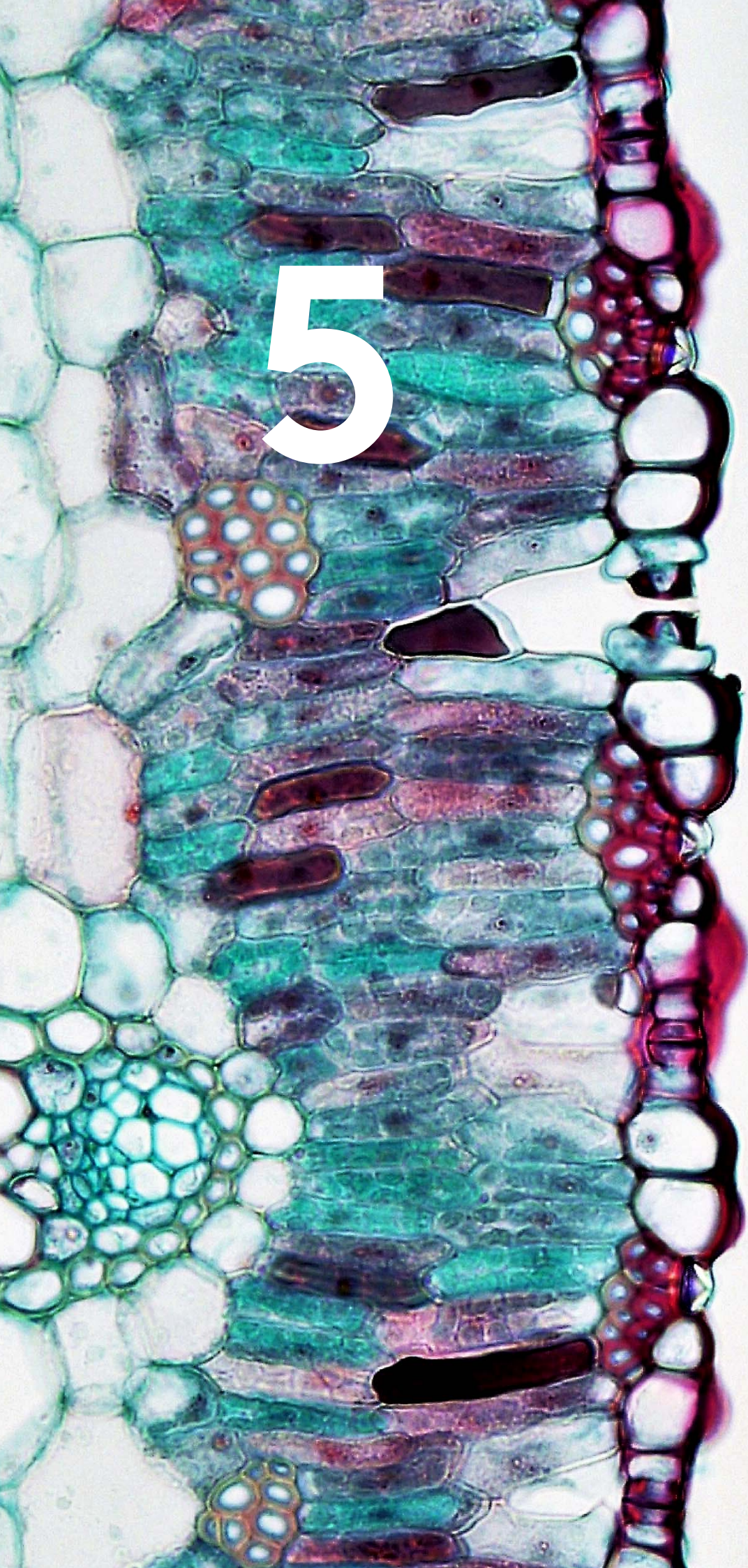
5 Results

The numerical analyses' results allowed to obtain comparable values only for the elastic stages, according to the applied setting. Then, the values of Young's Modulus and Yield strength were calculated through the analysis of the stress-strain curves.

After the experimental tests were carried out, the three main stages of the stress-strain curve were identified (elastic, plastic, densification stage); therefore, for each test, the values of Young's Modulus, Yield strength, IPCF (Initial peak of crushing force), the densification strain and the EA (Energy absorption) were calculated or extracted by the graphs.

5.1 Numerical results

As it was discussed in chapter 4.2.1, the material properties of the explicit model were set in order to obtain an elastic-perfectly plastic material. This means that the strain-hardening is negligible and so the material will continue to
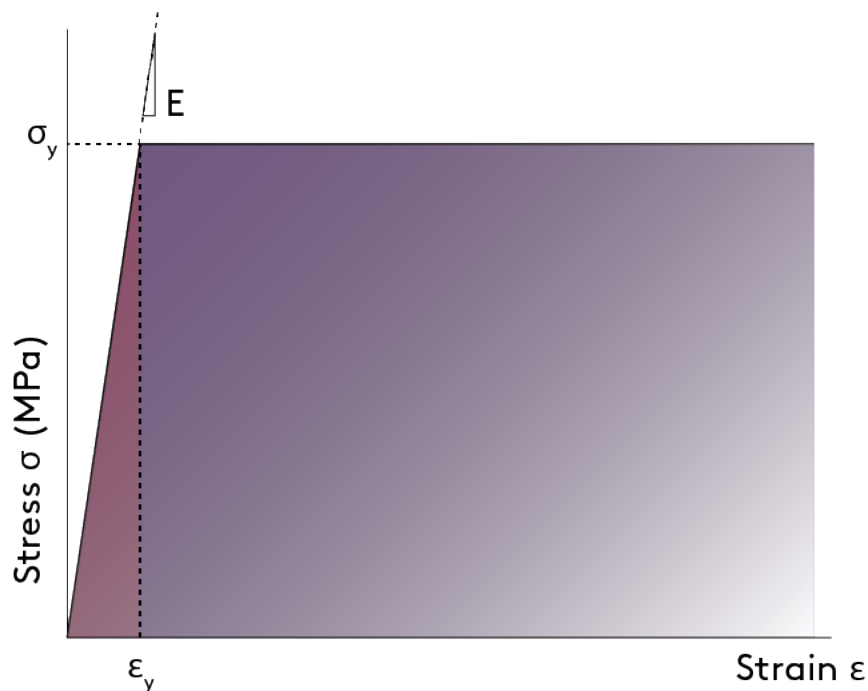
Figure 58 *Elastic-perfectly plastic stress strain curve*

deform plastically from the initial yielding till fracture, whilst the stress remains σ_y. (**Figure 58**) [1].

Therefore, in order to analyse the results of the numerical tests, the elastic stage was considered, and then the comparable parameters are Young's modulus and the Yield strength.
The elastic modulus was obtained as the slope of the straight line given by linear fitting of data points within the linear deformation region at the beginning of the compressive stress-strain curve (strain range of 0-0.02). The yield stress was computed as the intersection between the compressive stress-strain curve and the 0.2% offset line parallel to the elastic region (**Figure 59**).
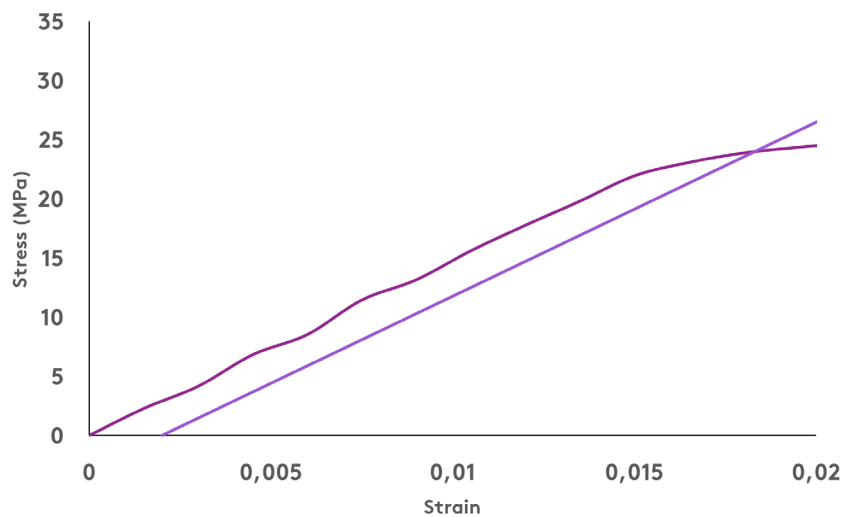
***Figure 59** Calculation of Yield stress with 0.2% offset method*

1.1.1
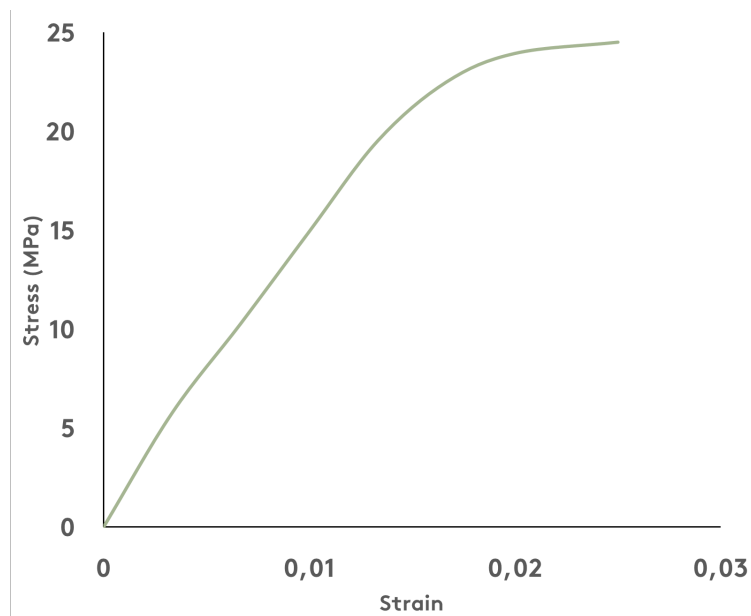
Figure 60 *1.1.1 stress-strain curve (numerical results)*

The elastic stage of the stress-strain curve ends at a strain of 0.019. The value of Yield stress is around 24 MPa. The Young's modulus, that characterise the trend of the linear stage is 1280 MPa. In **Figure 63** the stress-strain curve of the numerical test, while in **Figure 65** a representation of the test at different strains.

As it is possible to see from the numerical model, the contact points among the unit cells are affected by stress.
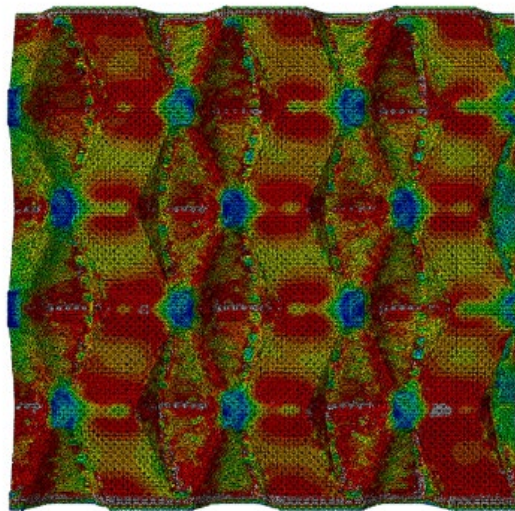
Figure 61 *Stress concentration at connection point of BLS 1.1.1*
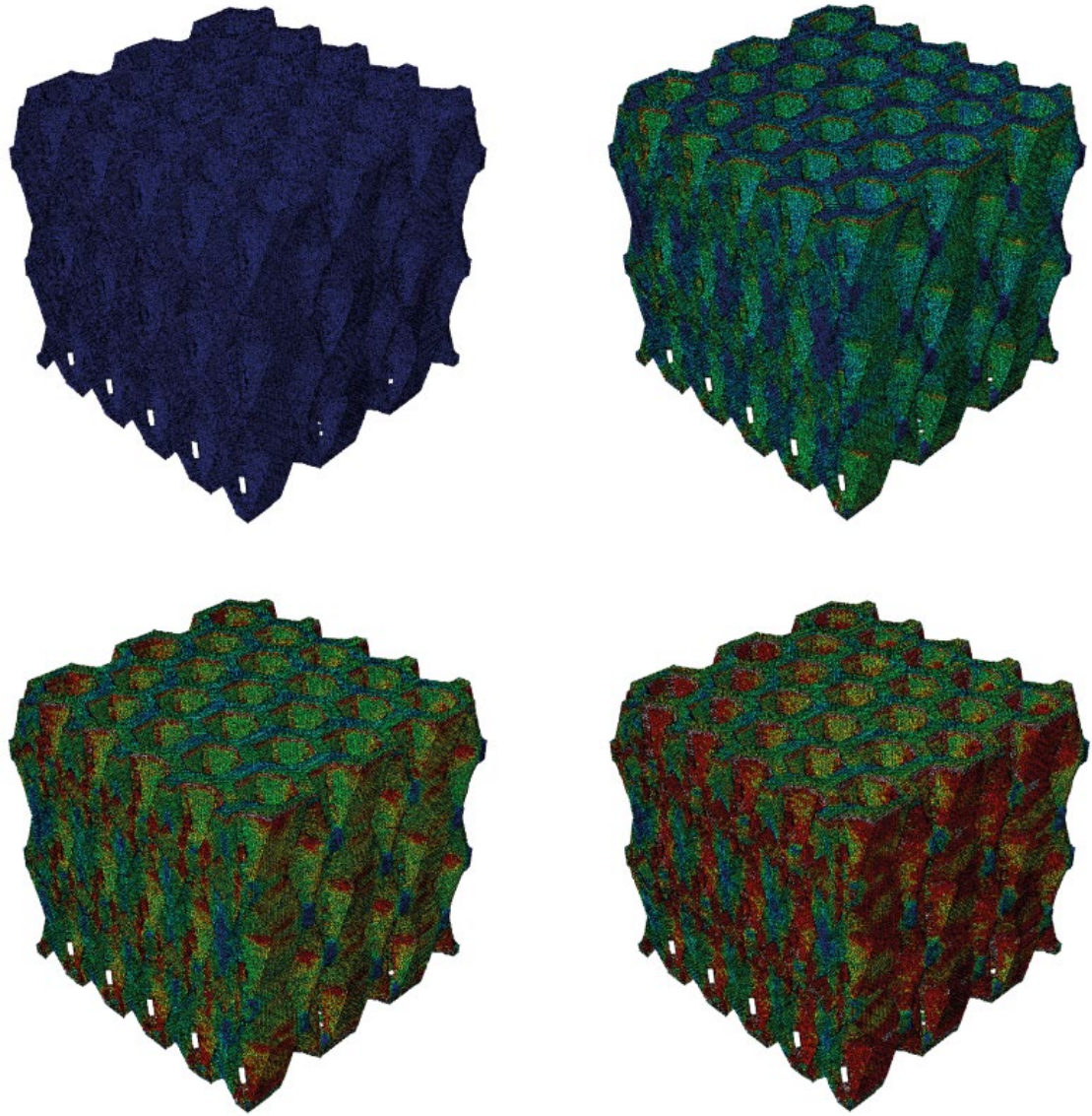
Figure 62 *1.1.1 Von Mises at different strain (from strain 0 to strain 0.02)*

2.1.1
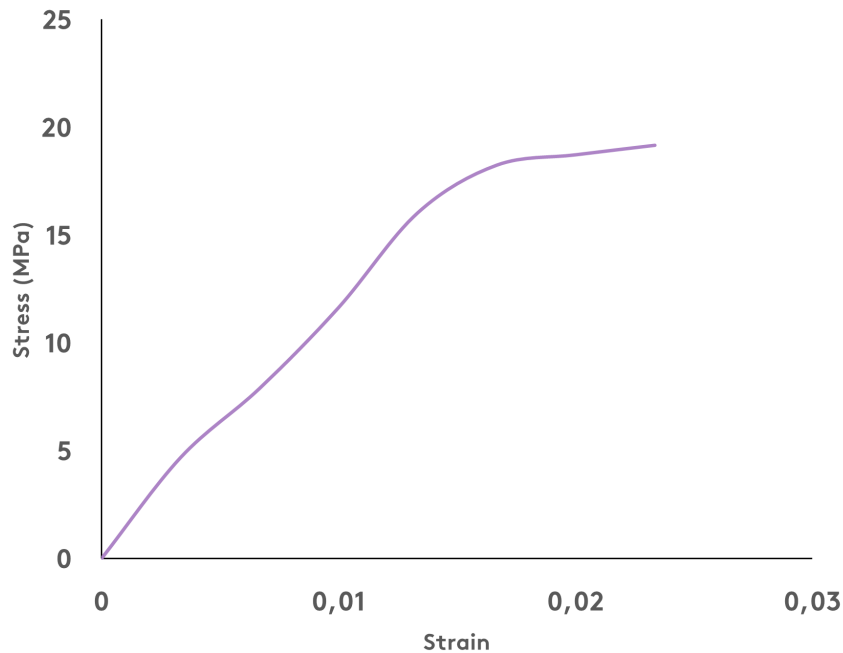
Figure 63 2.1.1 stress-strain curve (numerical results)

The elastic stage of the stress-strain curve ends at a strain of 0.018. The value of Yield stress is around 19 MPa. The Young Modulus, that characterise the trend of the linear stage is 1105 MPa. In **Figure 63** the stress-strain curve of the numerical test,
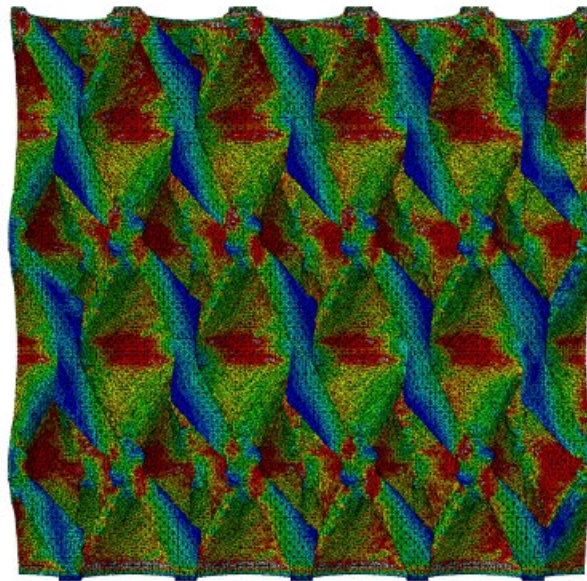
Figure 64 Stress concentration at connection point of BLS 2.1.1

while in **Figure 65** a representation of the test at different strains. As it is possible to see from the numerical model, the contact points among the unit cells are affected by stress.

***Figure 65** 2.1.1 Von Mises at different strain (from strain 0 to strain 0.02)*
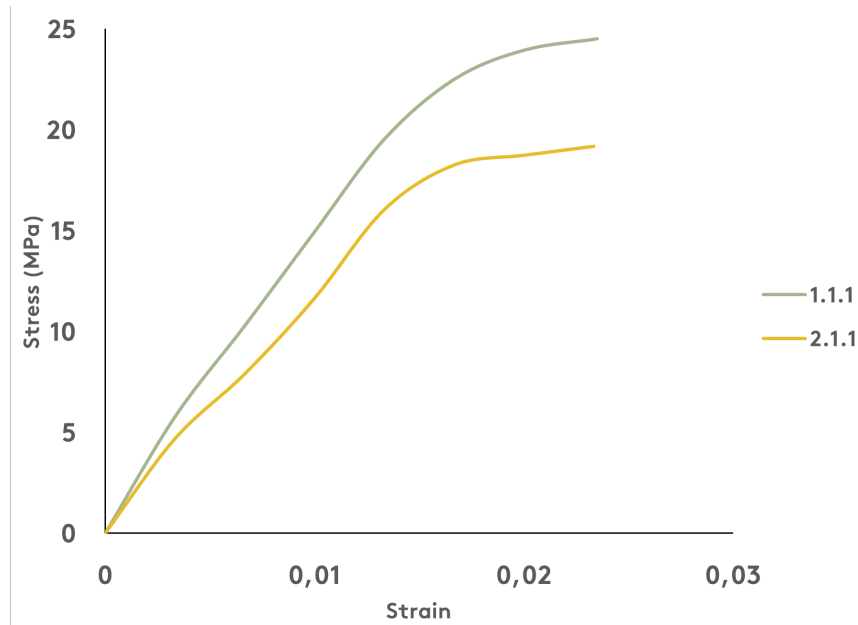
Figure 66 *Numerical results of 1.1.1 and 2.1.1*

The numerical analyses were carried out on BLS 1.1.1 and 2.1.1 (stress-strain curves in **Figure 66**). The results of elastic modulus and yield strength (**Table 11**) shows higher values for the lattice structure based on unit cell 1, while the elastic stage for both of the structures is reached with a strain of almost 0.2.

The results reflects the fact that BLS 1.1.1 shows higher resistance to compression, compared to structure 2.1.1.
Also, it can be noticed that, for both of the structures, the stress is localized at the contact points among the cells. These results are confirmed by the experimental tests, since it is possible to observe that, with higher strains, the fractures happen at those points.

Comparison between numerical and experimental data of BLSs 1.1.1 and 2.1.1
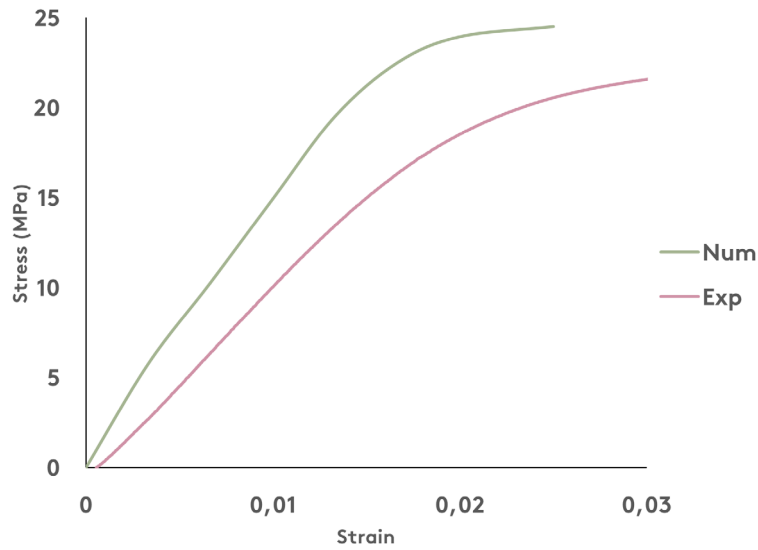
Figure 67 *Comparison between numerical and experimental results of 1.1.1*
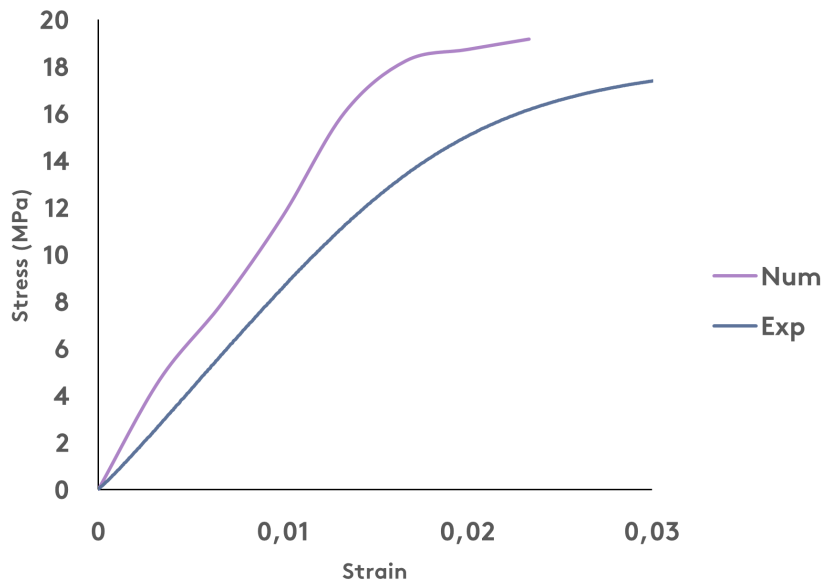
Figure 68 *Comparison between numerical and experimental results of 2.1.1*

A comparison of the numerical and experimental results was carried out for both BLS 1.1.1 and 2.1.1: in **Figure 68** and **Figure 67** and are shown the stress-strain curves, while a recap of the mechanical properties was made in **Table 11**. According to the setting of the FEM model, only the results related to the elastic stage could be compared with the experimental data.

The yield strains computed for the numerical analyses are practically the same of the values obtained with the experimental tests (ca. 0.02), while the numerical yield stresses are higher than the experimental ones.

Moreover, the slope of the elastic stage, for both 1.1.1 and 2.1.1 is higher in case of the experimental results.

The discrepancy between the numerical and the experimental results is mainly based on two reasons:

- The material model definition
- The surface roughness and possible internal defects

The material model did not consider the anisotropy of the model due to the manufacturing process: in fact, since the process is FDM, the lattice structures are composed by layers created by the fused filament.

The simplification of the geometry as an isotropy model led to discrepancies between the results of experimental and numerical tests, that present higher values also for this reason. [50]

1.1.1	NUM	EXP
Young's Modulus (MPa)	1764	696
σy (MPa)	29	18.6
εy	0.018	0.02

2.1.1	NUM	EXP
Young's Modulus (MPa)	1470	804
σy (MPa)	24.2	16
εy	0.018	0.02

Table 11 *Numerical and experimental results of 1.1.1 and 2.1.1*

A general observation about the manufacturing process should be made: structures printed in FDM present several defects, related to the used filament, the 3D printing parameters, the geometric details and the use or absence of support. All these defects affect the mechanical properties.

Roughness and internal defects can lead to reduced stiffness, especially in structures comprising relatively thin members, because it contributes surplus, non load-bearing material at the surface, reducing their effective load-bearing areas. Under compressive testing, this would result in the fabricated specimens potentially having lower stiffness than predicted by FE simulations.

With these factors in mind, it is clear that FE models do not at present completely capture the deformation mechanics of the experimentally assessed lattices, but they could show the stress distributions in the various lattice types. [51]

5.2 Experimental results

The values obtained by the compressive tests allowed to create a Load-Displacement graph. Therefore, the values of the curve were respectively converted from load (F) to stress (σ) and from displacement (U$_2$) to strain (ε).

$$\varepsilon = \frac{U_2}{L}, \sigma = \frac{F}{A} \text{ ; where L= 30 mm and A= L*L= 900 mm}^2$$

The compressive stress-strain curve (**Figure 69**) of a cellular solid can often be simplified into three regimes: the linear elastic regime, the plateau regime, and the densification regime. For many types of cellular solids, the plateau regime starts from the crush strain, ε_y, or crush stress, σ_y, representing the initiation of the new deformation mechanism of the cell wall or the cell wall failure, and ends at a critical strain, ε_{cd}, representing the onset of densification. With further compression, more cell walls come into contact with each other. The cellular material is completely compacted when the strain reaches a complete densification strain, ε_d, causing a steep increase in the slope of the stress-strain curve. The densification strain is the critical strain when the cell walls jam together. [52]
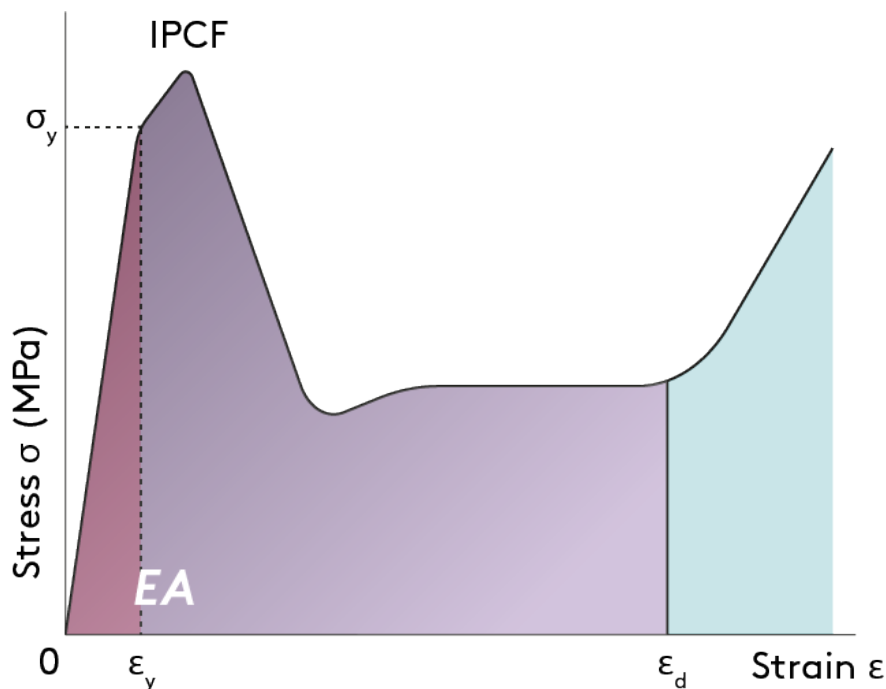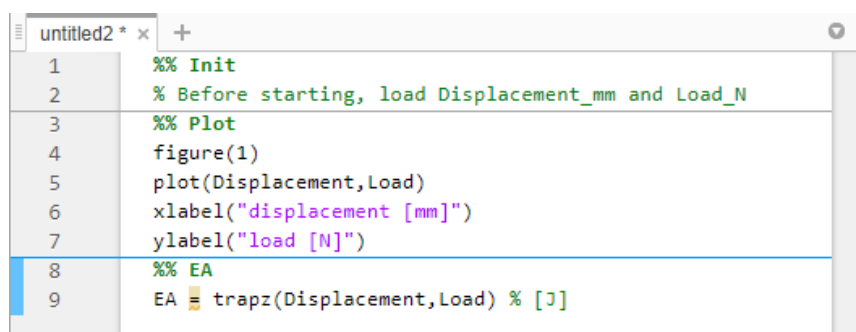
Figure 69 *Stress-strain curve*

The original unit cell is the 1; the unit cell 2 consists of a slight variation of the first one.

The structure 1.1.1 and 2.1.1, made respectively by the original unit cell 1 and 2, were modified in order to double and half the ratio between cells' height and diameter of the lofted profile; the fourth structure has no variation of the ratio diameter/height, but the dimension of fillets is modified in order to investigates the effect of radius at some critical point. Indeed, all the structures' compressive tests have been analysed (definition of stages compared to the strains; definition of Young's Modulus and Yield point; definition of IPCF and EA;) and the behaviour of the specimens is observed through the photos and videos, taken during the compressive tests. For each structure a representation of the stress-strain curves and of the deformation of the specimens during the experimental test is given.

The elastic modulus was obtained as the slope of the straight line given by linear fitting of data points within the linear deformation region at the beginning of the compressive stress-strain curve (strain range of 0-0.02). The yield stress was computed as the intersection between the compressive stress-strain curve and the 0.2% offset line parallel to the elastic region. The IPCF was estimated as the compressive stress corresponding to the first local maximum in the stress-strain curve. The EA was calculated in MATLAB by considering a strain range of 0-ε_d (**Figure 70**).

```matlab
%% Init
% Before starting, load Displacement_mm and Load_N
%% Plot
figure(1)
plot(Displacement,Load)
xlabel("displacement [mm]")
ylabel("load [N]")
%% EA
EA = trapz(Displacement,Load) % [J]
```

Figure 70 EA calculation in MATLAB

Note that the layers of unit cells are numbered top-down, for easier identification.

Structure 1

1.1.1
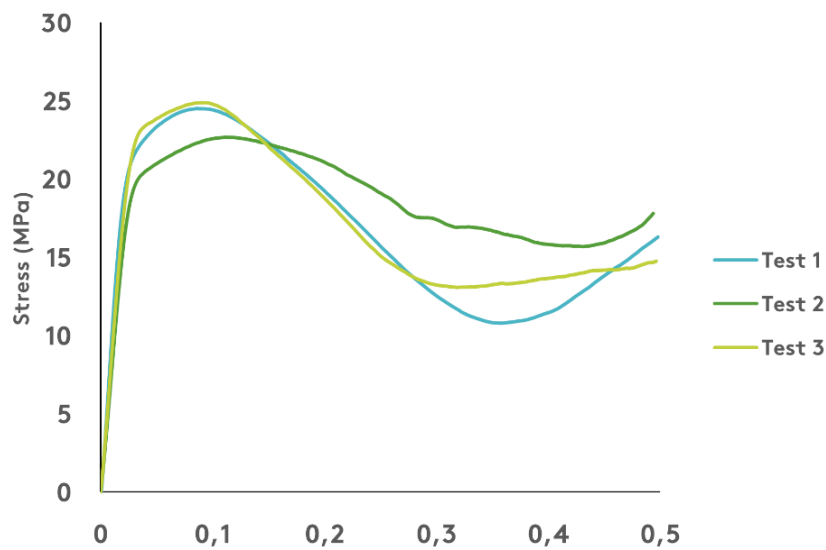
Figure 71 1.1.1 stress-strain curves

In **Figure 71** the stress-strain curves are represented: in this stage the initial peak is reached by the structure with a strain of 0.093±0.005. At this point of the curve, the structure withstands the load without visible damage. From 0.15 the first fractures between the layers of cells are visible and with the increase of plate displacement, the cracks are getting larger; around 0.25 the structure results damaged, and the layers of unit cells are fractured at the contact points. In **Figure 72** is shown the behaviour of the specimen under compressive test at different strains and in **Table 12** it is shown a recap of the mechanical properties.

1.1.1	Test 1	Test 2	Test 3	Avg.	St. dev.
E (MPa)	1035	809	896	913	±113
σy (MPa)	19	18	20	19	±1
εy	0.02	0.02	0.02	0.02	±0
IPCFσ(MPa)	24	23	25	24	±1
IPCFε	0.09	0.1	0.09	0.093	±0.005
EA (J)	182	225	210	205.6	±21.8
εd	0.4	0.45	0.47	0.44	±0.03

Table 12 1.1.1 mechanical properties
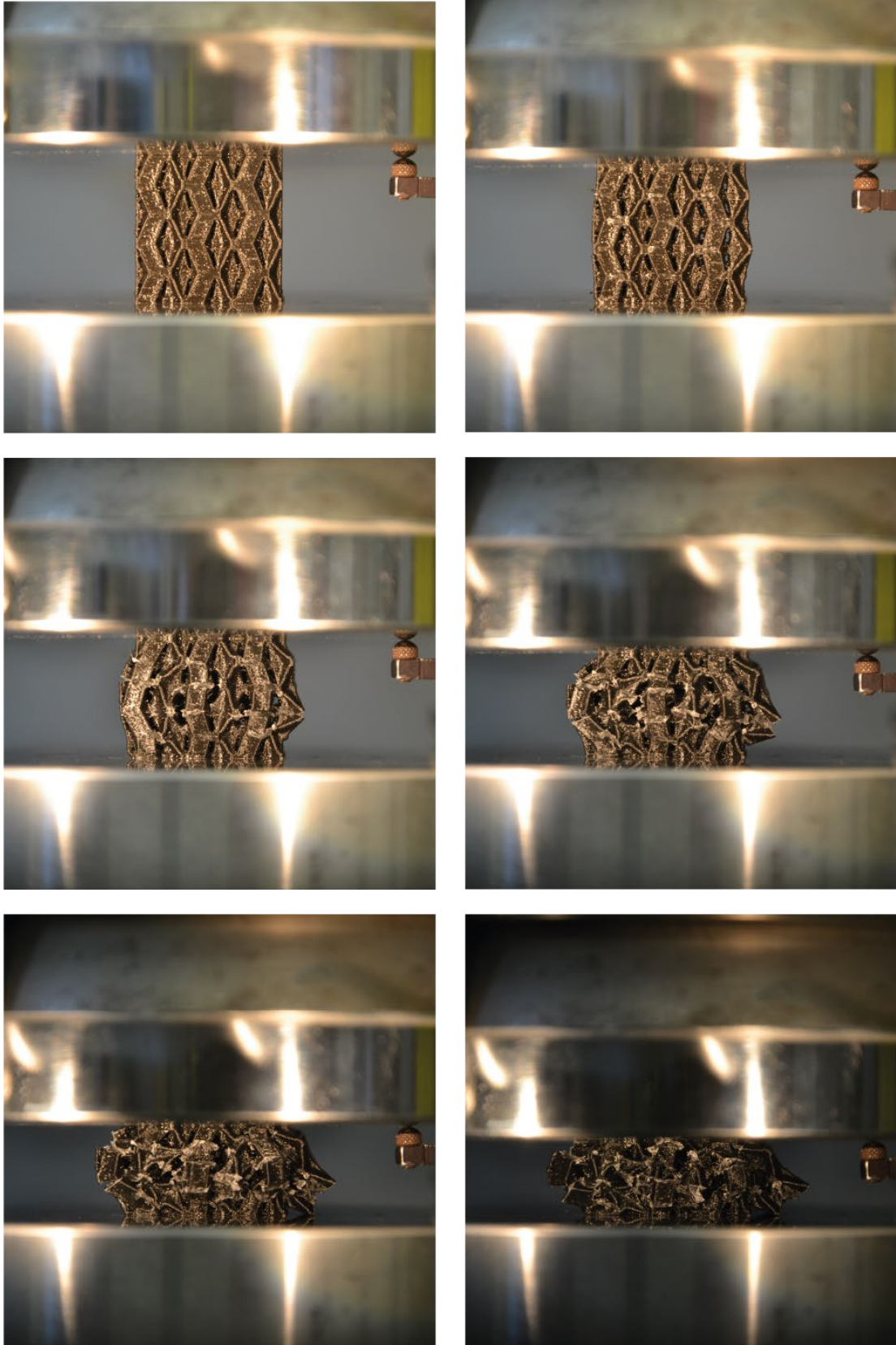
Figure 72 *1.1.1 Compression test of specimen (strain 0, 0.1, 0.2, 0.3, 0.4, 0.5)*

1.1.2
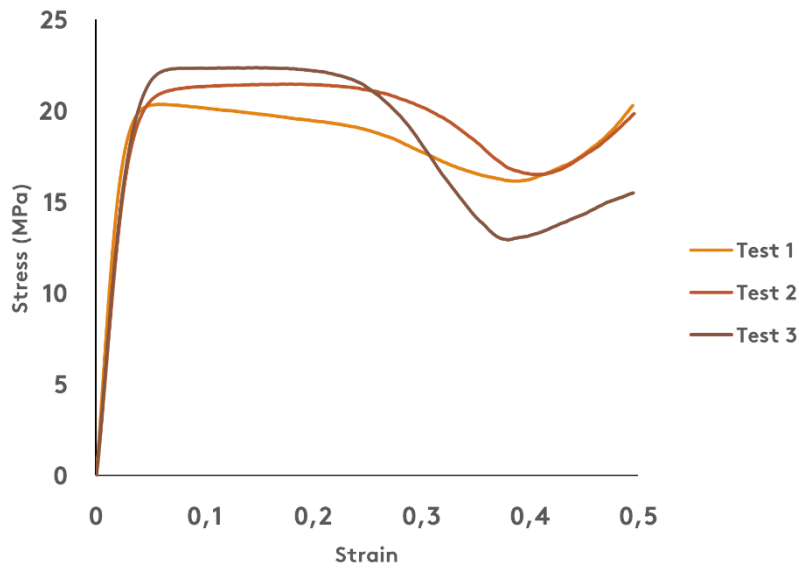
Figure 73 *1.1.2 stress-strain curves*

In **Figure 73** it is possible to see the stress-strain curve. In the plastic stage, the initial peak is reached by the structure with a strain of 0.05±0.01. At this point of the curve, the structure tends to be compacted, but it withstands the load without visible damage, up to strain 0.25. From that point, the first fractures between the layers of cells happen, around 0.3 the structure results damaged. The compression involves all the layers of cells in the same way: the space between the cells is reducing in a homogeneous way during compression; the "X shape" remains intact (**Figure 74**) and the connection between the unit cells result to be stronger. In **Table 13** are presented the mechanical properties.

1.1.2	Test 1	Test 2	Test 3	Avg.	St. dev.
E (MPa)	798	682	694	724	±63
σy(MPa)	16	15	15	15.3	±0.5
εy	0.02	0.02	0.02	0.02	±0
IPCFσ(MPa)	20	21	22	21	±1
IPCFε	0.06	0.06	0.03	0.05	±0.01
EA (J)	196	210	205	203.6	±7.09
εd	0.4	0.4	0.4	0.4	±0

Table 13 *1.1.2 mechanical properties*
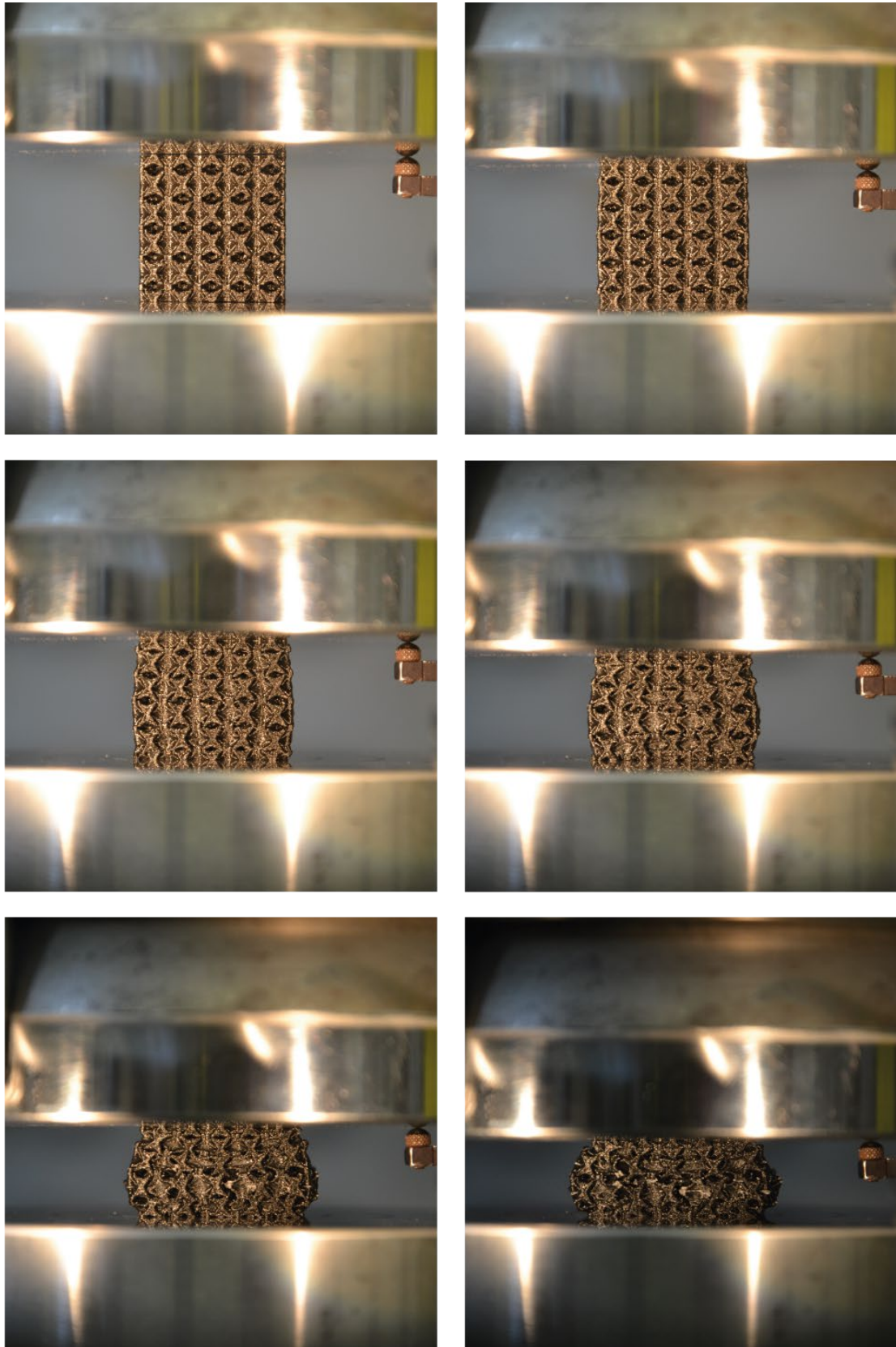
Figure 74 *1.1.2 Compression test of specimen (strain 0, 0.1, 0.2, 0.3, 0.4, 0.5)*

1.1.3
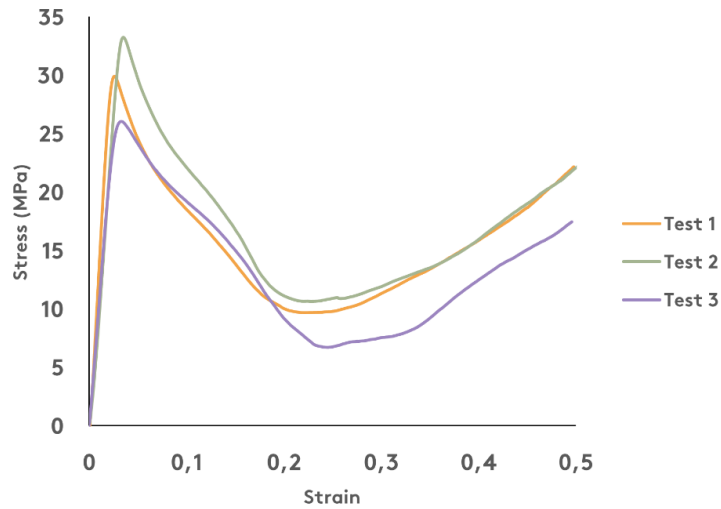
Figure 75 *1.1.3 stress-strain curves*

From strain 0.15 the first fractures between the first and second layer of cells happen, around 0.2 the structure results damaged with severe fractures. During the compressive test the third layer of unit cells, that in this case composes the base of the structure, is not severely damaged because the weak point results to be the connection between cells; then, since the structure's base is composed by the nodes feature, the final layer is not subject to fracture (**Figure 76**). About the critical point, it should be observed that the modified geometry of the cell increases the local stress at the contact points between the unit cells; the effect is more visible because the cell's height is doubled. In **Figure 75** the stress-strain curve of the compressive test is shown and in **Table 14** the mechanical properties are collected.

1.1.3	Test 1	Test 2	Test 3	Avg.	St. dev.
E (MPa)	1458	1079	1040	1192	±230
σy (MPa)	20	31	24	25	±5.5
εy	0.02	0.03	0.025	0.025	±0.005
IPCFσ (MPa)	30	33	26	29.6	±3.5
IPCFε	0.025	0.035	0.03	0.03	±0.005
EA (J)	109	128	118	118.3	±9.5
εd	0.25	0.27	0.32	0.28	±0.03

Table 14 *1.1.3 stress-strain curve*
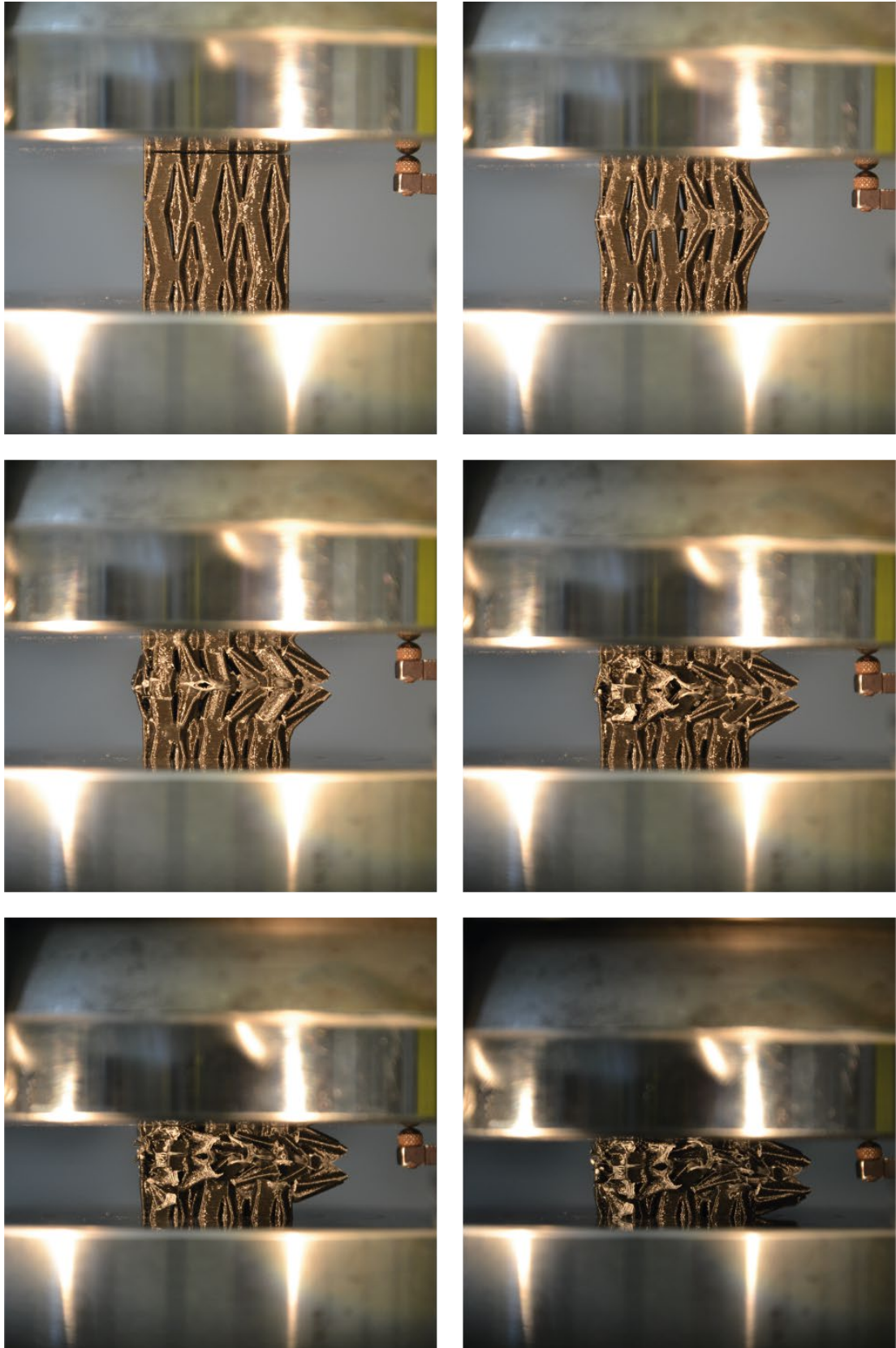
Figure 76 1.1.3 Compression test of specimen (strain 0, 0.1, 0.2, 0.3, 0.4, 0.5)

1.2.1
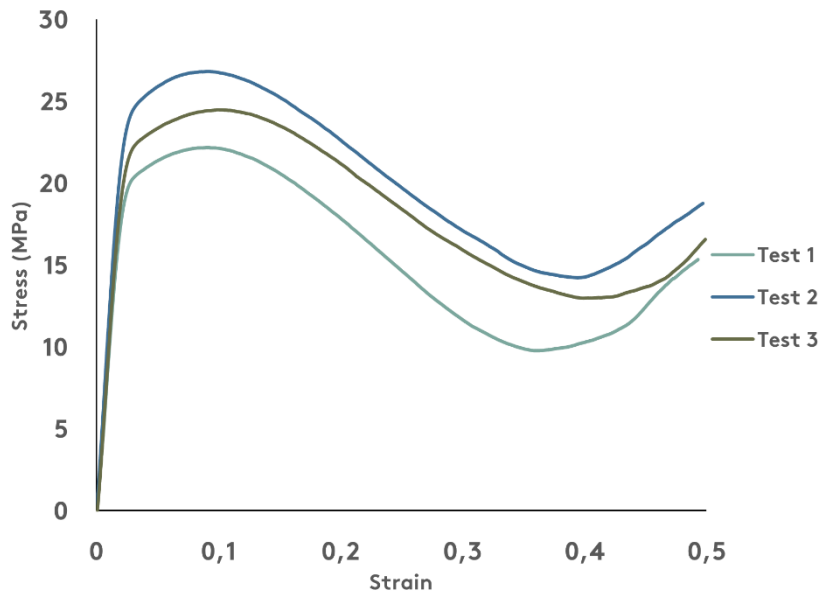
Figure 77 *1.2.1 stress-strain curves*

The stress-strain curve of the compressive test of a specimen of BLS 1.2.1 is shown in **Figure 77** while the mechanical properties are collected in **Table 15**. The elastic stage of the structure ends around a strain of 0.02 then the plastic stage starts. In this stage the initial peak is reached by the structure with a strain of 0.09. From 0.1 the first fractures between the layers of cells appear, at strain 0.2 the unit cells are still joined together but around 0.25 some fractures start to damage the lattice. Also in this case, the fractures appear at the connection points among the unit cells, as it is possible to see in **Figure 78**.

1.2.1	Test 1	Test 2	Test 3	Avg.	St. dev.
E (MPa)	941	1008	1036	995	±48
σy (MPa)	18	22	19	19.6	±2
εy	0.02	0.02	0.02	0.02	±0
IPCFσ(MPa)	22	27	24.5	24.5	±2.5
IPCFε	0.09	0.09	0.09	0.09	±0
EA (J)	173	225	219	205.6	±28.5
εd	0.4	0.4	0.4	0.4	±0

Table 15 *1.2.1 mechanical properties*
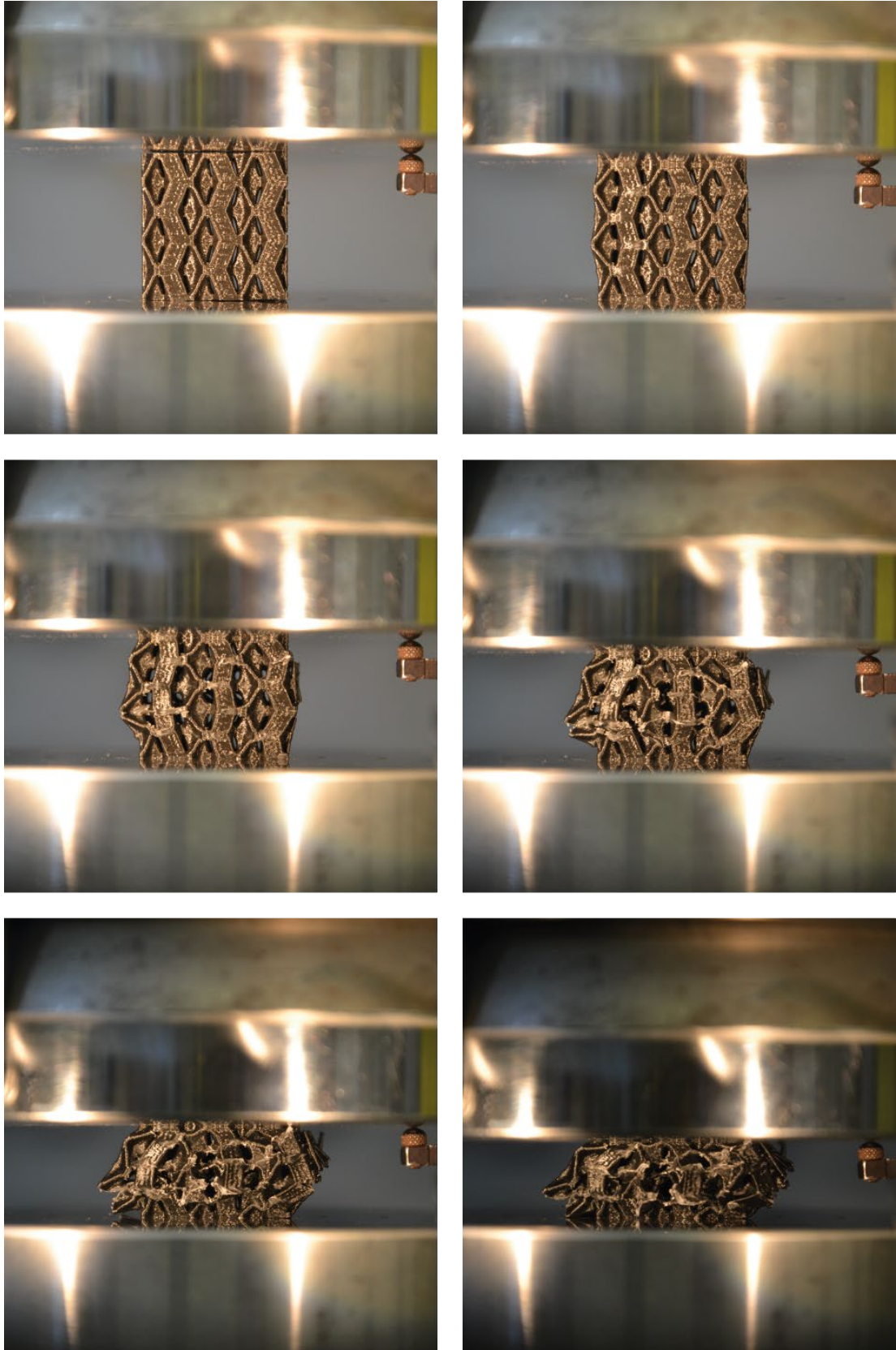
Figure 78 *1.2.1 Compression test of specimen (strain 0, 0.1, 0.2, 0.3, 0.4, 0.5)*

Structure 2
2.1.1
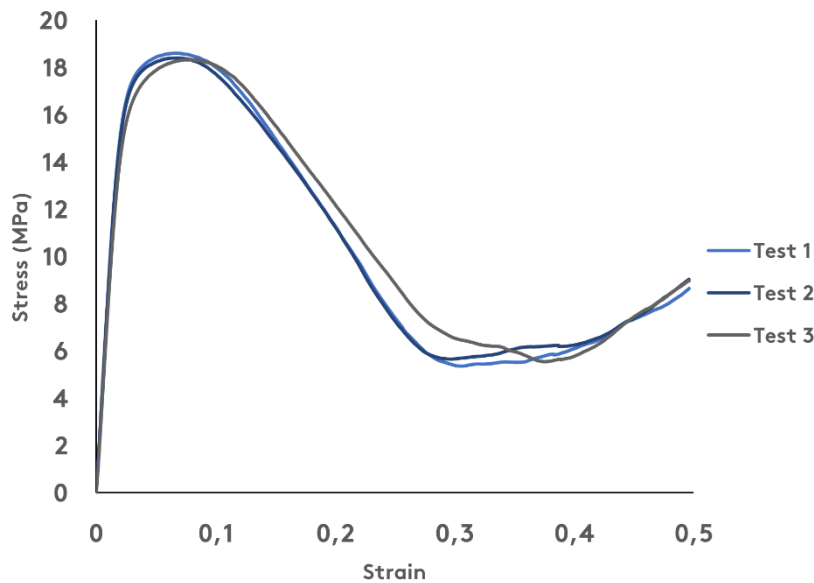
Figure 79 2.1.1 stress-strain curves

In **Figure 80** is possible to observe the behaviour of the specimen under compressive test. The elastic stage of the structure ends around a strain of 0.02; then the plastic stage starts. Around a strain of 0.1 the first fractures between the layers of cells happen and at strain 0.15, the layers 2,3 and 4 are splitting and fracturing, while the first layer is still intact. The stress-strain curves are showed in **Figure 79**, while in **Table 16** the mechanical properties are collected.

2.1.1	Test 1	Test 2	Test 3	Avg.	St. dev.
E (MPa)	804	780	743	775.6	±30
σy(MPa)	16	16	15	15.6	±0.5
εy	0.02	0.02	0.02	0.02	±0
IPCFσ(MPa)	19	18	18	18.3	±0.5
IPCFε	0.06	0.07	0.07	0.06	±0.005
EA (J)	116	120	124	120	±4
εd	0.4	0.4	0.4	0.4	±0

*Table 16 2.1.1 mechanical properties*
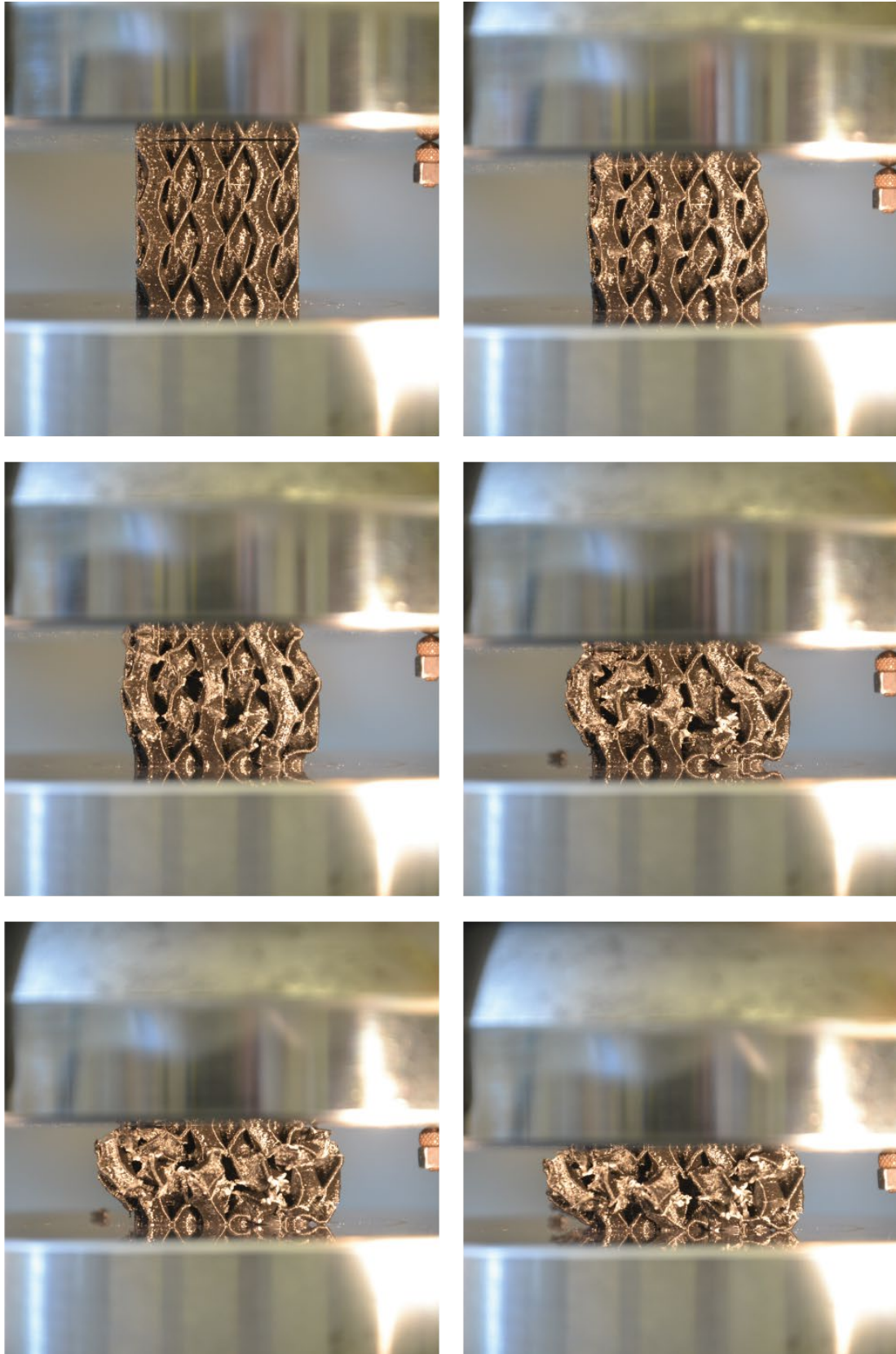
Figure 80 *2.1.1 Compression test of specimen (strain 0, 0.1, 0.2, 0.3, 0.4, 0.5)*

2.1.2
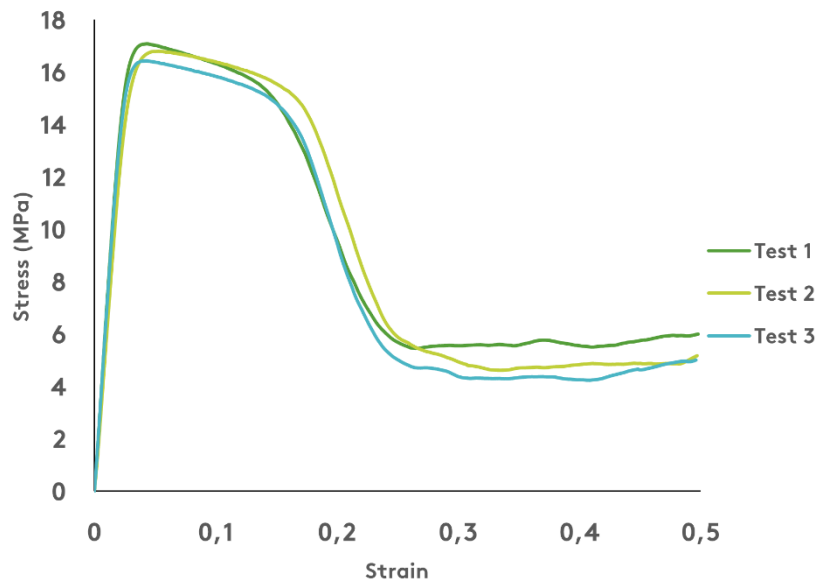
Figure 81 *2.1.2 stress-strain curves*

In **Figure 81** and **Figure 82** it is possible to see respectively the stress-strain curve of the compressive test and the behaviour of the specimen at different strain, from strain 0 to strain 0.5. In **Table 17** is presented a recap of the mechanical properties. The elastic stage of the structure ends around a strain of 0.025±0.001; then the plastic stage starts. From 0.1 the first fractures between the layers of cells happen, and at strain 0.2 the cells are fractured.

2.1.2	Test 1	Test 2	Test 3	Avg.	St. dev.
E (MPa)	682	605	615	634	±41
σy (MPa)	15	14.5	15.5	15	±0.5
εy	0.024	0.025	0.027	0.025	±0.001
IPCFσ(MPa)	17	17	16	16.6	±0.5
IPCFε	0.05	0.05	0.04	0.04	±0.005
EA (J)	124	120	108	117.3	±8.3
εd	0.49	0.48	0.44	0.47	±0.02

Table 17 *2.1.2 mechanical properties*
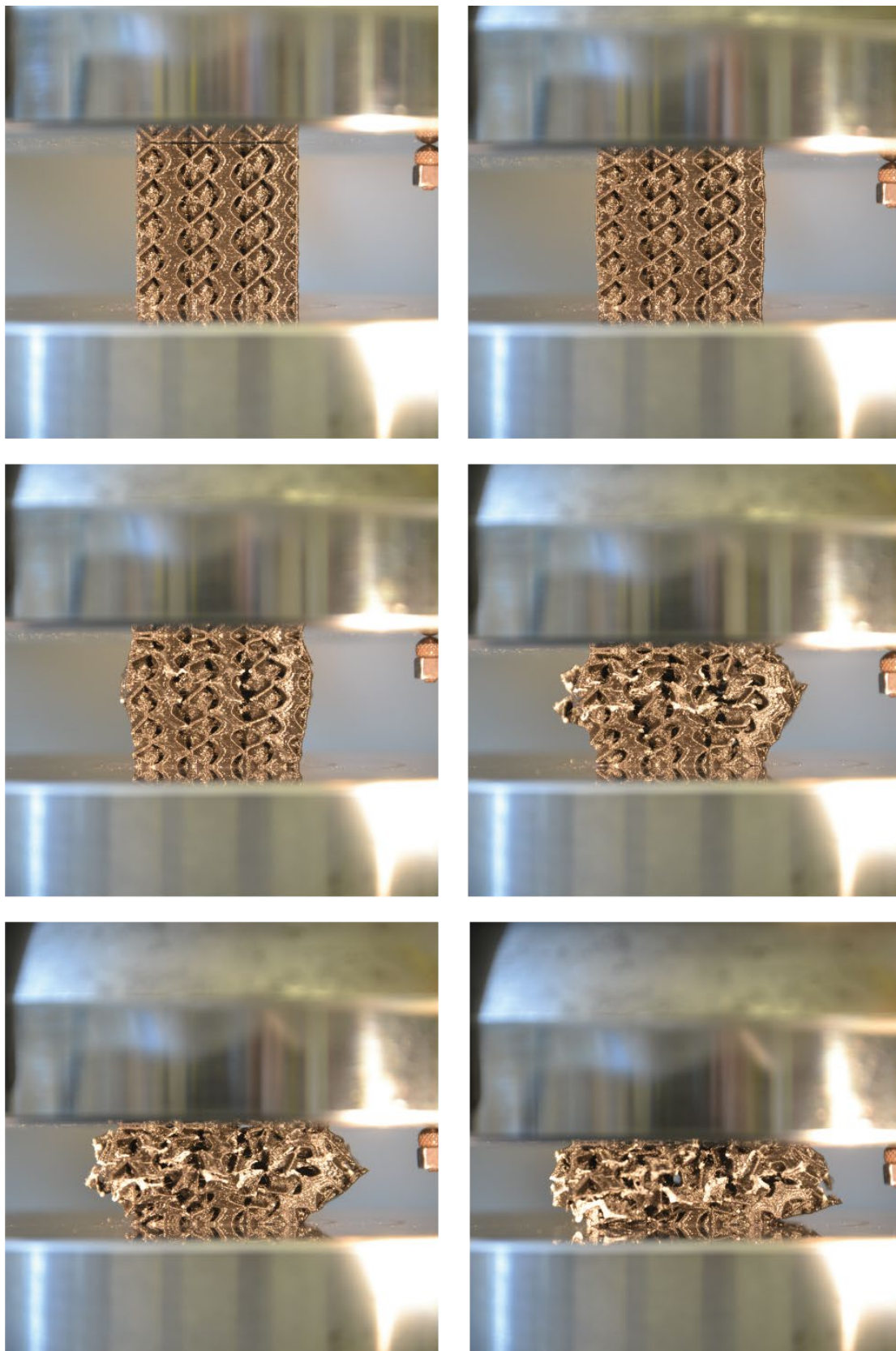
Figure 82 *2.1.2 Compression test of specimen (strain 0, 0.1, 0.2, 0.3, 0.4, 0.5)*

2.1.3
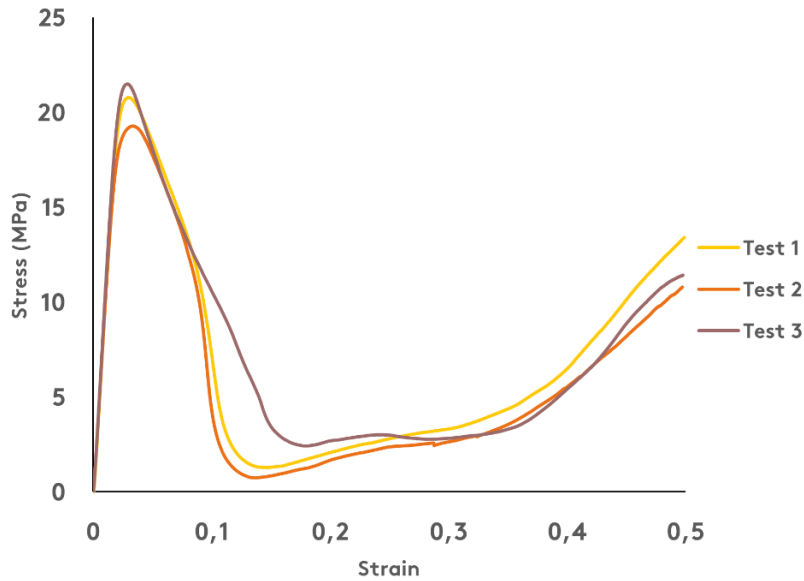
Figure 83 2.1.3 stress-strain curves

The initial fractures between the first layer and the second are visible right after the value of yield stress is reached, with a strain of 0.02, as it is possible to see in **Figure 84**. In **Table 18** the mechanical properties are presented. The initial peak is reached by the curve with a strain of 0.03. the curve decreases almost constantly from the strain of 0.03 to 0.15. From strain 0.1, the first fractures between cells become more evident, getting larger at strain 0.2. The trend of the curve is then gradually increasing because of densification stage (**Figure 83**). From strain 0 to 0.4, the last layers of unit cells (5) stay almost intact, as with the BLS 1.1.3, the reason is that the lattice structure base is composed by the diaphragms.

| 2.1.3	Test 1	Test 2	Test 3	Avg.	St. dev.
E (MPa)	1006	932	1030	989.3	±51
σy (MPa)	19	18	20	19	±1
εy	0.02	0.02	0.02	0.02	±0
IPCFσ(MPa)	21	19	21	20.3	±1.1
IPCFε	0.03	0.03	0.03	0.03	±0
EA (J)	53	49	66	56	±8.8
εd	0.3	0.3	0.3	0.3	±0

Table 18 2.1.3 mechanical properties
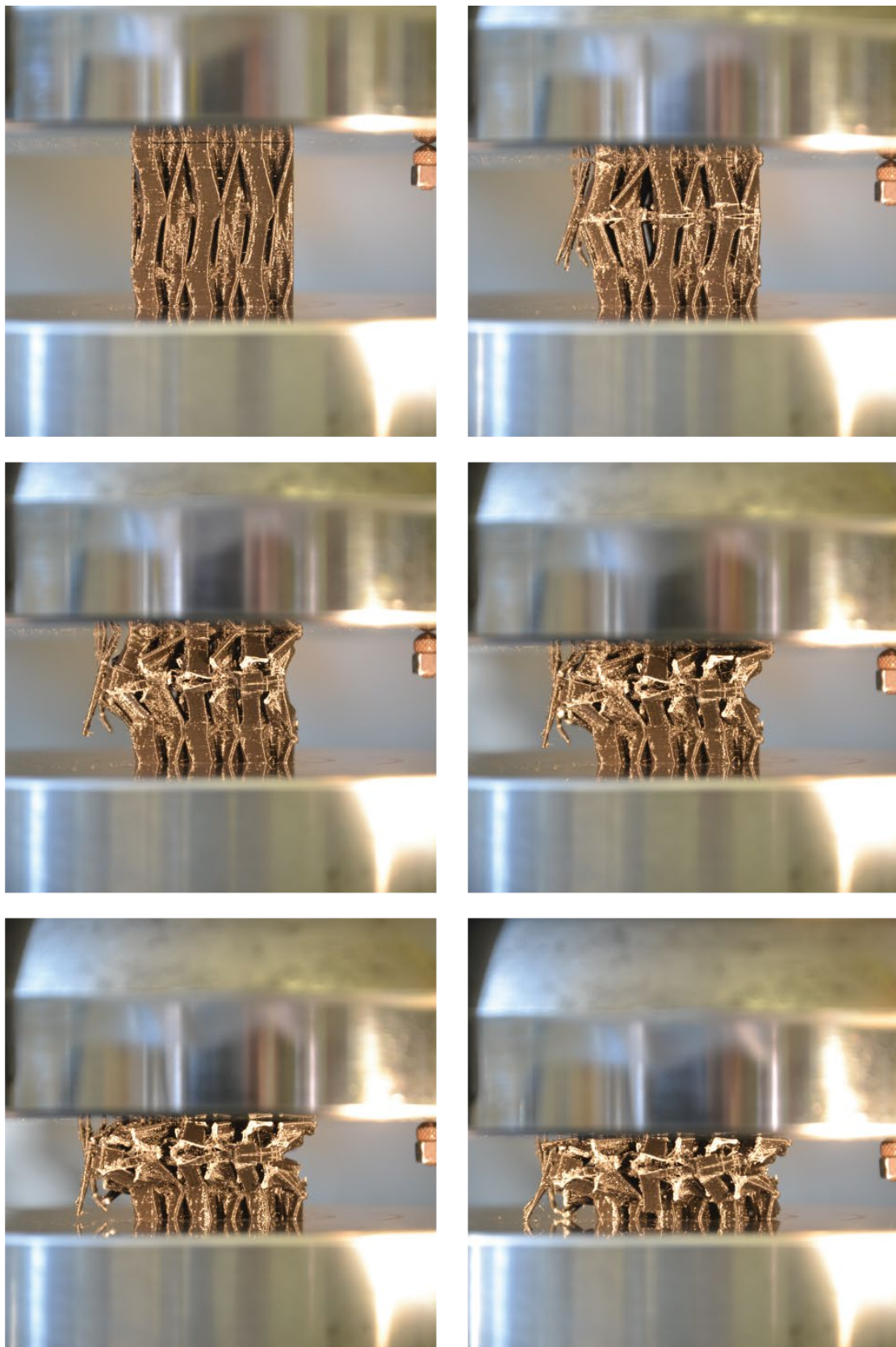
Figure 84 2.1.3 Compression test of specimen (strain 0, 0.1, 0.2, 0.3, 0.4, 0.5)

2.2.1
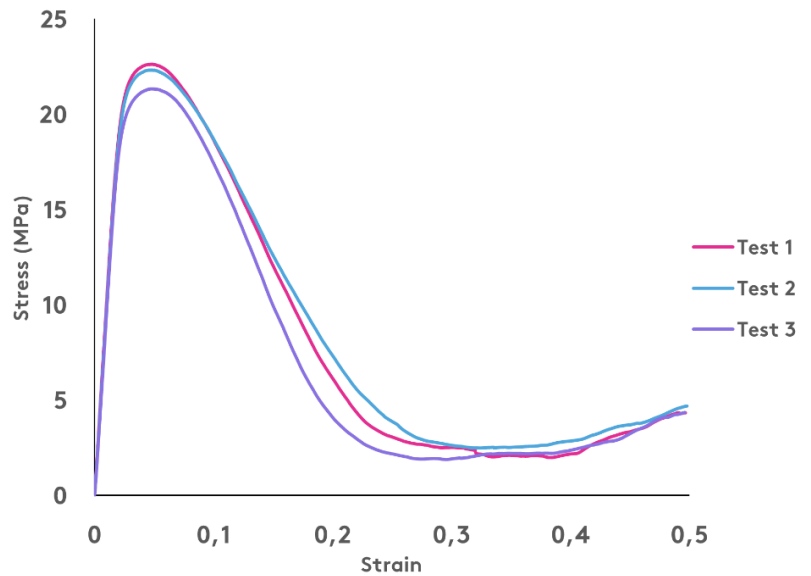
Figure 85 2.2.1 stress-strain curves

The elastic stage of the structure ends around a strain of 0.02 and a yield stress reached of 19.6±0.57 MPa; then the plastic stage starts. In this stage the initial peak is reached by the structure with a strain of 0.046±0.005. At this point of the curve, the structure results to be compressed, but it withstands the plate displacement without visible damage. From 0.1 the first fractures between the layers of cells happen, but at strain 0.2, severe cracks between layers 2 and 3 appear; layer 5 is almost intact. With a strain of 0.4, it starts the densification stage. In **Figure 85** and **Figure 86** the stress-strain curve and the behaviour of the specimen under compression are represented. In **Table 19** the mechanical properties.

2.2.1	Test 1	Test 2	Test 3	Avg.	St. dev.
E (MPa)	969	956	936	953.6	±16.6
σy (MPa)	20	20	19	19.6	±0.57
εy	0.02	0.02	0.02	0.02	±0
IPCFσ(MPa)	23	22	21	22	±1
IPCFε	0.04	0.05	0.05	0.046	±0.005
EA (J)	67	104	88	86.3	±18.5
εd	0.4	0.4	0.4	0.4	±0

Table 19 2.2.1 mechanical properties

119
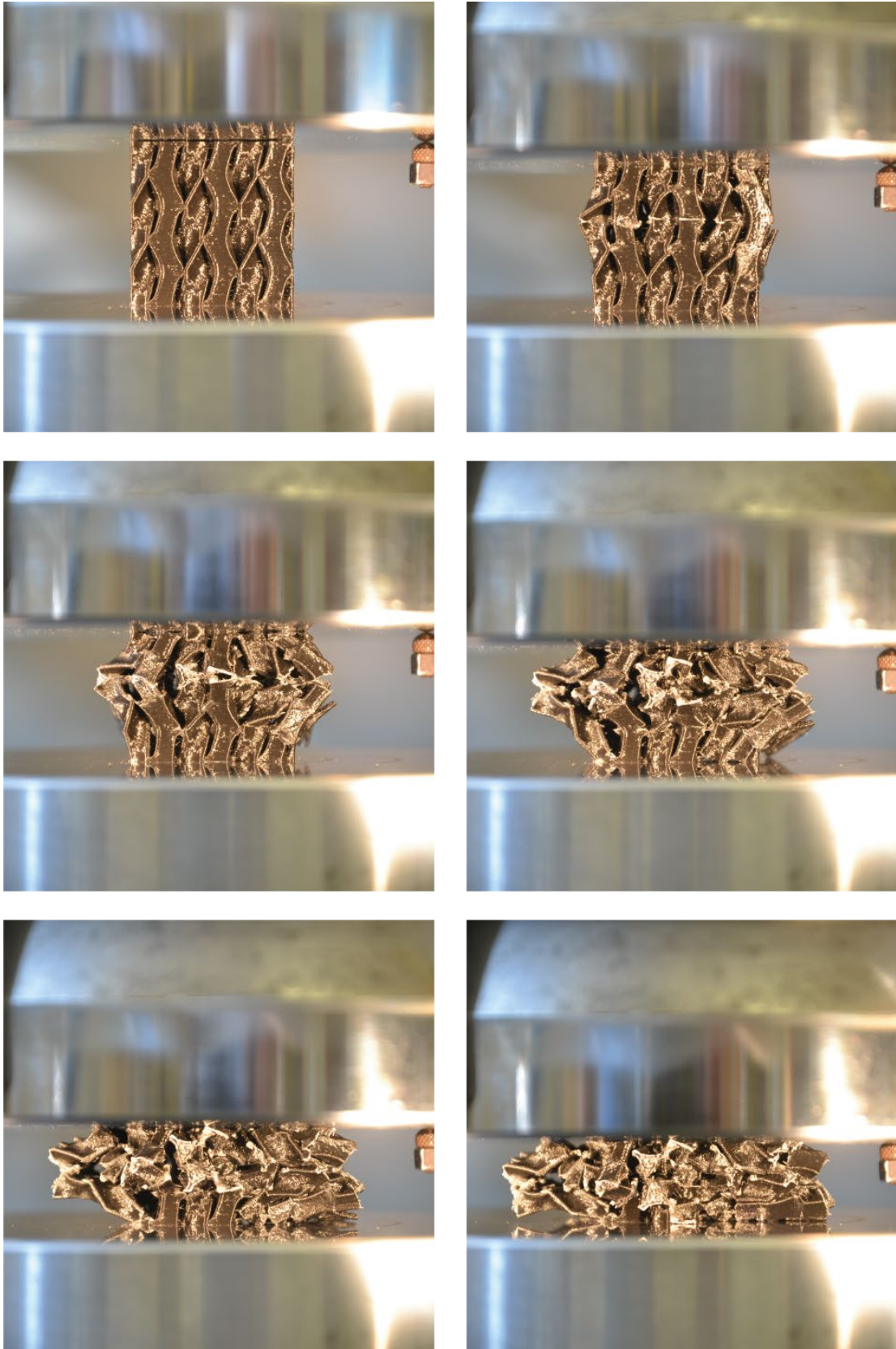
Figure 86 *2.2.1 Compression test of specimen (strain 0, 0.1, 0.2, 0.3, 0.4, 0.5)*
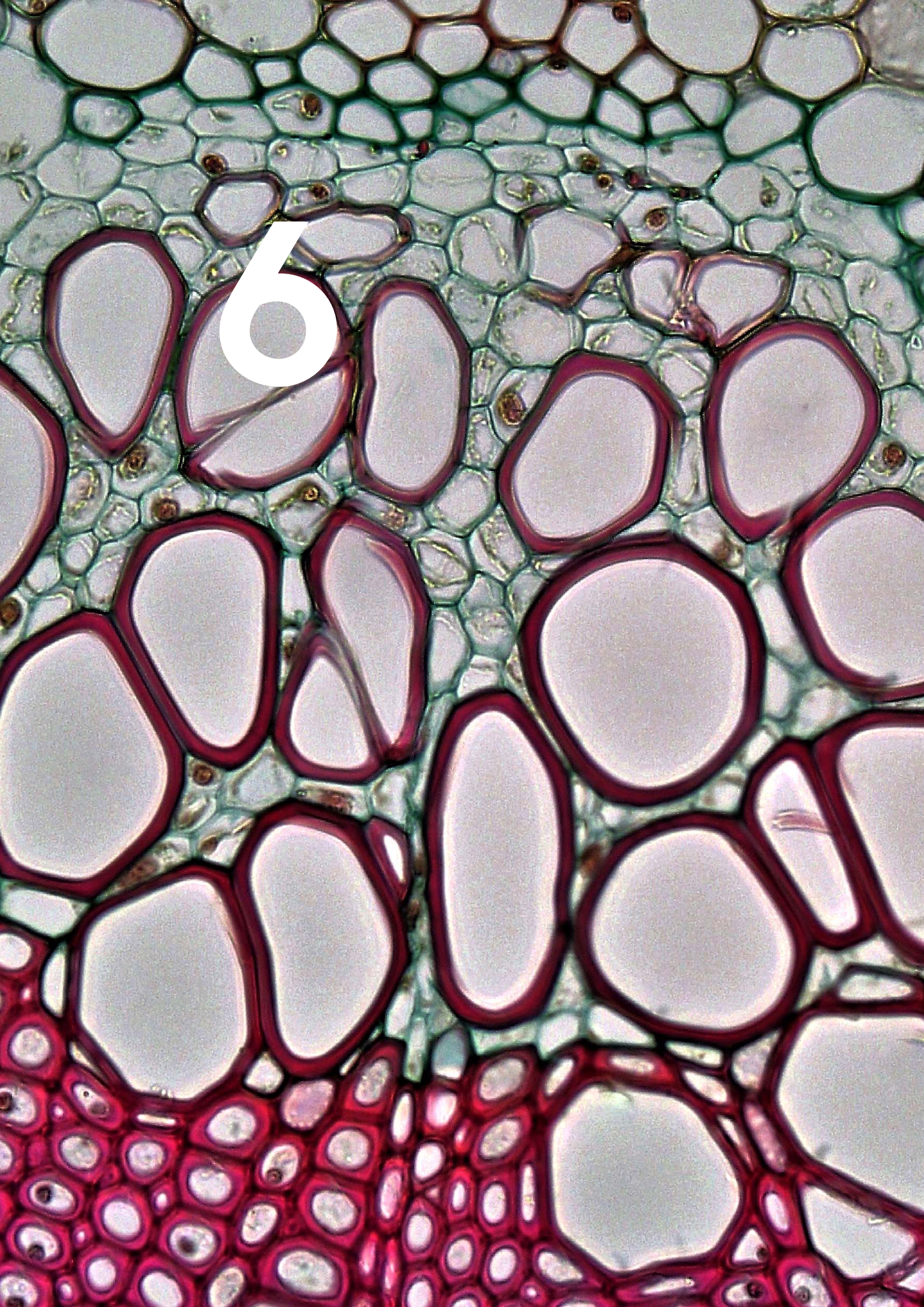
6

6 Discussion

Among the different structures, the common aspects or differences have been identified and then a comparison between structure x.1.1 and x.1.2, x.1.1 and x.1.3, x.1.1 and x.2.1 was carried out. Then, a comparison between the structures composed by unit cell 1 and unit cell 2 was made.

Note that only one of the stress-strain curves for each BLS is reported, in order to show its general trend and to allow for a graphical comparison.

1.1.1 and 1.1.2
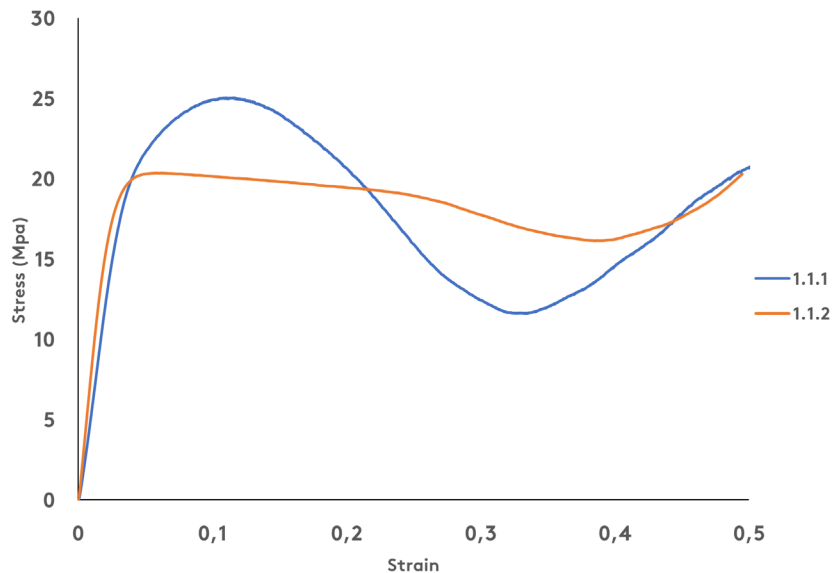
Figure 88 1.1.1 and 1.1.2 stress-strain curves

The BLS 1.1.1 is the lattice composed by the original version of the unit cell 1. Compared to 1.1.2; it shows a higher IPCF (24±1 MPa compared to 21±1 MPa), but the 1.1.2 shows a more constant trend of the curve (**Figure 88**).

Based on the observation of the compression of the specimens at same strain 0.3 (**Figure 89**), with the same porosity (both of the BLSs are characterised by a value of P=48%) the structure 2 results to have better behaviour against deformation, standing the compression without splitting. 1.1.1's EA is slightly higher (205.6±21.8 J compared to 203.6±7.09 J).
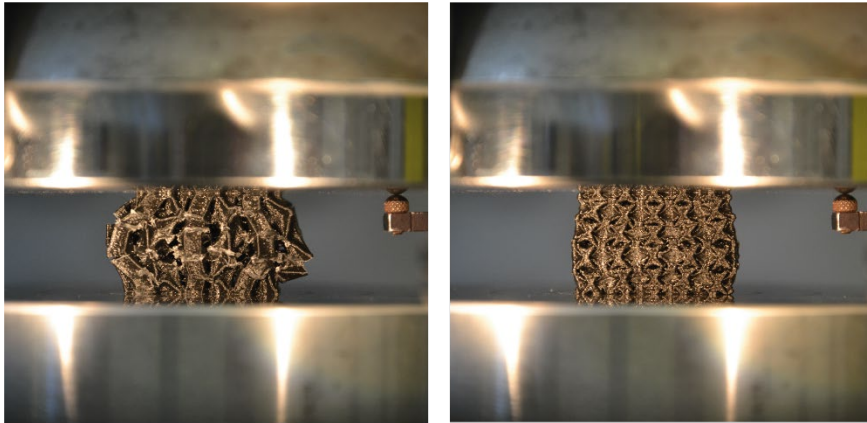
Figure 89 1.1.1 and 1.1.2 at strain 0.3

1.1.1 and 1.1.3

The highest IPCF if reached by the structure 1.1.3, but right after the peak, the trend of the curve tends to decrease faster (29.6±3.5 MPa compared to 24±1 MPa); besides, the EA is higher for BLS 1.1.1 (205.6±21.8 J compared to 118.3±9.5 J) and its curve is characterised by a rounded shape (**Figure 90**); in this case the IPCF is reached at a higher strain (0.093±0.005 compared to 0.03±0.005).
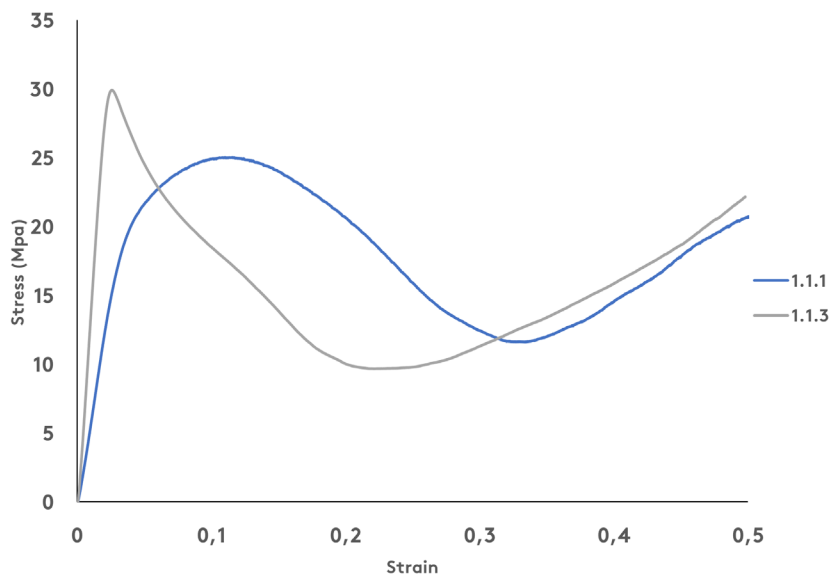
Figure 90 1.1.1 and 1.1.3 stress-strain curves

At the same strain of 0.1 the structure 3 is already breaking at the connection point of the cells between layer 1 and 2 (**Figure 91**). The yield strength of the structure 1.1.3 is the highest among all the variation of structure 1 (25±5.5 MPa).
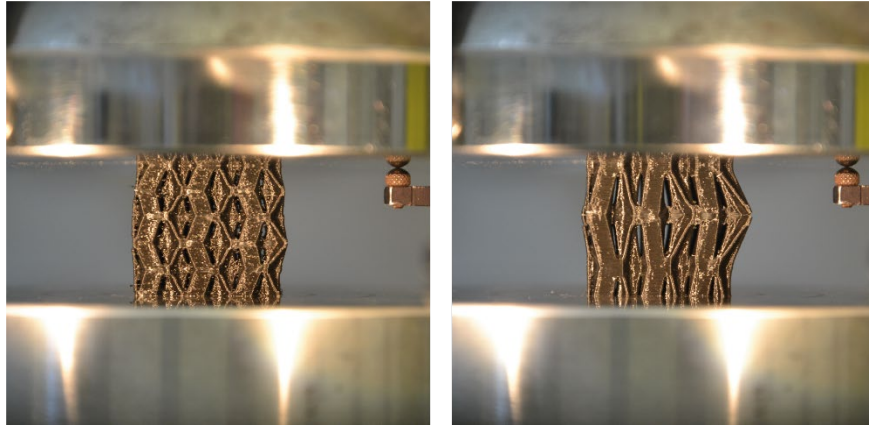
Figure 91 1.1.1 and 1.1.3 at strain 0.1

1.1.1 and 1.2.1

The EA of BLS 1.1.1 and 1.2.1 are almost identical (205.6±21.8 J compared to 205.6±28.5); while IPCF of 1.2.1 is slightly higher (24±1 MPa compared to 24.5±2.5 MPa); in general, the trend of the curve is more "stable" than the one of structure 1.1.1. The stress-strain curves are showed in **Figure 92**. By comparing the photos of the specimens during the
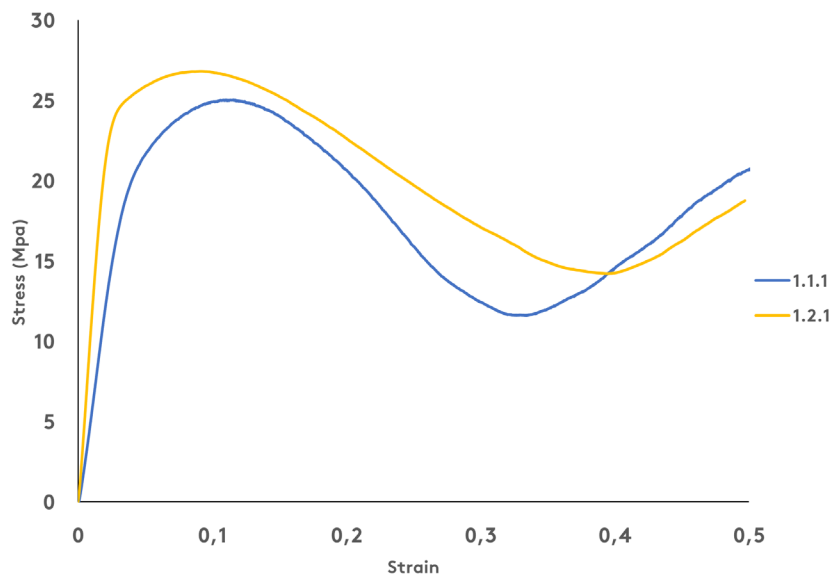
Figure 92 1.1.1 and 1.2.1 stress-strain curves

compressive tests, at the same strain of 0.2 in **Figure 93**, it is possible to see that the connection between the unit cells is stronger for the case with bigger fillets.
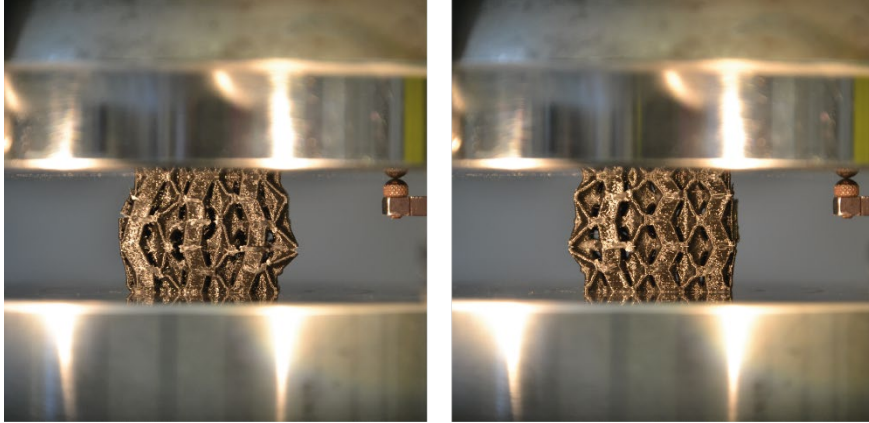
Figure 93 *1.1.1 and 1.2.1 at strain 0.2*

2.1.1 and 2.1.2
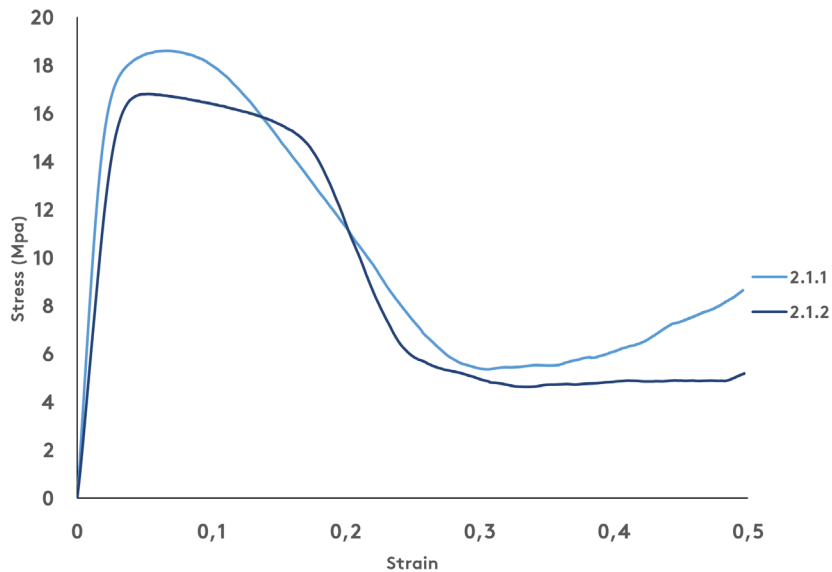
Figure 94 *2.1.1 and 2.1.2 stress-strain curves*

The BLS 2.1.1 is the lattice composed by the original version of the unit cell 2. Compared to 2.1.2, it shows a higher IPCF (18.3±0.5 MPa compared to 16.6±0.5 MPa), but 2.1.2 shows a diverse trend of the curve, as it is possible to see in **Figure 94**: from strain 0 to strain 0.3 the BLS 2.1.1 has a curve with a rounded peak, then the values of stress gradually decrease up

to the densification stage. The peak of the curve is reached with a lower value of stress, and it is possible to identify a point where the decreasing trend of the curve is changing. Around strain value 0.17, the stress values decrease faster, as it could be noticed by observing the slope of the curve: this behaviour is related to the effect of compression on specimen, that is starting to show some fractures at a strain of 0.15. Although, at strain 0.1, the first structure is fractured between the layers of cells, and those cracks get worse with the increasing of the strain. The EA of the structures is almost the same: 120±4 J and 117.3±8.3 J are the mean values of 2.1.1 and 2.1.2.

2.1.1 and 2.1.3
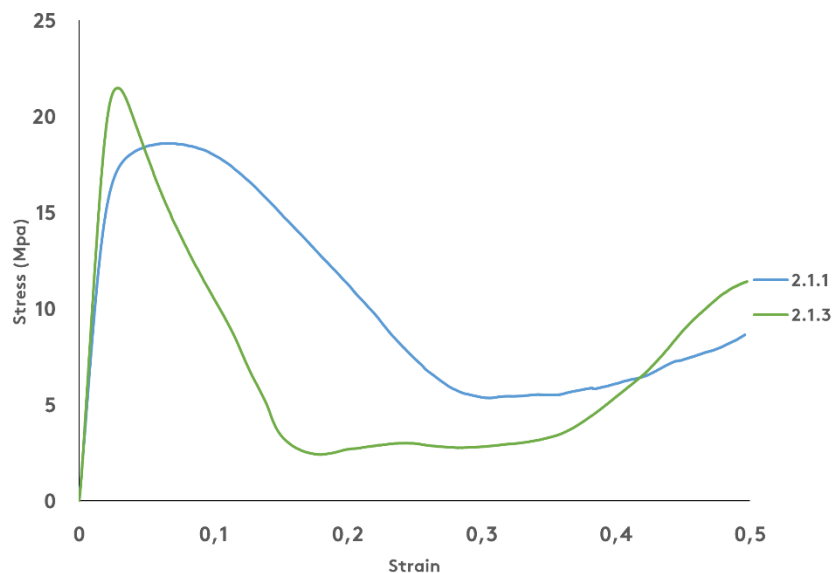
Figure 95 *2.1.1 and 2.1.3 stress-strain curves*

With a strain of 0.1, the BLS 2.1.3 is already showing some cracks; the fractures are identified at the contact points among cells. Also, the BLS 2.1.1 at the strain 0.1 showed the first fractures (**Figure 96**), but with strain 0.15 they are becoming more severe. The IPCF of 2.1.3 is higher (20.3±1.1 MPa compared to 18.3±0.5 MPa), but the trend of the curve also shows a faster decreasing of stress values right after the peak is reached, at strain 0.03. The BLS 2.1.1 curve's peak is not made by a sharp angle, but the trend of the curve is characterised by a rounded peak and a different slope. The EA
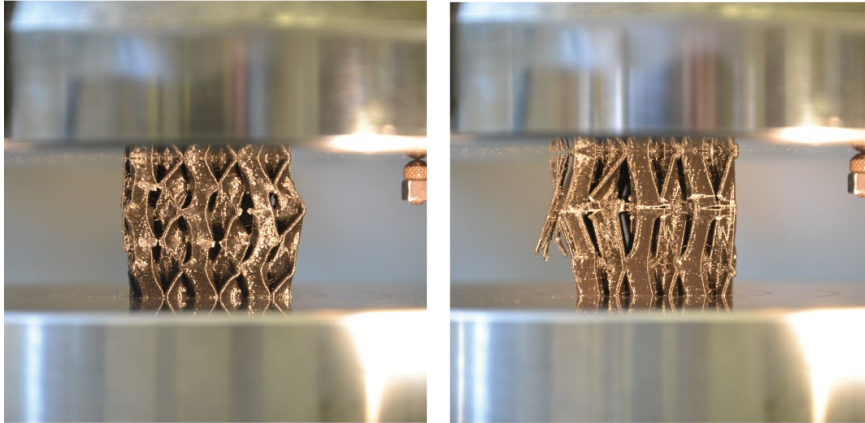
Figure 96 2.1.1 and 2.1.3 at strain 0.1

of 2.1.1 is higher than 2.1.3 (120±4 J compared to 56±8.8 J). In **Figure 95** a comparison of the stress-strain curves of the BLSs is represented.

2.1.1 and 2.2.1
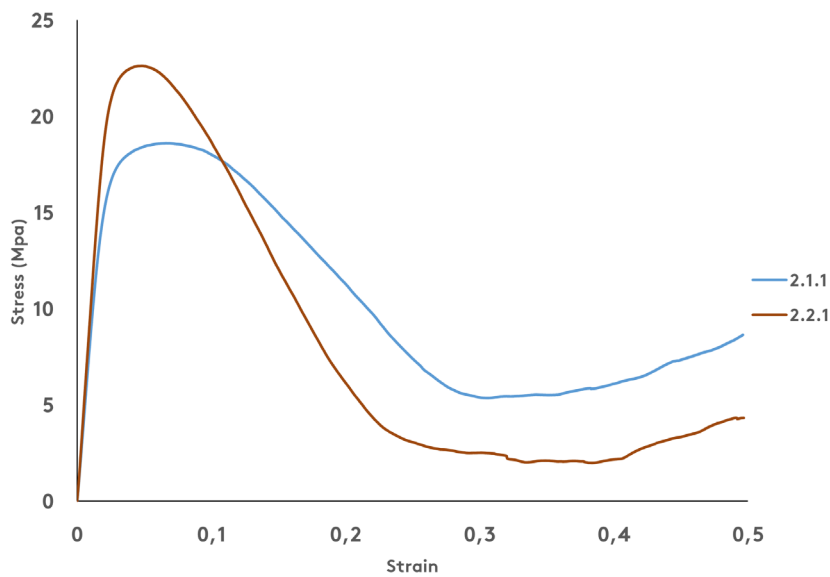
Figure 97 2.1.1 and 2.2.1 stress-strain curves

At a strain of 0.1 (**Figure 98**), BLS 2.2.1 is already showing some fractures, while the structure 2.1.1 is deformed but still intact and it is not showing cracks. In **Figure 97** the stress-strain curves of the BLSs. In general, the fractures are visible at different layers of the lattices: for structure 2.1.1 the most involved layers are the third and fourth, while for BLS 2.2.1, the

128

considered layers are the second and third. The IPCF is higher for 2.2.1 (22±1 MPa compared to 18.3±0.5)
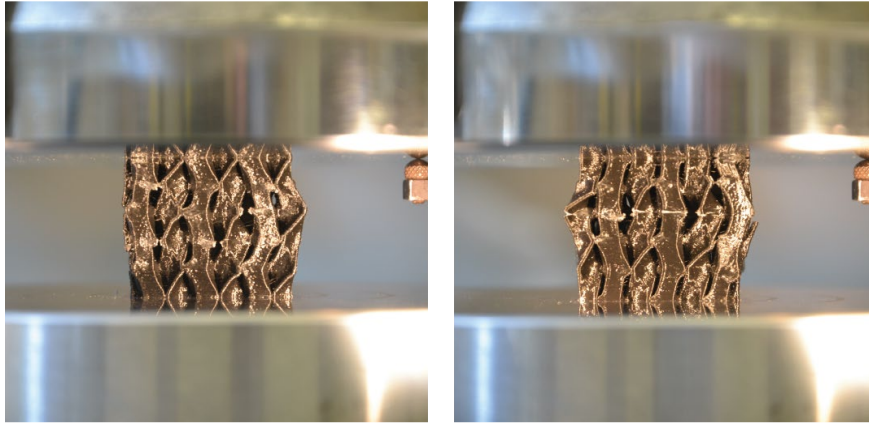
Figure 98 2.1.1 and 2.2.1 at strain 0.1

1.1.1 and 2.1.1
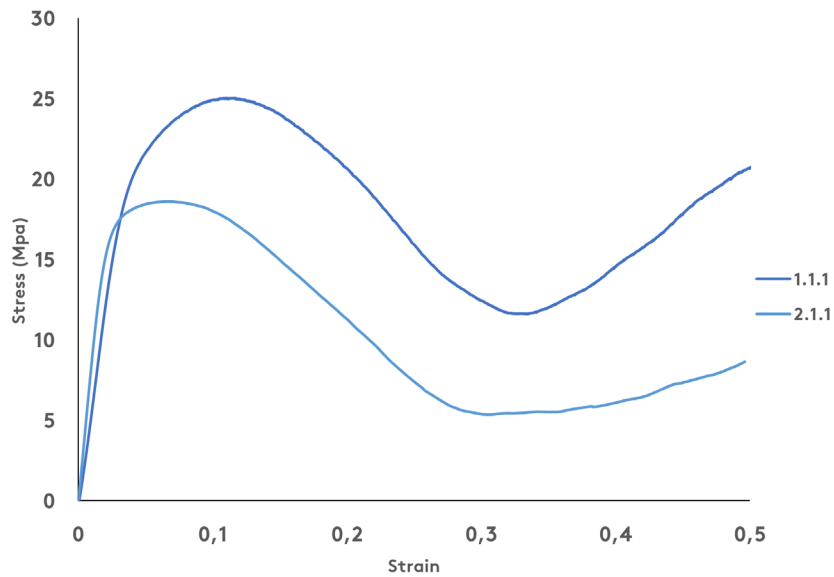
Figure 99 1.1.1 and 2.1.1 stress-strain curves

The trend of the two curves is similar, but 1.1.1 has a higher EA (205.6±21.8 J compared to 120±4 J), higher value of IPCF (24±1 MPa compared to 18.3±0.5 MPa) and also of Yield strength (19±1 MPa compared to 15.6±0.5 MPa). At strain 0.1, 2.1.1 is already showing fractures while 1.1.1 starts to show cracks at 0.15. The deformation of the structure did not happen in the

same way: for BLS 2.1.1, during the compressive test, the layers 2,3 and 4 are splitting and fracturing while the first layer is still intact (**Figure 100**). In general, both of the curves are characterised by a constant decreasing of values after the structures reach the IPCF (**Figure 99**).
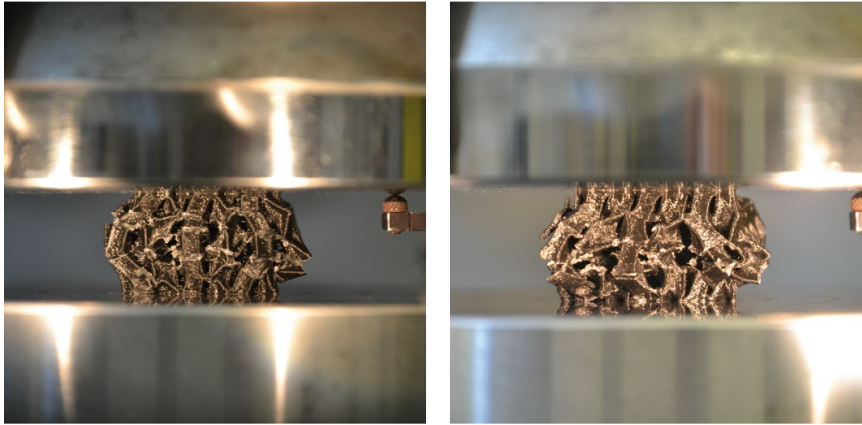
Figure 100 1.1.1 and 2.1.1 at strain 0.3

1.1.2 and 2.1.2
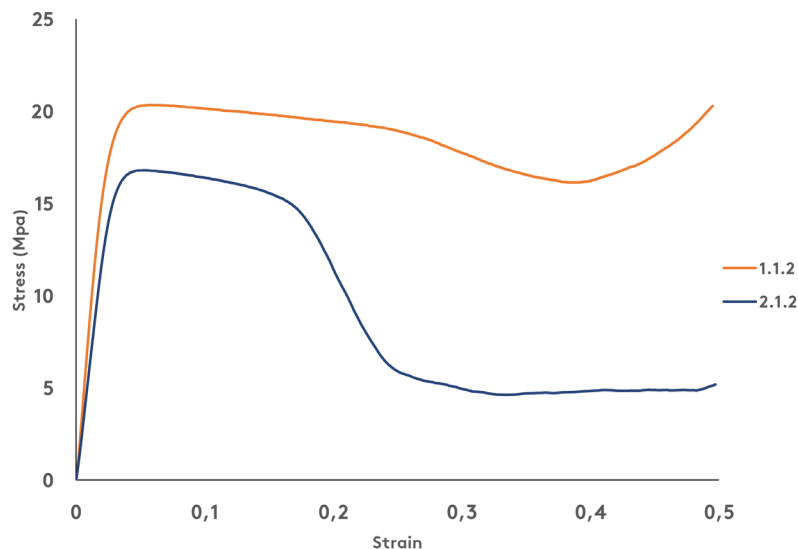
Figure 101 1.1.2 and 2.1.2 stress-strain curves

Both of the structures consist of a variation of the original version, obtained by halving the height, therefore by changing the ratio between height and diameter of the unit cells.
Also in this case, the structure based on unit cell 1 shows higher EA (203.6±7.09 J compared to 117.3±8.3 J) and higher value of IPCF (21±1 MPa compared to 16.6± 0.5 MPa).
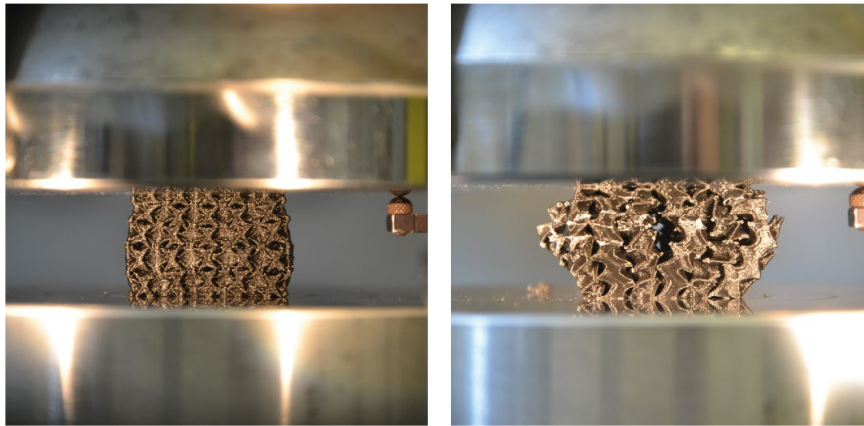
Figure 102 1.1.2 and 2.1.2 at strain 0.3

The BLS 2.1.2 has severe fractures between cells starting from strain 0.15: the curve values are decreasing from this point, establishing a change of the slope of the curve. The BLS 1.1.2 has a different behaviour; the slope of the curve remains constant from strain 0.05 to strain 0.25, then the stress values are decreasing faster up to strain 0.4, as is possible to see in **Figure 101**. A comparison of the structure under compressive test at strain of 0.3 is showed in **Figure 102**.

1.1.3 and 2.1.3
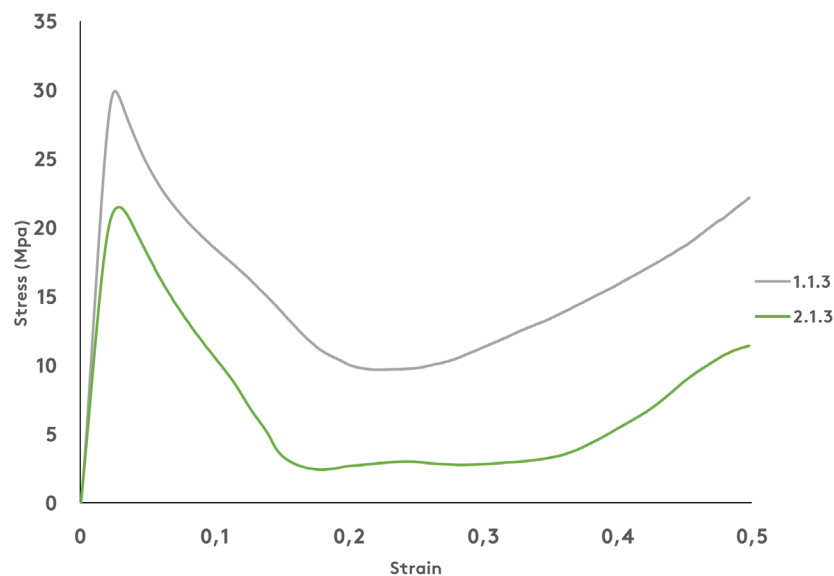
Figure 103 1.1.3 and 2.1.3 stress-strain curves

As it was previously discussed in chapter 3, these two lattices both have the ratio between radius of the profile and height
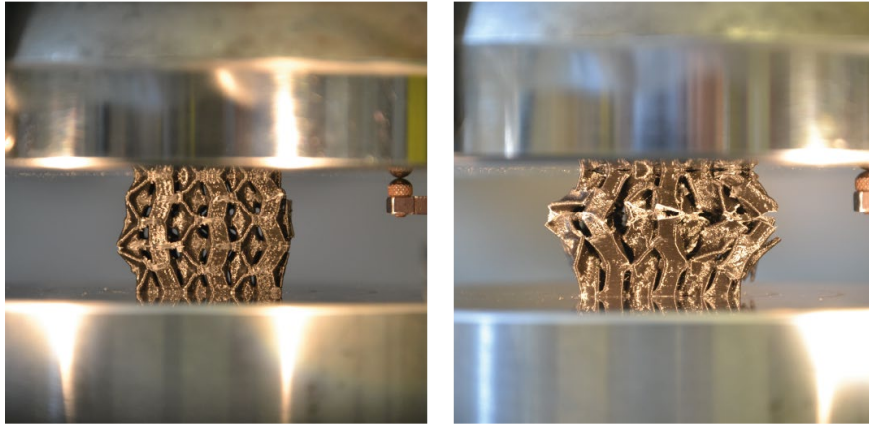
Figure 104 *1.2.1 and 2.2.1 at strain 0.2*

of the unit cell doubled. At the same moment of the compressive tests, at the same strain, it could be observed a similar behaviour of the two BLSs, but 1.1.3 shows a higher resistance to compression (**Figure 103**). It is visible the deformation of the lattice but is not yet visible the fracture between unit cells layers 1 and 2. The BLSs 2.1.3 and 1.1.3 are the only two structures composed by two layers and half. Therefore, at their base, these structures are supported by the nodes: according to the photos and video of the specimens, it is possible to see that the last half layer of cells it is almost intact for most of the compressive test (**Figure 104**).
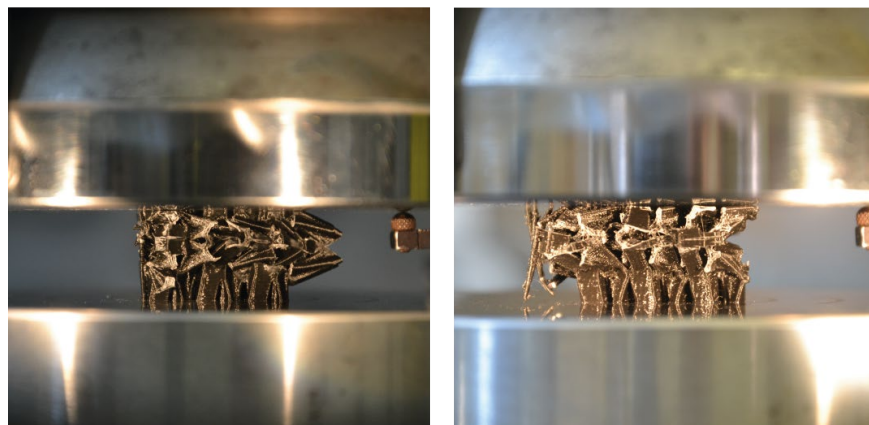
Figure 105 *1.1.3 and 2.1.3 at strain 0.4*

132
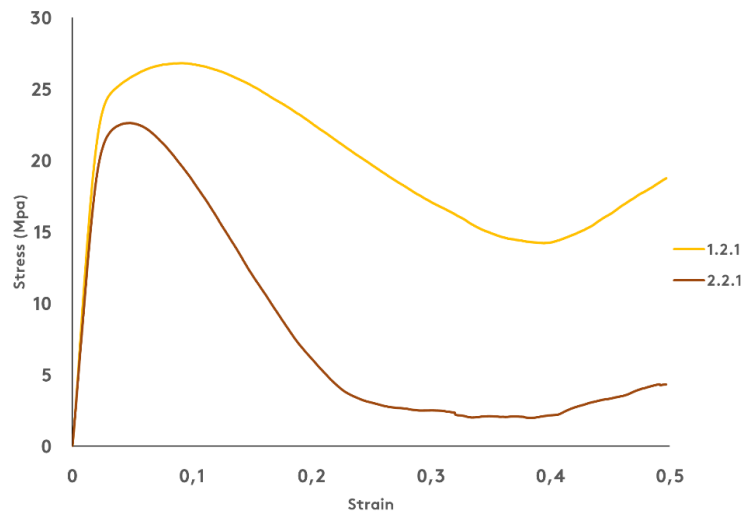
1.2.1 and 2.2.1

Figure 106 *1.2.1 and 2.2.1 stress-strain curves*

Both of the structure consist of a variation of the original versions of BLS; the variation consisted of an increase of fillet radius of the unit cells.

For structure 1, this modification helps the lattice to resist more under compression: in fact, since there is more material at the critical point of connection between the cells, the structure still fracture in those points at with higher strains. According to the curves in **Figure 106**, the BLS 1.2.1 shows both a higher IPCF (24.5±2.5 MPa compared to 22±1 MPa) and EA (205.6±28.5 J compared to 86.3±18.5 J).

In **Figure 107** a comparison of all the stress-strain curves of the BLSs is represented.
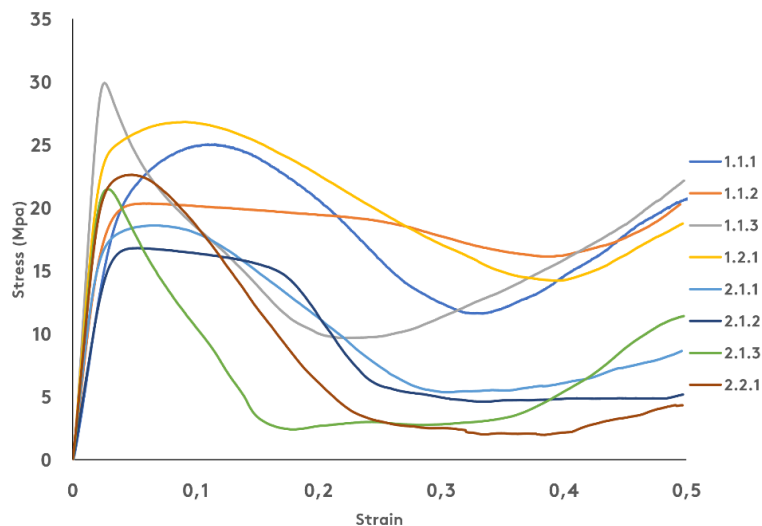
Figure 107 *Comparison of all the BLSs' stress-strain curves*

Structure 1

The failure mode of 1.1.1 and 1.1.2 is slightly different and this is related to the presence of nodes, the quantity of which is doubled in the second structure; for this reason, the second structure supports compression without splitting. For both of the structures, the fractures appear at the junction point of the unit cells: in any case, the unit cell per se is not breaking into two parts; this means that the feature of the node is effective.

Also BLS 1.1.3 is a variation of BLS 1.1.1: the height of the unit cells is doubled; this means that the quantity of nodes is halved, and this explains the reason why the resistance to compression is lower and the trend of the curve at the first stages. This factor also influences the behaviour of the lattices: buckling happens because of the ratio between the diameter of the profile and the height of the cell, which is doubled. It should be noticed that 1.1.3 has the highest value of Young's modulus, then the BLSs 1.1.3 is the stiffest among all the lattices.

According to these observations, the structure 1.1.2 (with unit cell with halved height) perform better under compression than the BLS 1.1.3 (based on unit cell with doubled height); BLS 1.1.2 also seems to be better than the original structure 1: with the same porosity, the EA of structure 2 is higher and the specimen resists better the compression.

The porosity of the structure 1.2.1 is slightly lower than the one of BLS 1.1.1 (P= 46% vs P= 48%), because of the increase of the value of fillets. Nevertheless, the addition of material in the correct points helps the structure to better resist the compression; in fact, the PLA is added at the most critical zone of the structure 1.2.1; the connection between the unit cells is stronger for the case with bigger fillets.

In general, it is suggested that the part were the unit cells are in contact is a critical point: in order to avoid this problem or to reduce this effect, the shape of the cell should be modified in order to increase the quantity of material in that part (e.g., by increasing the dimension of the fillet such as unit 1.2.1); also, it seems that when the layers of unit cells are vertically packed, it would be better to increase the contact zone

between them. Actually, by observing how the structure geometry is obtained, it is evident that the reason why fracture happens between cells is not just the necessity to increase the fillet radius.

By analysing the shape, it is possible to see that on the top and bottom of the cell, there is a vertical extrusion that allows the unit cells to enter in contact. Then, the profile is lofted in order to generate the shape. Probably, the sudden change of cross section, make the structure weaker at those points. In **Figure 108** it is possible to see the extrusion of the profile, highlighted with grey colour.
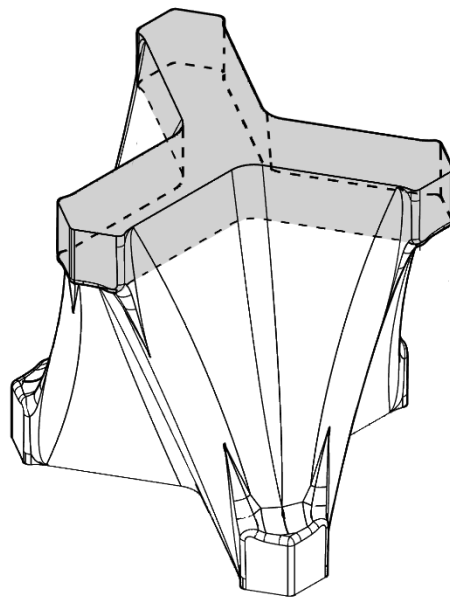
Figure 108 Unit cell 1 profile extrusion

Structure 2

As for unit cell 1, the second variation of the BLS based on unit cell 2 has the height of the unit cell halved. The curve of BLS 2.1.2, like for 1.1.2, has a different behaviour, related to the presence of nodes, the quantity of which is doubled in this lattice.

In general, the fracture happens in the zone where the unit cells enter in contact: also in this case, like with BLSs of series 1, the unit cell per se are not failing; this means that the

135

feature of the node is effectively helping the structure to stand the compressive plate.

Lattice structure 2.1.3 consist of a variation of 2.1.1, the ratio between height and diameter of the unit cells is doubled. Then, because of the value of this ratio, there is an increased effect of buckling.
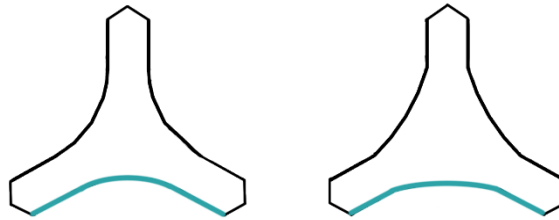
Figure 109 Original unit cell 2 profile and unit cell 2 with varied fillet

According to the analyses and the results of structure 1.1.1 and 1.2.1, it is expected that the structure 2.2.1 shows a better resistance to compression because of the presence of bigger fillets. Indeed, by observing the unit cells, it is possible to notice that the variation of fillet in the second case is not involving the connection point of the unit cells, but it is only related to the general shape of the cell.

Therefore, by comparing 2.1.1 and 2.2.1, it is evident that the better structure in this case is the first one.

Structure 2.2.1 with varied value of fillets is not as much "stable" as 2.1.1 because the unit cell profile is composed by a core and three slenderer wings: by increasing the fillets, the core becomes even bigger when compared to the wings (**Figure 109**); this geometrical feature is not ideal for compression; the local stress in fact is more concentrated at the connecting point of the unit cells and the structure itself is not capable of adequately resist axial compression because it represents a critical point.

In general, note that in **Figure 110** it is possible to see that, when the structure cracks, in the internal part of the lattices there are defects and voids: this cause influenced the behaviour of all the structures under compression, too.
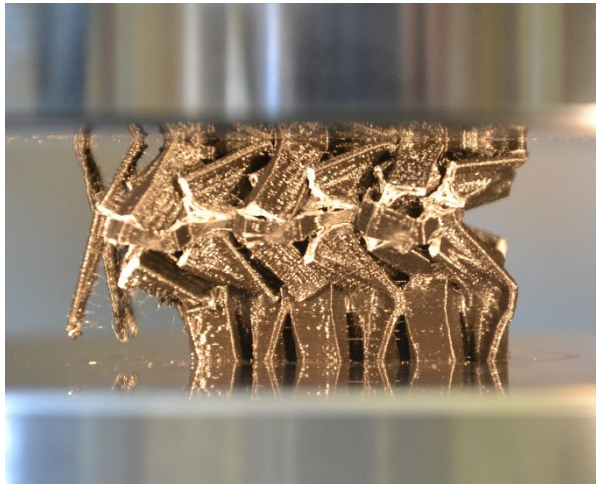
Figure 110 specimen 2.1.3 fractures

Comparison between structure 1 and 2

By comparing the unit cell 1 and the unit cell 2, the biggest difference is how the lofted profile is generated: in case of structure one, the profile has a geometry that is more "constant and balanced", while the second one is composed of a bigger core and three slenderer wings. The unit cells profiled are represented in Figure 108.

By increasing the fillet, like in BLS 1.2.1 and 2.2.1 there are different effects on the structures: for BLS based on unit cell 1, this modification helps the lattice to resist more under compression: in fact, since there is more material at the critical point of connection between the cells, the structure still fractures in those points but at higher strains. For BLS based on unit cell 2, this improvement is not happening. The increase of the radius fillet is not involving the connection
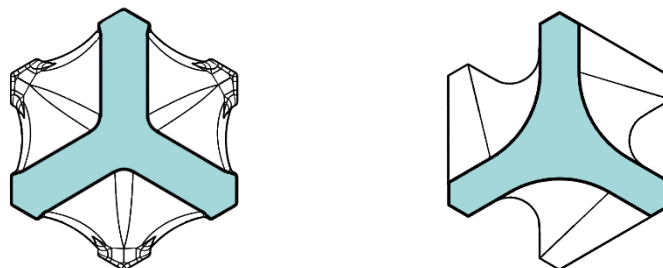
Figure 111 Unit cell 1 and unit cell 2 profiles

137

point of the cells but only the core of the unit. The dimension increment of this part of the cell is worsening the situation, since the three wings become too slender and even unsuitable to properly stand the compressive plate. Then, the connection point among the unit cells (**Figure 112**) results to be a weak point.

In conclusion, the lofted profile of structure 2, that was considered for a possible torsion application, is not ideal for compression; all the structures made by unit cells 2 and their variations are showing lower resistance to compression; also, the specimens during the compressive tests were more likely to fail because of fractures at lower strain. The main issue is that the stress is more concentrated at the connecting point of the unit cells; but, because of the geometry of the lofted profile, the structure is not capable to adequately resist axial compression, since contact points represent a critical zone that easily fractures.

According to the results, among all the BLSs, the two best structures are 1.1.2 and 1.2.1.

1.2.1 is characterised by slightly higher value of EA (205.6±28.5 J in comparison to 203.6±7.09 J). However, by observing the failure mode and the behaviour of the specimens during the compressive tests, the BLS 1.1.2 is less damaged than the other one under the same strain; there are no visible fractures between the unit cells while BLS 1.2.1 shows some cracks
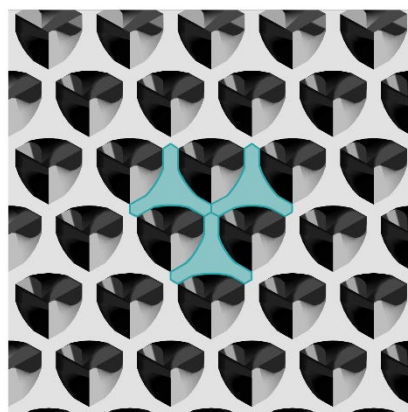
Figure 112 *Unit cell packing of BLS 2.2.1*

among the layers of units. The porosity of these lattices is almost the same, 48% (1.1.2) and 46% (1.2.1).

The BLSs during the compressive tests are showed in **Figure 113**.
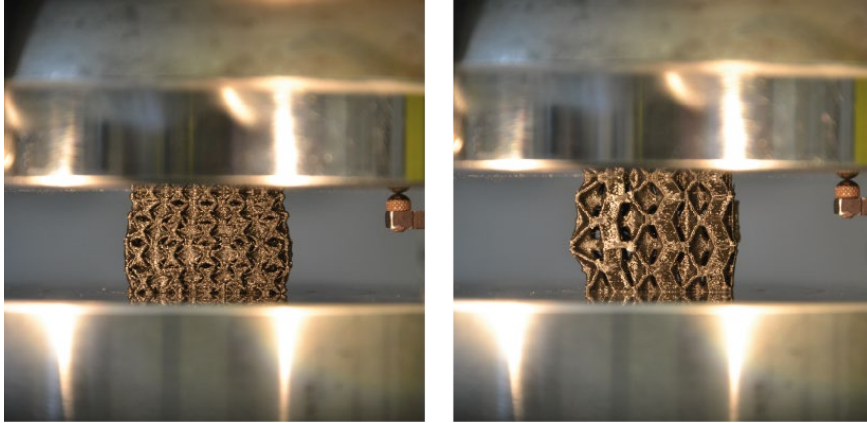
Figure 113 1.1.2 and 1.2.1. at strain 0.3

In conclusion, three main observations could be made: the feature of the node or diaphragm, inspired by the bamboo is effectively making the structures more resistant to compression, considering that during the experimental tests it is always possible to see that the unit cells are not breaking into two parts.

Another positive aspect of this feature could be identified in structure variations 3 (the BLSs with doubled height of the cells): in fact, it is possible to notice that the cube bases are composed of the bamboo's diaphragm feature. These elements allow the last layer of cell to remain almost intact during the compressive tests, avoiding the cells to expand and split.

The weak point of the structures in fact results to be the connection point of the unit cells: the solution to this problem has been found in structure 1.2.1, which has increased dimension of fillets, compared to the original structure.

Finally, according to the dimensional variations, halving the height of the unit cell by keeping all the other dimensions unvaried (also porosity remains unchanged) allows to have a different and better failure mode: when compressed, the structures 1.1.2 was more compact and it was the only structure to not show fracture between the unit cells. In **Figure**

115, **Figure 114**, **Figure 116** and **Figure 117** a comparison for each of the mechanical properties considered was made.
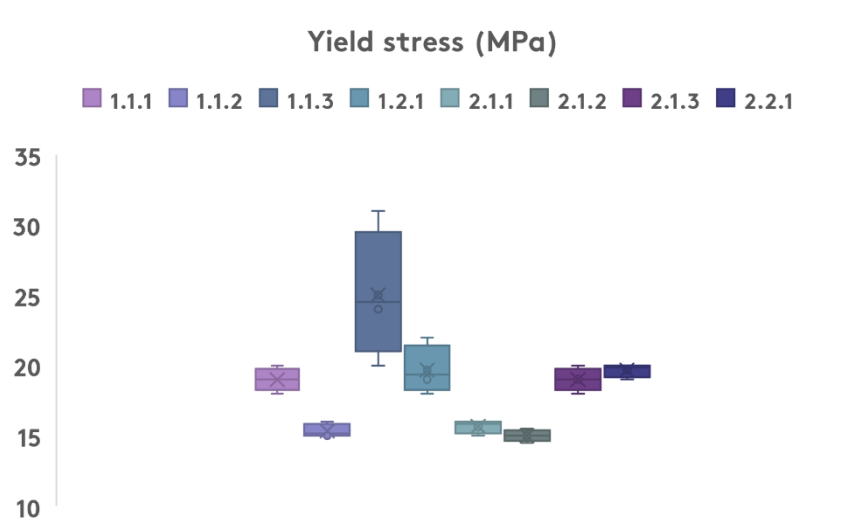
Figure 114 BLSs Yield stress
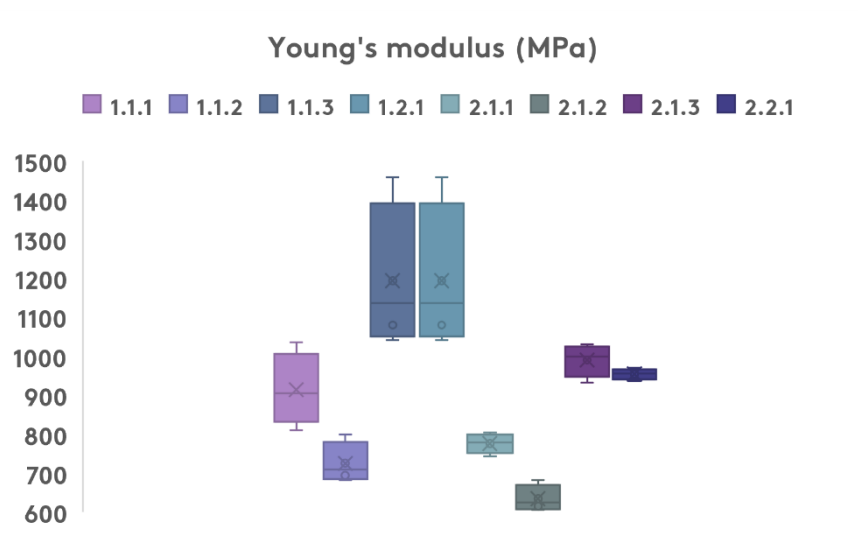
Figure 115 BLSs Young's Modulus
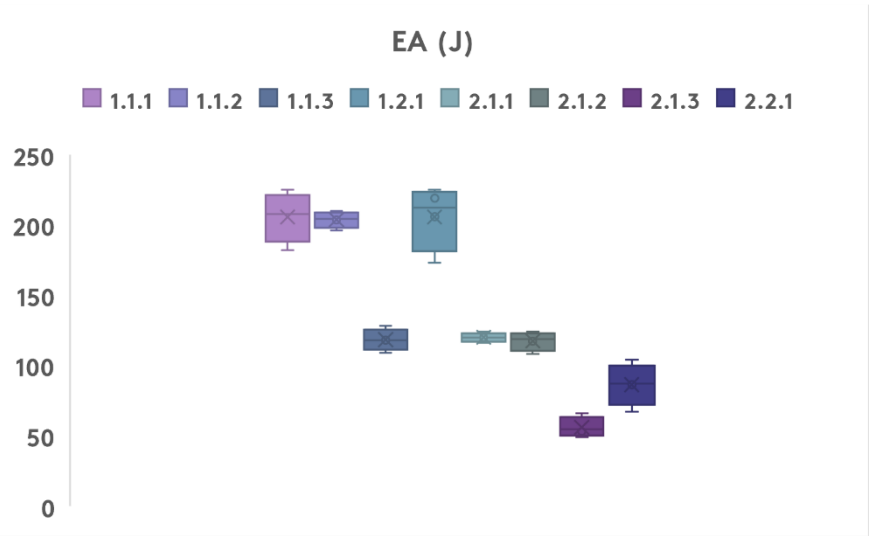
Figure 116 *BLSs EA*
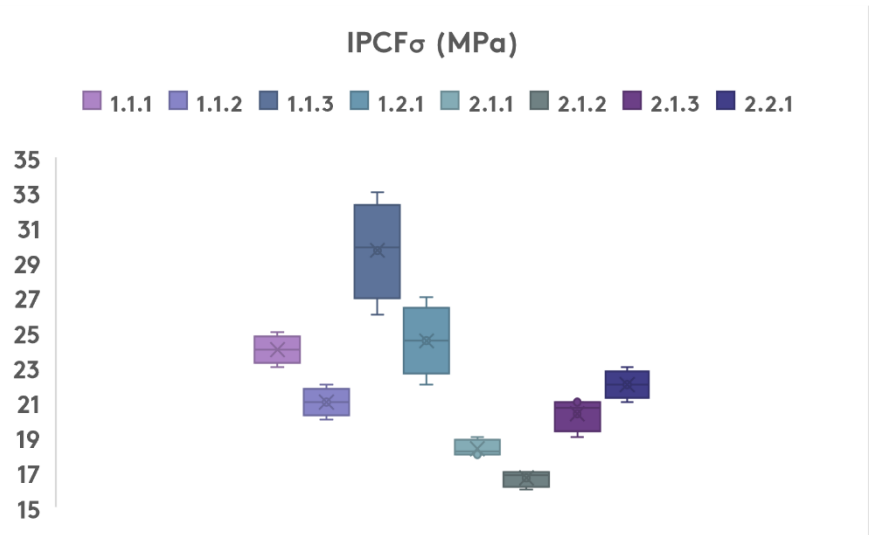
Figure 117 *BLSs IPCF*

1.1.1	Test 1	Test 2	Test 3	Avg.	St. dev.
E (MPa)	1035	809	896	913	±113
σy (MPa)	19	18	20	19	±1
εy	0.02	0.02	0.02	0.02	±0
IPCFσ (MPa)	24	23	25	24	±1
IPCFε	0.09	0.1	0.09	0.093	±0.005
EA (J)	182	225	210	205.6	±21.8
εd	0.4	0.45	0.47	0.44	±0.03

2.1.1	Test 1	Test 2	Test 3	Avg.	St. dev.
E (MPa)	804	780	743	775.6	±30
σy (MPa)	16	16	15	15.6	±0.5
εy	0.02	0.02	0.02	0.02	±0
IPCFσ (MPa)	19	18	18	18.3	±0.5
IPCFε	0.06	0.07	0.07	0.06	±0.005
EA (J)	116	120	124	120	±4
εd	0.4	0.4	0.4	0.4	±0

1.1.2	Test 1	Test 2	Test 3	Avg.	St. dev.
E (MPa)	798	682	694	724	±63
σy (MPa)	16	15	15	15.3	±0.5
εy	0.02	0.02	0.02	0.02	±0
IPCFσ (MPa)	20	21	22	21	±1
IPCFε	0.06	0.06	0.03	0.05	±0.01
EA (J)	196	210	205	203.6	±7.09
εd	0.4	0.4	0.4	0.4	±0

2.1.2	Test 1	Test 2	Test 3	Avg.	St. dev.
E (MPa)	682	605	615	634	±41
σy (MPa)	15	14.5	15.5	15	±0.5
εy	0.024	0.025	0.027	0.025	±0.001
IPCFσ (MPa)	17	17	16	16.6	±0.5
IPCFε	0.05	0.05	0.04	0.04	±0.005
EA (J)	124	120	108	117.3	±8.3
εd	0.49	0.48	0.44	0.47	±0.02

1.1.3	Test 1	Test 2	Test 3	Avg.	St. dev.
E (MPa)	1458	1079	1040	1192	±230
σy (MPa)	20	31	24	25	±5.5
εy	0.02	0.03	0.025	0.025	±0.005
IPCFσ (MPa)	30	33	26	29.6	±3.5
IPCFε	0.025	0.035	0.03	0.03	±0.005
EA (J)	109	128	118	118.3	±9.5
εd	0.25	0.27	0.32	0.28	±0.03

2.1.3	Test 1	Test 2	Test 3	Avg.	St. dev.
E (MPa)	1006	932	1030	989.3	±51
σy (MPa)	19	18	20	19	±1
εy	0.02	0.02	0.02	0.02	±0
IPCFσ (MPa)	21	19	21	20.3	±1.1
IPCFε	0.03	0.03	0.03	0.03	±0
EA (J)	53	49	66	56	±8.8
εd	0.3	0.3	0.3	0.3	±0

1.2.1	Test 1	Test 2	Test 3	Avg.	St. dev.
E (MPa)	941	1008	1036	995	±48
σy (MPa)	18	22	19	19.6	±2
εy	0.02	0.02	0.02	0.02	±0
IPCFσ (MPa)	22	27	24.5	24.5	±2.5
IPCFε	0.09	0.09	0.09	0.09	±0
EA (J)	173	225	219	205.6	±28.5
εd	0.4	0.4	0.4	0.4	±0

2.2.1	Test 1	Test 2	Test 3	Avg.	St. dev.
E (MPa)	969	956	936	953.6	±16.6
σy (MPa)	20	20	19	19.6	±0.57
εy	0.02	0.02	0.02	0.02	±0
IPCFσ (MPa)	23	22	21	22	±1
IPCFε	0.04	0.05	0.05	0.046	±0.005
EA (J)	67	104	88	86.3	±18.5
εd	0.4	0.4	0.4	0.4	±0

Table 20 BLSs mechanical properties recap
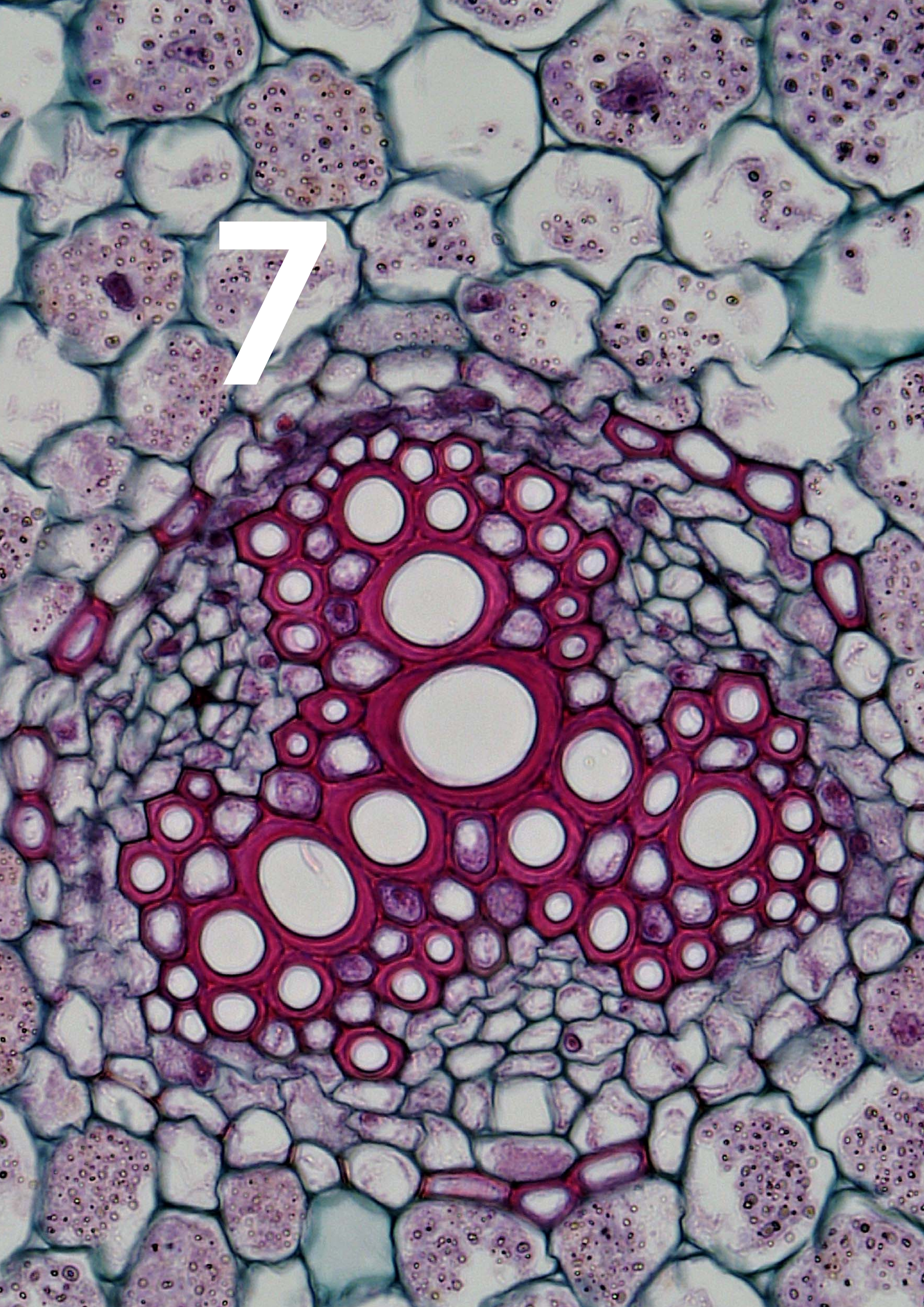
7 Conclusions and future developments

In this work, PLA FDM-manufactured bio-inspired lattice structures have been designed and then experimentally and numerically studied with the purpose of resistance to compression and energy absorption applications. A literature review has been carried out to develop novel bio-inspired unit cells and to understand in detail the different aspects to be considered to make the structures resistant to compressive load. A numerical model has been developed to predict compressive mechanical properties i.e., elastic modulus and yield stress, while the validation of the model has been carried out by direct comparison with experimental data. Two unit cells were developed and for each of them four lattice structures were made: morphological variations were introduced to the original unit cell in order to analyze the effect on compressive strength. The height of the unit cell was doubled or halved, and the dimension of fillet was varied. Structure based on unit cell 1 have a porosity of 46-48%, while the BLSs based on unit cell 2 have a porosity of 55-57%.

According to the analysis of stress-strain curves and of mechanical properties obtained by the experimental tests, structure 1.1.3 has the highest stiffness (1192±230 MPa), the highest Yield stress (25±5.5 MPa) and the highest IPCF (29.6±3.5 MPa), but its EA is the lowest among the unit cell 1 variations (118.3±9.5 J). Its curve in fact is characterised by a high peak, but then the values of the curve tend to decrease fast. The highest value of EA is shown by BLS 1.2.1: 205.6±28.5 J.

In general, according to the results, the structures based on unit cell 1 performs better under compressive load than the unit cell 2. The main reason is that the profile used to generate the shape of the second unit cell is composed of a big core and three slender wings, which make the structure weak at the connection points between the cells. This is evident from the failure mode of the specimens but also from the resulted EA. The geometry of the profile of unit cell 2 in fact was considered

for hypothetical torsion applications, therefore is not ideal for compression.

Three main geometrical features should be considered and discussed: the nodal diaphragm, the effect of fillet radius and the effect of height variation.

- The bamboo-inspired feature effectively made the structure more resistant to compression; as it could be seen for each of the considered structures, during the compressive tests, the unit cells that compose the BLSs are not breaking into two parts. This behaviour confirms the initial hypothesis made on this morphological element. Another positive aspect of this feature could be identified in structure variations 3 (the BLSs with doubled height of the cells): in fact, since the lattice bases are composed of the bamboo's diaphragm feature, the last layer of cell remains almost intact during the compressive tests, avoiding the cells to expand and split.

- By observing the specimens under the compressive test, some difference could be identified when dealing with the original structure 1.1.1 and with its variations with halved height 1.1.2 and with doubled height 1.1.3 (these structures have the same porosity).
  During experimental tests, structure 1.1.2 showed a better resistance to compression and a different failure mode: no fractures were visible among the different layers of unit cells as opposed to both BLS 1.1.1 and 1.1.3. As expected, structure 1.1.3 is prone to buckling because of its unit cells' doubled height.

- BLS 1.2.1 with bigger fillets also showed a better resistance to compression when compared to original BLS 1.1.1. The increase of radius fillet in fact allowed the structure to avoid severe fracture between unit cells: the EA of the structure is slightly higher than the EA of 1.1.1, and an increased value of Young's Modulus make

the structure stiffer at the contact point among unit cells.

7.1 Future developments

According to the results, a hybrid structure composed by halved-height unit cells 1 (1.1.2) with bigger fillets (1.2.1) could be considered for further research and tests. The vertical packing of the unit cells could also be modified in order to allow the structure to have as a base the diaphragms, in order to help the BLS to resist the compression and to avoid splitting between the cells that composes the layer placed at the base of the structure. A FE model of this hybrid structure could be considered for further developments.

The two unit cell considered were not thought only for applications that require resistance to compression. In fact, the feature of diaphragm could provide resistance to bending load; while the shape of the unit cell 2, inspired by the buttress core of Burj Khalifa, was considered for hypothetical torsion applications. Therefore, it would be interesting to analyse the effect of these morphological features on the structure's resistance to different typologies of load.

Another further development could be the possibility to test the structure under dynamic tests, in order to analyse the behaviour for impact applications.

Experimental tests and FEA should be conducted in order to understand the behaviour of the structures under different loads.

7.2 Potential applications

Despite the objective of this research work was the development and testing of design of novel structures for energy absorption, a part of research was focused on the future developments for potential applications. The aim was to define application fields that better exploit all the potentials of the FDM process, but also to consider the need of making the final product feasible in terms of industrial production. Indeed, the developed BLSs could be manufactured only through additive manufacturing process; then it is important to define not only the possible applications field, but also constraints and limits of 3D printing, according to the aspect of industrial production.

The terms "energy absorption" is immediately referred to the idea of protection [1]: there are different possibilities to develop an impact resistant structure to implement various protective devices, then, a macro distinction need to be considered:

- many applications for energy absorption are related to personal protection, from helmets to knee pads or elbow guards;
- energy absorption for transportation and storage of goods. More in detail, transportation of delicate and valuable object could be considered, such as musical instruments.

Another interesting field for this type of applications could be the biomedical and biomechanics field:

- from corrective insoles, prosthesis and innovative 3D printed casts and splints to soles that are specifically designed for different sports.

In order to identify advantages and disadvantages of additive manufacturing technologies, they need to be defined not only from a technical point of view, but it also important to consider the economical aspect of this type of process.
Additive manufacturing (AM) is a prototypical example of a flexible manufacturing technology, as it conceptually enables

a vast variety of outcomes in manufacturing in any given sequence on one stable manufacturing system. Other than consumables (materials) and the actual AM machine, only the product's digital 3D model is necessary for manufacturing. Setup and changeover costs are negligible as only a different CAD file needs to be uploaded into the machine when changing the product to be manufactured; neither tools nor molds are necessary. As a result, AM enables product individualization without cost penalties. By adding material layer by layer until the product is finalized, AM has fewer process and design restrictions. Furthermore, an increase in design complexity does not mean higher production costs, contrary to conventional technologies where production unit costs usually increase with a higher complexity of product design. [53]

Product designs can be optimized according to their desired function rather than restricted from production technology or supply chain constraints. Furthermore, firms are able to offer highly customized products that match customer preferences. Product customization potentially yields an increase in customers' perceived product value and, thus, higher willingness to pay.

Figure 119 A complicate shape obtained with AM technology (brake caliper by Bugatti) [102]

An important constraint to consider is relatively low production throughput speed compared to conventional production methods (e.g., injection molding). While product variety can be increased without cost penalties in manufacturing, AM cannot exploit economies of scale when increasing the production volume of a product variant. Therefore, mass production of standardized parts will likely remain the domain of conventional manufacturing technologies. [53]

Also, 3D printed objects must be limited in size: the build space of AM machines sets a physical limit to product dimensions; the volume that can be obtained with standard 3D printers ranges from 80 to 400 cubic mm. [39]

Therefore, FDM should not be seen as a constraint, because of the complex shape of the lattices (that cannot be produced through traditional manufacturing processes), but it is a process that has many advantages that could be investigated and exploited. Freedom of shape, precision in reproducing details and easy personalisation of each variant of the product are some of the possibilities that this process offers. In **Figure 119** an example of a complicate shape and rich of details, obtained through AM technology.

Materials
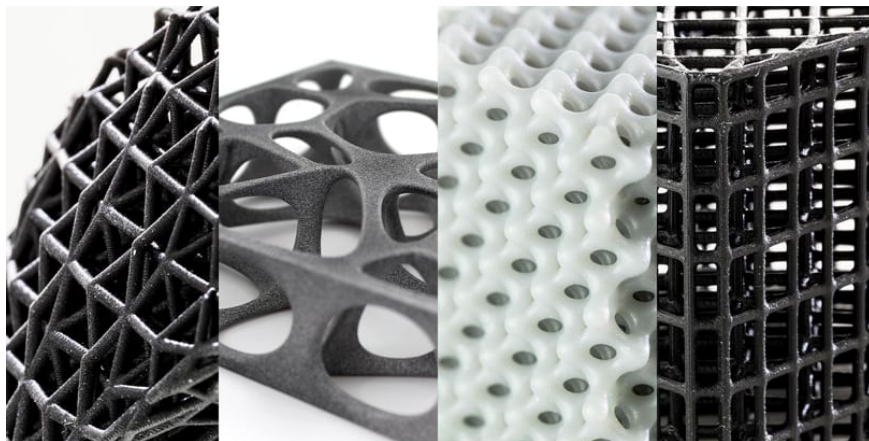
Figure 120 Various cell structures and materials [103]

In order to consider future application fields and developments, the BLSs could be made in other polymers or

150

materials and then tested to understand the mechanical behaviour and how the resistance to impact is changing from the structure made by the original material, PLA. In **Figure 120** an example of different materials and typology of unit cells. Other common polymers that are already used for 3D printing are ABS and PA.

- PLA (Polylactic acid) is a thermoplastic polymer widely used for prototyping; it is made from renewable resources such as sugarcane or corn starch. It is stronger and stiffer than ABS and PA and it is characterised by low melting temperature and minimal warping. These factors make PLA one of the easiest materials to 3D print successfully. Unfortunately, its low melting point causes it to lose virtually stiffness and strength at temperatures above 50 degrees. In addition, PLA is brittle: 3D printed objects made by this material are not durable and have low impact resistance. Although PLA is the strongest of these three plastics, its poor chemical and heat resistance make it adaptable almost exclusively to hobbyist applications.
- ABS (Acrylonitrile Butadiene Styrene), while weaker and less rigid than PLA, is a tougher, lighter filament, with better impact resistance. It requires effort to print because it's more heat resistant and prone to warping. The improved durability over PLA lends ABS to some more practical applications, such as prototyping and low-stress end-use parts.
- PA (Polyamide or commonly known as Nylon) is flexible and durable, but also less strong and stiff than PLA and ABS; it is also characterised by an impact resistance ten times that of ABS. It requires extra care to print and it needs to be extruded at high temperatures. Due to its tendency to absorb moisture from the air, it must be kept in a dry environment. Nylon is tougher and more resistant to chemicals than ABS and PLA, but its low strength and stiffness keep it from being used in the manufacturing industry. As a result, have been introduced nylon-fibre mixtures. [54]

Composite fibres improve specific properties of traditional 3D printed parts. This results as an important advantage over traditional thermoplastics used in 3D printing. In **Figure 121** Carbon fibre 3d printed bike frame the one-piece frame of a bicycle, made in 3D printed carbon fibre.

Carbon fibre filaments use tiny fibres that are infused into a base material; several filaments can be bought with carbon fibre fill: PLA, PETG, PA, ABS, and PC. The fibres cause the filament to increase in strength and stiffness and allow the 3D printed parts to be lighter and dimensionally stable, as the fibres will help prevent shrinking as it cools. Print settings (printing temperature, speed, bed adhesion, and extrusion rates) will be very similar to the normal settings used for the base material that the fibres were added to. However, due to the fibres, these materials are more likely to clog and can require special hardware to avoid damaging the printer. [55]

Figure 121 Carbon fibre 3d printed bike frame [104]

Product applications
CRASH BOX

With the rapid development of automobile industry in the world, safety performance has become one of the most important indexes of a vehicle; the increasingly interest in crashworthiness of vehicles has resulted in extensive research on the structural response of thin-walled metallic tubes, which are the most conventional energy-absorbing devices and have

been widely employed in the vehicle design and manufacture. Moreover, with the development of passive safety technology, how to improve vehicle safety performance is increasing attention. The crash box structure and design space limit its energy absorption capability [24]: to handle this problem, a filled crash box with BLS could be developed.

BICYCLE HELMETS

Personal protection is an issue when dealing with bicycle helmets: one of the most interesting aspect of this object that can be optimized is the energy absorbing capacity.

Most of the helmets are composed by the same elements: a hard outer shell attached to an inner layer. In case of impact, the outer shell dissipates a significant amount of the mechanical energy (34%), its function is to protect the head from sharp objects and to distribute the impact load over a larger area. The inner layer is mainly a foam, it absorbs the mechanical energy from the impact and distributes it over a large area, reliving the head from as much load as possible. The foam can be of many types but expanded polystyrene (EPS) is a common choice in bicycle helmets. How the material in the helmet is structured is limited by available manufacturing techniques and materials.

3D printing allows not only for the development and the manufacturing of new inner structures, but also for individual customization through tailor made helmets specifically designed for the user and its use case. [15]

A very innovative product and service is offered by HEXR: in order to allow users to buy customised and unique bicycle helmets, the company sends a fitting cap to capture head measurements at home with a

Figure 122 Hexr helmet [105]

153

smartphone fitting app. Once the company receives the data, they start the production and 3D print the helmet (**Figure 122**), that will be quality checked and then send to the client. Besides the big innovation of size customisation of the helmet, another main feature is the replacement of the internal EPS foam with a honeycomb structure made from Polyamide 11. [56]

A similar product is sold by KAV, a company that produces 3D printed custom hockey and bicycle helmets (**Figure 123**). The offered service is almost analogous to the HEXR one: a Fit Kit is sent to the client and then it is organised an online fitting session with one of their experts in order to ensure that the measurements are precise. Therefore, the helmet is 3D printed according to the measures and it is later sent to the final user.

Figure 123 KAV bycicle helmet [106]

An interesting diatom-inspired bicycle helmet concept and prototype was developed by Paula Studio. The helmet is composed by three honeycomb layers with various dimensions that were thought to absorb the shock due to possible impact but also to make the helmet as lightweight as possible.

Another interesting concept was based on the research and development of a new ultra-lightweight sandwich structure optimized for bending, inspired by butterflies' wings. The microstructure of the wing could be described as a gyroid: the sandwich was inspired by this geometry and then the designed structure was reinforced and implemented with carbon fibre-reinforced plastic (CFRP) rods. The structure was manufactured through the stereolithography (SLA) technique, and it was tested by finite element simulations and 3-point bending, quasi-static experimental tests. [57]

Another innovative project thought for bicycle helmet wouldn't have been possible without Additive Manufacturing. The company Kupol developed a helmet designed to react to impacts from any angle and absorb rotational forces, which are the characteristics of most cycling accidents. The most innovative aspect of the helmet is the replacement of the classical internal foam with a novel safety system. This system was composed by three main elements: an internal component designed to collapse on impact to take the brunt of the force; kinetic bumpers under the shell that cushion the head in the event of a fall at low speeds and over 100 sucker-like pods that offer an ideal fit and protection against quick rotational movements. All these features make this helmet safe, lightweight and breathable.

MUSICAL INSTRUMENTS CASES
Transport of delicate and valuable objects such as musical instruments requires adequate protection: they need lightweight but resistant cases in order to be easily transported. There are different typologies of cases, from the soft to the hard ones and the preference from one typology to another depends on the instruments. The shape, the value of the object and the habits of the final users help to define which case is more suitable.

For example, for electric guitars is preferred a rigid case, while for the classic ones is used the soft case. Flutes, trumpets, violins are the typologies of instruments that require a rigid case which, in general, is more expensive.

Hard cases are characterised by a rigid external shell (materials such as wood, metal, or carbon fibre, and often a combination of these is employed), while the inner part is shaped in order to secure the instrument but also to protect it from impact. The inner part is composed by padded foam: polyurethane or PVC foam that compose inserts and cushions. The core foam that is placed inside the rigid shell could be substituted by the BLSs: the 3D printed lattices' shape could be changed in order to be adapted to the different instruments and their dimensions; maybe with modular elements and an external rigid shell with fixed size.

SHOES MIDSOLES

Adidas recently launched the Adidas Futurecraft 4D pair of shoes with the first 3D printed midsole. Adidas teamed up with Carbon3D, a firm that has pioneered a new AM technology. The midsole material is made out of a blend of UV curable resin and polyurethane, a stiff and durable elastomer. This high-performance monolithic component has different lattice structures in the heel and forefoot, to account for different cushioning needs of the foot while running (**Figure 124**). The lattice geometry, that consists of 20000 individual struts, is designed to provide optimum cushioning and impact control. The design also considers years of athlete data gathered by Adidas. As a result of AM technology, each sole is customized to an individual's unique footprint and running pattern. [58] [59]

Figure 124 Adidas Futurecraft 4D midsole [107]

Also New Balance collaborated with a 3D printing company, 3D Systems, to develop midsoles using SLS technology and a thermoplastic elastomer material. The objective was to design the midsoles with new geometries thought for maximum shock absorbance and weight saving. [60]

INSOLES

The most well-known type of orthotic is the shoe insole, which is mostly used to non-surgically correct foot and ankle problems.

Phits™ Insoles is a company that directly translate gait analysis into custom 3D-printed insoles. To realize this innovation, their dynamic measurement foot scan solutions was combined with a specific 3D printing software. Patients benefit greatly from customization since these orthotics can be matched to the specific issues and they also match each individual foot perfectly. [61]

CASTS AND SPLINTS

Another possible medical application to implement is the plaster cast: a covering made of plaster of Paris that is put around part of someone's body, forming a hard case to protect them while a broken bone repairs itself. [62]

The skin under the plaster itches, and it is not possible to avoid the contact with the skin; the cast is heavy and it is complicated to take a shower without damaging it: in general it is required to temporarily cover the cast with waterproof materials; also complications like ulcerations and infections can arise [63]. A new 3D printed cast should be lightweight, it should allow the skin to breath and it should be easy to practice everyday activities when wearing it.

Then, an interesting application for cast could involve the BLSs for this medical application. The lattice is made to protect the injured part of the body from impacts, waterproof, made in PLA; polylactic acid is a polymer that is biodegradable and naturally decomposes in a short period [64]. For this application, durability is not a long-term issue: in general, the cast should be worn from three to four weeks (this period varies according to injuries, but typically the recommended period to wear a cast is no more than a month). [65]

It is well known that 3D printing world and DIY (Do-It-Yourself) community go hand-in-hand. In fact, in 2014, on the website Thingiverse, it was possible to download the STL files of a wrist brace in order to 3D print it: +LAB, the 3D printing Lab of Politecnico di Milano, created the prototype that could be easily adapted. Additive manufacturing technologies allow to easily customise the dimension of the casts according to everyone's size, avoiding the necessity of casts specialised staff like orthopaedic plasterer. [66]

Even if in 2014 the possibility to wear a 3D printed brace or splint was only achievable by means of amatorial and-hobbyists' solutions, during last years this possibility became reality and it was realised by various companies or services.

For example, the Children's Hospital Colorado gives their patients the possibility to choose 3D printed casts and splints instead of the classical plaster casts. To ensure that the child's cast fits them perfectly, a paediatric orthopaedic expert moves a digital scanner around the injured limb while they hold it still. This typically takes less than a minute and ensures the cast is customised on the child and their injury. While the cast is 3D printed (around four days), a temporary cast or splint to wear is provided.

In this case, the products are specifically aimed to children: it is more comfortable during everyday activities and also it avoids the itchiness and the difficulty in wearing bulky orthopaedic casts. [67]

The discomfort of traditional cast is experienced not only by children, but also by any adult person. Therefore, a similar service is offered by Cortex Cast, Novacast, ActivArmor (**Figure 125**) Fathom, Exiom, Ortho Baltic: they 3D scan patients' limbs or use algorithms to define the dimensions of the customised cast. [68] [69] [70]

Figure 125 *Activarmor 3D printed cast [108]*

PROSTHESIS

The medical field benefits from the wide range of advantages offered by AM: thanks to the mass-customization opportunities and the flexibility of the manufacturing and design processes, 3D printing becomes a real alternative for this sector and it is tackling a particular issue: prosthetics. Many companies such as Unyq are using the advantages of generative design and additive manufacturing to create a brand-new approach to prosthetics both in terms of form and functionality. Manufacturing adapted and quality devices for amputees is actually a struggle all over the world, as these prosthetics are expensive and most of the time, poorly adapted to the patient's particularities. [71]

In a study published in 2015, a 3D-printable foot prosthesis was designed and manufactured using PLA filament. The research aimed to minimize the costs, so that the product can be printed at home, and donated to residents of developing

countries; the results were appealing. However, the low heat resistance of PLA might cause excessive deformation and it is not the ideal material as far as its mechanical properties are concerned. Different types of ABS and PC-ABS are often used in the industry for load-bearing parts. The energy storing nature of these plastics is beneficial for the user during the push-off phase. Carbon and glass fibre filaments are also used with FDM in order to create strong composite material parts [72].

Being light and small, strong and durable are the objectives for a good prosthetic foot. Therefore, the main factors to consider are as follows:

- materials. The materials in a prosthetic foot differ by activity level. Wood, plastic and foam are usually found in feet thought for individuals who have low activity levels and require stability. Carbon fibre feet are lightweight and meet the functional needs for shock absorption and energy efficiency.
- Function. For people who cannot walk, the function of prosthetic feet is largely cosmetic. For those who are most active, a prosthetic foot must mimic a normal foot during the act of walking. It must act as a shock absorber, adapt to uneven terrain and provide a smooth rollover from heel to toe.
- Multi-axial motion. Some prosthetic feet are designed to allow the foot to move in multiple planes; to raise and lower the forefoot; to move the forefoot to the left and right and so on. Multi-axial motion is also needed to walk comfortably on uneven ground.
- Energy storage. The carbon fibre acts as a spring, compressing as the weight is applied and propelling the user forward as the foot rolls, returning energy to the step as the spring releases. Some prostheses have one spring in the heel and a second spring in the forefoot, for walking at various speeds, running, climbing hills or descending stairs. [73]

As an example, dynamic prosthetic foot should be lightweight and suitable for different activities: hiking, jogging, golfing,

biking; but mainly they are used for walking. [74] For this application, materials such as carbon fibre or ABS are ideal in order to make the structure more resistant and durable.

Customizable functional prostheses creation is now possible thanks to 3D printers: getting adapted devices and prosthetics will benefit the patients and improve their quality of life during a limb loss. Moreover, developing a complex project as prosthetics is expensive with traditional manufacturing techniques: if the objective is to adapt it to the morphology of the patient, additive manufacturing appears to be the most efficient technique [71]. The geometric freedom provided by 3D printing helps customize prostheses to meet the varying needs of patients. The CAD models are adjustable after testing with amputees, based on their feedback. Using this method an optimal geometry can be created for low-volume production or for individual custom prostheses. [72]
3D printing allows to adapt the prosthesis to everyone's necessities and needs, but also it could be useful when dealing with paediatric prosthetic feet and children's growth. In fact, a child will require a new prosthesis approximately every 6 months until adulthood to accommodate growth and development. [75]

The BLS results to be ideal for this typology of biomedical application not only for the manufacturing process that allow for personalization and customization of the product, but also for the ability to absorb energy. After hypothetical impact test, the structure could also be applied to dynamic prosthetic foot that are not just used for walking, but also for other activities (biking, hiking, jogging…).
Another important factor is its porosity: the final product would be lightweight, and this is a fundamental requirement for prosthetic feet.
According to the different typologies of prosthetic feet, mainly related to the activity level of the user, the properties of the foot could be modulated according to the different needs: for example, in different zones of the prosthesis, the geometrical aspects of the unit cell could be adapted to provide site-specific stiffness where needed.

In **Figure 126** and **Figure 127** a graphical representation of a prosthetic foot with bio-inspired lattice structure is shown.

Figure 127 Potential application of BLSs
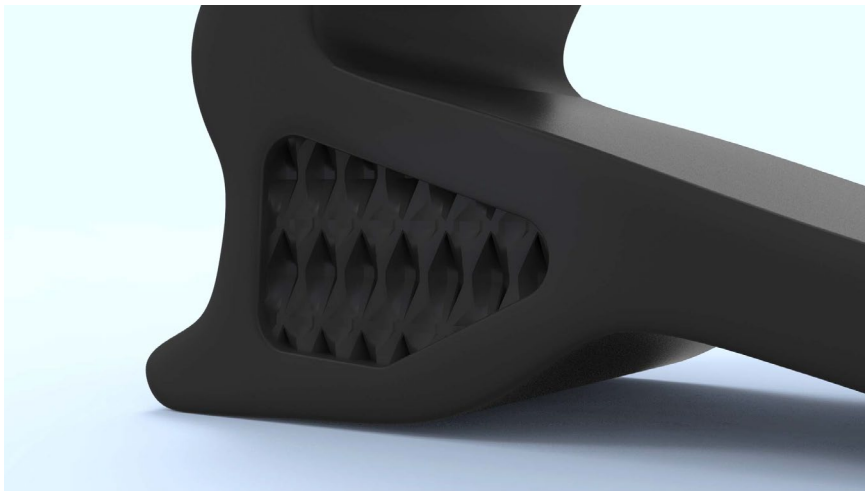
Figure 126 Potential application of BLSs

References

[1]   G. Lu and T. X. Yu, Energy Absorption of Structures and Materials, Cambridge: Woodhead Publishing, 2003.

[2]   T. Thomas and G. Tiwari, "Crushing behavior of honeycomb structure: a review," *Int. J. Crashworthiness,* pp. 555-579, 2019.

[3]   X. Wang, R. Qin, F. Gao and B. Chen, "Energy absorption performance of hexagonal multi-cell tube with hierarchy under axial loading," *Thin-walled structures,* December 2021.

[4]   S. Palanivelu, W. Van Paepagem, J. Degrieck, J. Vantomme and D. Kakogiannis, "Comparison of the crushing performance of hollow and foam-filled small scale composite tubes with different geometrical shapes for use in sacrificial cladding structures," *Composites: Part B,* pp. 434-445, 2010.

[5]   F. Tarlochan, S. Ramesh and S. Harpreet, "Advanced composite sandwich structure design for energy absorption applications: Blast protection and crashworthiness," *Composites Part B: Engineering,* pp. 2198-2208, July 2012.

[6]   T. Maconachie, M. Leary, B. Lozanovski, X. Zhang, M. Qian, O. Faruque and M. Brandt, "SLM lattice structures: Properties, performance, applications and challenges," *Materials & Design,* 2019.

[7]   L. J. Gibson, "Modelling the mechanical behavior of cellular materials," *Mater. Sci. Eng. A,* pp. 1-36, 1989.

[8]   M. Ashby, "The properties of foams and lattices," *Phys. Eng. Sci.,* pp. 15-30, 2005.

[9]   H. Niknam and A. H. Akbarzadehab, "Graded lattice structures: Simultaneous enhancement in stiffness and energy absorption," *Materials & Design,* November 2020.

[10]   C. Tang, J. Liu, Y. Yang, S. Jiang and W. Hao, "Effect of process parameters on mechanical properties of 3D printed PLA lattice structures," *Composites part C,* November 2020.

[11]   Y. Du, D. Gu, L. Xi, D. Dai, T. Gao, J. Zhu and C. Ma, "Laser additive manufacturing of bio-inspired lattice structure: Forming quality, microstructure and energy absorption behavior," *Materials Science and Engineering: A,* 31 January 2020.

[12]   Y. Tang, G. Dong, Q. Zhou and Y. F. Zhao, "Lattice Structure Design and Optimization With Additive Manufacturing Constraints," *IEEE Transactions on Automation Science and Engineering ,* pp. 1546-1562, 27 April 2017.

[13]   N. S. Ha and G. Lu, "A review of recent research on bio-inspired structures and materials for," *Composites Part B,* 2020.

[14]   S. Yin, H. Wang, J. Li, R. O. Ritchie and J. Xu, "Light but tough bio-inherited materials: Luffa sponge based nickel-plated composites," *Journal of the Mechanical Behavior of Biomedical Materials,* pp. 10-18, June 2019.

[15]   A. Olsson and M. Naarttijarvi, "Design optimization for 3D printed energy absorbing," 2017.

[16]   G. Yao, R. Liu, Z. Xu, R. Xin, L. Chen, Z. Yu and Z. Zhang, "Study on quasi-static mechanical properties of four 3D-printed bio-inspired structures based on

functional relationship," *Composite Structures,* 15 October 2021.

[17]   L. Hao, D. Raymont, C. Yan, A. Hussein and P. Young, "Design and additive manufacturing of cellular lattice structures," in *The International Conference on Advanced Research in Virtual and Rapid Prototyping (VRAP)*, Leiria, Portugal, 2011.

[18]   A. Bacciaglia, A. Ceruti and A. Liverani, "Proposal of a standard for 2D representation of bio-inspired lightweight lattice structures in drawings," *Proceedings of the Institution of Mechanical Engineers, Part C: Journal of Mechanical Engineering Science,* August 2020.

[19]   J. Fu, Q. Liu, K. Liufu, Y. Deng, J. Fang and Q. Li, "Design of bionic-bamboo thin-walled structures for energy absorption," *Thin-Walled Structures,* pp. 400-413, 2019.

[20]   M. Zou, S. Xu, C. Wei, H. Wang and Z. Liu, "A bionic method for the crashworthiness design of thin-walled structures inspired by bamboo," *Thin-Walled Structures,* pp. 222-230, 2016.

[21]   F. Fu, "Shear Wall, Core, Outrigger, Belt Truss, and Buttress Core System for Tall Buildings," in *Design and Analysis of Tall and Complex Structures*, 2018.

[22]   S. Liu, Z. Tong, Z. Tang, Y. Liu and Z. Zhang, "Bionic design modification of non-convex multi-corner thin-walled columns for improving energy absorption through adding bulkheads," *Thin-Walled Structures,* pp. 70-81, 2015.

[23]   C. Qi, S. Yang and F. Dong, "Crushing analysis and multiobjective crashworthiness optimization of

tapered square tubes under oblique impact loading," *Thin-Walled Structures,* pp. 103-119, 2012.

[24] Z. Li, L. Duan, T. Chen and Z. Hu, "Crashworthiness analysis and multi-objective design optimization of a novel lotus root filled tube (LFT)," *Structural and Multidisciplinary Optimization,* pp. 865-875, 2017.

[25] X. Deng and W. Liu, "Crushing analysis and multi-objective crashworthiness optimization of multi-cell conical tube subjected to oblique loading," *Advances in Mechanical Engineering,* 2019.

[26] L. Zhang, Z. Bai and F. Bai, "Crashworthiness design for bio-inspired multi-cell tubes with quadrilateral, hexagonal and octagonal sections," *Thin-Walled Structures,* pp. 42-51, 2018.

[27] P. Hao and J. Du, "Energy absorption characteristics of bio-inspired honeycomb column thin-walled structure under impact loading," *Journal of the Mechanical Behavior of Biomedical Materials,* pp. 301-308, 2018.

[28] J. Xiang and J. Du, "Energy absorption characteristics of bio-inspired honeycomb structure under axial impact loading," *Materials Science and Engineering: A,* pp. 283-289, 1 June 2017.

[29] Y. Xiao, H. Yin and G. Wen, "Crashworthiness design of horsetail-bionic thin-walled structures under," *International Journal of Mechanics and Materials in Design,* December 2016.

[30] N. S. Ha, G. Lu and X. Xiang, "Energy absorption of a bio-inspired honeycomb sandwich panel," *Journal of Materials Science,* pp. 6286-6300, 2019.

[31] X. Yang, J. Ma, Y. Shi, Y. Sun and J. Yang, "Crashworthiness investigation of the bioinspired bi-

directionally corrugated core sandwich panel under quasistatic crushing load," *Materials & Design,* pp. 275-290, 2017.

[32]   J. Li, T. X. Yu, J. Xu, H. Chen and S. Yin, "Effects of architecture level on mechanical properties of hierarchical lattice materials," *International Journal of Mechanical Sciences,* pp. 282-292, 2019.

[33]   D. Hu, Y. Wang, B. Song, L. Dang and Z. Zhang, "Energy-absorption characteristics of a bionic honeycomb tubular nested structure inspired by bamboo under axial crushing," *Composites Part B: Engineering,* pp. 21-32, 1 April 2019.

[34]   Y. Zhang, X. Xu, J. Wang, T. Chen and C. H. Wang, "Crushing analysis for novel bio-inspired hierarchical circular structures subjected to axial load," *International Journal of Mechanical Sciences,* pp. 407-431, May 2018.

[35]   H. Tsang and S. Raza, "Impact energy absorption of bio-inspired tubular sections with structural hierarchy," *Composite Structures,* pp. 199-210, 2018.

[36]   W. Zhang, S. Yin, T. X. Yu and J. Xu, "Crushing resistance and energy absorption of pomelo peel inspired hierarchical honeycomb," *International Journal of Impact Engineering,* pp. 163-172, March 2019.

[37]   Q. He, J. Feng, Y. Chen and H. Zhou, "Mechanical properties of spider-web hierarchical honeycombs subjected to out-of-plane impact loading," *Journal of Sandwich Structures and Materials,* April 2018.

[38]   P. Pearce, Structure in nature is a strategy for design, The MIT Press, 1980.

[39]   L. Rampino and R. Gatti, "Digital Fabrication and Product Aesthetics," in *Evolving perspectives in product design*, Milano, Franco Angeli, 2018, pp. 153-168.

[40]   B. Zheng, Y. Liu, J. Liu, S. Yin and J. Xu, "Novel mechanical behaviors of DNA-inspired helical structures with chirality," *International Journal of Mechanical Sciences,* October 2019.

[41]   A. Seharing, A. H. Azman and S. Abdullah, "A review on integration of lightweight gradient lattice structures in additive manufacturing parts," *Advanced in Mechanical Engineering,* 1 June 2014.

[42]   X. Wang, S. Xu, S. Zhou, W. Xu, M. Leary, P. Choong, M. Qian, M. Brandt and Y. M. Xie, "Topological design and additive manufacturing of porous metals for bone," *Biomaterials,* no. 83, pp. 127-141, 2017.

[43]   "Prusa 3D," [Online]. Available: https://www.prusa3d.com/original-prusa-i3-mk3/. [Accessed 11 November 2021].

[44]   "3Dnet," [Online]. Available: https://3dnet.no/collections/featured-1/products/3dnet-pla-1-75-ny?variant=34430795284644. [Accessed 11 November 2021].

[45]   "MTS," [Online]. Available: https://corp.mts.com/cs/groups/public/documents/library/mts_006225.pdf. [Accessed 11 November 2021].

[46]   "MTS," [Online]. Available: https://www.mts.com/-/media/materials/pdfs/brochures/mts-series-809-test-system-brochure.pdf?as=1. [Accessed 11 November 2021].

[47]   "MTS," [Online]. Available: https://www.mts.com/-
        /media/materials/pdfs/test-standards/100-332-
        871_PlasticsISO604.pdf?as=1. [Accessed 11 November
        2021].

[48]   ABAQUS User's Manual, version 2016, 2015.

[49]   HyperMesh 13.0 Manual.

[50]   P. Baikerikar and C. J. Turner, "Comparison Of FEA
        Simulations And Experimental Results For As-Built
        Additively Manufactured Dogbone Specimens,"
        Engineering, 6 August 2017.

[51]   I. Maskery, L. Sturm, A. O. Aremu, A. Panesar, C. B.
        Williams, C. J. Tuck, R. D. Wildman, I. A. Ashcroft and
        R. J. Hague, "Insights into the mechanical properties
        of several triply periodic minimal surface lattice
        structures made by polymer additive manufacturing,"
        Polymer, pp. 62-71, 12 September 2018.

[52]   Q. M. Li, I. Magkiriadis and J. J. Harrigan,
        "Compressive Strain at the Onset of Densification of
        Cellular Solids," *Journal of Cellular Plastics,* pp. 371-
        392, 6 September 2006.

[53]   C. Weller, R. Kleer and F. T. Piller, "Economic
        implications of 3D printing: Market structure models
        in light of additive manufacturing revisited,"
        International Journal of Production Economics, pp.
        43-56, June 2015.

[54]   "Markforged," [Online]. Available:
        https://markforged.com/resources/blog/pla-abs-
        nylon. [Accessed 27 October 2021].

[55]   "Simplify 3D," [Online]. Available:
        https://www.simplify3d.com/support/materials-

guide/carbon-fiber-filled/. [Accessed 27 Ottobre 2021].

[56]   "HEXR," [Online]. Available: https://hexr.com/.

[57]   M. Pelanconi and A. Ortona, "Nature-Inspired, Ultra-Lightweight Structures with Gyroid Cores Produced by Additive Manufacturing and Reinforced by Unidirectional Carbon Fiber Ribs," *Materials,* December 2019.

[58]   "Carbon," [Online]. Available: https://www.carbon3d.com/resources/whitepaper/the-adidas-story/. [Accessed 2021 October 27].

[59]   "Trueventor," 15 March 2018. [Online]. Available: https://www.truventor.ai/blogs/adidas-future-craft/. [Accessed 27 October 2021].

[60]   "3D sourced," [Online]. Available: https://www.3dsourced.com/feature-stories/3d-printed-shoes/. [Accessed 27 October 2021].

[61]   "Materialise," [Online]. Available: https://www.materialise.com/en/cases/worlds-first-dynamic-printed-insoles. [Accessed 27 October 2021].

[62]   "Cambridge Dictionary," [Online]. Available: https://dictionary.cambridge.org/it/dizionario/inglese/plaster-cast. [Accessed 11 October 2021].

[63]   "The Medical Futurist," 21 March 2016. [Online]. Available: https://medicalfuturist.com/plaster-casts-on-a-broken-limb-in-2016-please-print-out-mine/. [Accessed 11 October 2021].

[64]   "S.M.A.R.T. - TRASH," [Online]. Available: http://www.smart-trash-eduformat.com/pla-produzione.html. [Accessed 11 October 2021].

[65] "Healthdesk," 24 January 2019. [Online]. Available: http://www.healthdesk.it/medicina/frattura-caviglia-bastano-tre-settimane-gesso-invece-che-sei. [Accessed 11 October 2021].

[66] "Thingiverse," 22 July 2014. [Online]. Available: https://www.thingiverse.com/thing:403001. [Accessed 12 October 2021].

[67] "Children's Hospital Colorado," [Online]. Available: https://www.childrenscolorado.org/doctors-and-departments/departments/orthopedics/services/3d-printed-casts/. [Accessed 11 October 2021].

[68] "Sculpteo," 29 April 2019. [Online]. Available: https://www.sculpteo.com/blog/2019/04/29/can-additive-manufacturing-heal-bones-with-a-3d-printed-cast/. [Accessed 12 October 2021].

[69] "Exiom," [Online]. Available: Exiom.com. [Accessed 12 October 2021].

[70] "Ortho Baltic," [Online]. Available: https://www.orthobaltic.eu/orthoses/orthoses.html. [Accessed 26 October 2021].

[71] "Sculpteo," 5 April 2019. [Online]. Available: https://www.sculpteo.com/blog/2019/04/05/3d-printed-prosthetics-the-best-projects/. [Accessed 13 October 2021].

[72] B. Rochlitz and D. Pammer, "Design and Analysis of 3D Printable," *Periodica Polytechnica Mechanical Engineering,* pp. 282-287, 2017.

[73] Ottobockus. [Online]. Available: https://www.ottobockus.com/prosthetics/info-for-new-amputees/prosthetics-101/finding-the-best-foot-for-you/. [Accessed 26 October 2021].

[74] "Leimkuehler," [Online]. Available: https://leimkuehleroandp.com/feet-and-ankles/. [Accessed 26 October 2021].

[75] F. Mitchell, "Prosthetic limbs for children," *The Lancet - Child & Adolescent Health,* 1 December 2020.

[76] R. Budde, "The story of Velcro," *Physics World 8(1):22-22,* January 1995.

[77] W. L. Krinsky, "Beetles (Coleoptera)," *Medical and Veterinary Entomology (Third Edition),* pp. 129-143, 2019.

[78] S. Brady e U. Schmidt, «Woodcraft,» 10 February 2007. [Online]. Available: https://www.woodcraft.com/blog_entries/woodsense-bamboo. [Consultato il giorno 2 November 2021].

[79] M. D. Pisapia, "Marco De Pisapia," [Online]. Available: https://www.marcodepisapia.com/burj-khalifa-sul-tetto-del-mondo-a-828-metri-di-altezza/. [Accessed 2 November 2021].

[80] D. Ginzburg, F. Pinto, O. Iervolino and M. Meo, "Damage tolerance of bio-inspired helicoidal composites under lowvelocity impact," *Composite Structures,* vol. 161, pp. 187-203, 1 February 2017.

[81] C. S. Han, D. S. Kang and K. Kang, "Two nature-mimicking auxetic materials with potential for high energy absorption," *Materials today,* pp. 30-39, June 2019.

[82] X. Yang, Y. Sun, J. Yang and Q. Pan, "Out-of-plane crashworthiness analysis of bio-inspired aluminum honeycomb patterned with horseshoe mesostructure," *Thin-Walled Structures,* pp. 1-11, April 2018.

[83] C. Hundertmark, R. Tinter, M. Ortelt and M. Hauser, "Diatom-inspired Plastic Deformation Elements for Energy Absorption in Automobiles," *Journal of Bionic Engineering,* pp. 613-623, 2015.

[84] T. Demuth, Y. Jeanvoine, J. Hafner and J. G. Ángyán, "Polymorphism in Silica Studied in the Local Density and Generalized-Gradient Approximations," *Journal of Physics Condensed Matter,* pp. 3833-3874, May 1999.

[85] "Mathworks," [Online]. Available: https://it.mathworks.com/help/matlab/ref/trapz.html. [Accessed 8 November 2021].

[86] Q. Bui, A. Grillet and H. Tran, "A Bamboo Treatment Procedure: Effects on the Durability and Mechanical Performance," *Sustainability,* August 2017.

[87] [Online]. Available: https://helmet.beam.vt.edu/bicycle-helmet-ratings.html. [Accessed 24 November 2021].

[88] [Online]. Available: https://www.jamestowncontainer.com/polyurethane-packing-foam/. [Accessed 24 November 2021].

[89] [Online]. Available: https://www.macpanther-materials.de/pu-based-metal-foams.html. [Accessed 24 November 2021].

[90] [Online]. Available: https://3dprinting.com/tips-tricks/3d-printed-lattice-structures/. [Accessed 24 November 2021].

[91] [Online]. Available: https://www.nanopress.it/storie/il-materiale-piu-leggero-al-mondo-per-gli-aerei-del-futuro/78363/2/. [Accessed 24 November 2021].

[92] [Online]. Available: http://www.microlabgallery.com/gallery/Bamboo%20C%202b.aspx. [Accessed 24 November 2021].

[93] [Online]. Available: https://www.sciencephoto.com/keyword/radial-canal. [Accessed 24 November 2021].

[94] [Online]. Available: https://commons.wikimedia.org/wiki/File:Diatom_-_Cocconeis_sp._-_630x_(16703676292).jpg. [Accessed 24 November 2021].

[95] [Online]. Available: https://engineering.berkeley.edu/news/2020/04/tough-as-scales/. [Accessed 24 November 2021].

[96] [Online]. Available: https://www.flickr.com/photos/dr-harout/8354385553/. [Accessed 24 November 2021].

[97] [Online]. Available: https://casoar.org/en/2020/09/09/les-perles-noires-de-tahiti-remarquables-gemmes-de-polynesie-francaise/meb_nacre/. [Accessed 24 November 2021].

[98] [Online]. Available: https://amfg.ai/de/2019/08/28/7-komplexe-designs-im-3d-druck/. [Accessed 24 November 2021].

[99] [Online]. Available: https://oppositionalgeometryblog.wordpress.com/2015/10/01/plato-ca-428-ca-347-b-c/. [Accessed 24 November 2021].

[100] [Online]. Available: https://unsplash.com/photos/nb5_NM77RfI. [Accessed 24 November 2021].

[101] [Online]. Available:
https://unsplash.com/photos/ei57d-mVZP0.
[Accessed 24 November 2021].

[102] [Online]. Available: https://bionicproduction.com/3d-
druck-technologien/fused-deposition-modeling-fdm/.
[Accessed 24 November 2021].

[103] [Online]. Available:
https://www.fastradius.com/resources/understanding
-3d-printed-lattices-performance-and-design-
considerations/. [Accessed 24 November 2021].

[104] [Online]. Available:
https://leganerd.com/2021/07/16/il-primo-ponte-in-
acciaio-stampato-in-3d-e-stato-inaugurato-ad-
amsterdam/. [Accessed 24 November 2021].

[105] [Online]. Available:
https://www.buys365.ga/ProductDetail.aspx?iid=4267
53120&pr=. [Accessed 24 November 2021].

[106] [Online]. Available:
https://www.enstocks5b.top/products.aspx?cname=ki
ckstarter+helmet+bike&cid=14. [Accessed 24
November 2021].

[107] [Online]. Available:
https://www.pinterest.it/pin/373446994106504017/.
[Accessed 24 November 2021].

[108] [Online]. Available: https://activarmor.com/wp-
content/uploads/2021/03/ActivArmor-Use-Cases.pdf.
[Accessed 24 November 2021].